Elucidating the Ligand-induced Phase Behavior of Polymer-grafted Nanoparticle Thin Films

by
Wenjie Wu

A dissertation submitted to the Department of Chemical and Bimolecular Engineering,
Cullen College of Engineering
in partial fulfillment of the requirements for the degree of

DOCTOR OF PHILOSOPHY

in Chemical Engineering

Chair of Committee: Alamgir Karim

Committee Member: Megan Robertson

Committee Member: Jeremy Palmer

Committee Member: Devin Shaffer

Committee Member: Hadi Ghasemi

University of Houston
May 2022

DEDICATION

This dissertation is dedicated to my wife Jiayi Chen and my daughter Anne C.Wu.

Love you to the moon and back.

ACKNOWLEDGMENTS

I would like to take this opportunity to thank all the people who provides me support and help during my whole Ph.D. life. I feel so lucky to have all of them around me, accompanying me through those “up” and “downs”, not only during the research, but also in life. These 4 years’ experience has shaped me to a tenacious person and armed me with the strong problem-solving skills for any future challenges. This is a unique and precious experience I will cherish and appreciate through the whole rest of my life.

First and foremost, I would like to thank my Ph.D. advisor Dr. Alamgir Karim. He is always helpful and ready to provide me advice whenever I needed. At the same time, he also encouraged me to be a self-motivated person. He encouraged me to identify and solve the scientific problems by myself and let me try those “Saturday crazy” research ideas. Although sometime those ideas didn’t work, but I sharped my problem-solving and practical skills from those experience. Those skills I learned from him will continue to help me in my future career. I am also grateful to my committee members: Dr. Megan Robertson, Dr. Jeremy Palmer, Dr. Devin Shaffer, and Dr. Hadi Ghasemi for their valuable suggestions and help in my Ph.D. research.

I would like to appreciate our collaborators Dr. Michael Bockstaller and Dr. Krzysztof Matyjaszewski and their students Yue Zhai, Rongguan Yin, and Dr. Jaejun Lee at Carnegie Mellon University. Thank them for providing all the polymer-grafted nanoparticles (PGNPs) and TEM measurements. I also appreciate the great discussions about my Ph.D. research during the monthly DOE meeting with them. My whole Ph.D. research is built upon this collaboration.

I also want to acknowledge Dr. Jack Douglas at NIST for those great thoughts about the binary PGNPs blends phase separation. I believe the discussion of hydrodynamic suppression in PGNPs blends is one of the critical factor that make our paper published in ACS Nano. My acknowledgement also goes to the beam scientists at both NIST and Oak Ridge National Lab: Dr. Guangcui Yuan, Dr. Markus Bleuel, and Dr. John Akner. I also appreciate Dr. Tanguy Terlier for the ToF-SIMS measurement and analysis.

Many thanks to all the current and alumni of the Karim Research Group (KRG) at both University of Akron and University of Houston: Maninderjeet Singh, Dr. Ali Masud, Dr. Ali Ammar, Dr. Xiaoteng Wang, Dr. Asritha Nallapaneni, Dr. Sonal Bhadauriya, Dr. Ren Zhang, Chuqing Yuan, Kuan Cheng, Wafa Tonny, Kshitij Sharma, Samuel Wallaert, Mina Shanbedi, Aman Agrawal, Shenhui Zhao, Zihan Xiao, Edward Armijo, Van Do, to name a few. I enjoy working in this big family and appreciate all the great support and help from them. Special thanks to Maninderjeet Singh, a good “friend for life”.

Finally, my greatest gratitude and love goes to my family: my beloved wife Jiayi Chen, my lovely daughter Anne C. Wu, my mother Xiaoyu Xu, my father Xinhua Wu, my mother-in-law Weiwen Zhao, my father-in-law Yunxiang Chen, and my two cutest feline daughters Bao and Willow. I appreciate their unconditional love and support, which will continue to make me a tenacious person for any future endeavors.

ABSTRACT

High molecular mass polymer-grafted nanoparticles (PGNPs) have attracted significant attention in the past few decades with the potential to design next-generation polymer nanocomposites with enhanced optical and mechanical properties and thermal stabilities. A critical requirement for these new nanoparticles and their associated applications is the control of their morphology and the dispersion in the system. However, subsequent studies have demonstrated that the mobilities of the high molecular mass PGNPs decrease significantly, which leads to poor or no control over their phase morphologies. In this study, we aim to overcome this scientific problem and control the spatial organization of those materials *via* the interactions between the grafted polymer layer and the polymer matrix in both smooth and nanopatterned films. We firstly investigate a binary high molecular mass PGNPs blends using a direct immersion annealing method (DIA) that allows for facile tuning of the PGNPs phase boundary, phase separation kinetics, and the ultimate scale of phase separation after a sufficient 'aging' time. We show that the phase morphologies could be readily switched between phase-separated and homogenous state by changing the thermodynamic conditions of DIA solution quality. To overcome the low-mobility problem and exert the exquisite control over the distribution of high molecular mass PGNPs in a nanopatterned film, we developed a solvent vapor annealing soft lithography (SVA-SL) method. We revealed that the minimization of the entropic free energy from the topographic nanoimprint patterning along with the increased mobilities from solvent vapor drives the high molecular mass PGNPs to the 'mesa' region of nanopatterned films. Furthermore, reversible partitioning (selective *vs.* no

partitioning) in a nanopatterned film can be facilely achieved by introducing the enthalpic interactions into the system. Both the SVA-SL processing method and the reversible partitioning *via* tunning the interaction parameter is important. It allows for facile imprint patterning of PGNP materials and large-scale organization of the "sluggish" high molecular mass PGNPs. These approaches, along with the DIA method to control the morphologies of smooth film, have great potential to design the nanocomposite films with enhanced thermo-mechanical property of the resulting films, and a corresponding extended range of potential nanotech applications.

TABLE OF CONTENTS

LIST OF TABLES

LIST OF FIGURES

I. INTRODUCTION

During the last several decades, scientists have revealed that polymer can be used to develop multifunctional soft materials by adding nanoparticles into it.[1,2] This blend system is usually referred to as polymer nanocomposites (PNC).[3] By adding only a small amount of nanoparticles, the polymer matrices can acquire enhanced mechanical properties,[4–7] enhanced thermal stabilities,[8,9] electric conductivity,[10] and better permeability and selectivity for filtration,[11] which is due to the larger interfacial area and the synergistic interactions between the nanoparticles and the polymer matrix.[3] The distribution of nanoparticles in the PNC film plays the vital role in controlling the overall properties. For example, a well-mixed/miscible state of nanoparticles in polymer matrix is required for uniformly enhanced mechanical properties. However, due to the van der Waals attraction and the larger surface area, the nanoparticles tend to aggregate and form clusters within the film, which brings non-uniformity to the whole system.[5,6,12]

How to enhance the miscibility and control the phase morphologies of nanoparticles in the polymer matrix? One of the efficient ways is by directly grafting the polymer chains onto it. The morphology of nanoparticles can then be tuned from both the enthalpic and entropic interactions of grafted polymer chains and the polymer matrix. This kind of material is named as polymer-grafted nanoparticles (PGNPs).[13] With the development of surface initiated controlled radical polymerization (SI-CRP),[14–17] researchers have synthesized PGNPs with the variation of grafting density, chain length, and the composition of the grafted polymer chains, which helps them

successfully incorporated the PGNPs into different kinds of polymer matrix with well-controlled morphologies, including block copolymers,[18,19] homopolymer,[8,20–23] and another type of PGNPs.[24,25]

In this dissertation, we are specially interested in high molecular mass PGNPs, which has great potential to design next-generation polymer nanocomposites with enhanced mechanical properties and thermal stabilities of nanopatterned surfaces due to the strong entanglement between the grafted polymer chains and the matrix. However, subsequent studies have demonstrated that the mobilities of the high molecular mass PGNPs decrease significantly due to the 'solid-like' 'jammed state',[26,27] which brings difficulties in processing this material and controlling the morphologies of it for advanced applications.

The objective of the current work is then to understand the phase behaviors of binary high molecular mass PGNPs blends and to develop the facile method to control the morphologies of it in both smooth and patterned films. Generally, the PGNPs studied in this dissertation are densely grafted, where the interaction between the inner nanoparticle core is "blocked" from the grafted polymer chains. The phase behavior is then governed only by the interactions between the grafted polymer chains and the polymer matrix.

In Chapter II, a literature review about the background of the PGNPs system is provided. We firstly cover the application of (polymer-grafted) nanoparticles and the relationship between the morphologies and the properties. We then introduce the structures of PGNPs and how does it influence the dispersion of the PGNPs in the

polymer matrix. To have a fundamental understanding of the phase behaviors, we introduce the thermodynamics and kinetics of homopolymer blends phase separation and relate it to the system with PGNPs. In the last part of Chapter II, we provide detailed review about the strategies to have controlled dispersion of nanoparticles/PGNPs in the polymer matrix, including both "External-in" and "Internal-out" method. In Chapter III, we firstly start with a scientific problem that the binary high molecular mass PGNPs doesn't show any morphology development compared to the as-cast film *via* thermal annealing due to the lack of mobility. We introduce a solvent assisted method called direct immersion annealing (DIA) to solve this problem. More interestingly, by changing the solvent of DIA mixtures, we achieve reversible phase behavior between phase-separated and homogenous state of those PGNPs blends. To have a solid understanding of the phase behavior, we investigated both the thermodynamics and kinetics of the DIA induced phase separation. The thermodynamic is studied using the Flory-Huggins interaction parameter χ, while the kinetic is investigated by comparing the exponent of the power-law to the parent homopolymer blends. We then extend our investigation of the phase behavior of binary PGNPs blends to nanopatterned films (Chapter IV and V). Previous studies from our group revealed that the thermal annealing induced topographic soft-pattern confinement (TA-SL) can be used to selectively control the distribution of low molecular mass PGNPs in the chemically identical homopolymer matrix. In Chapter IV, we firstly reveal that the TA-SL can no longer induce the selective segregation of high molecular mass PGNPs in a chemically identical but smaller-sized PGNPs matrix. We develop a solvent vapor annealing soft lithography (SVA-SL) method to overcome

this scientific processing difficulty. The extension of selective partitioning is quantified using a partitioning parameter K_p, and the driving force for the selective ordering of the larger-sized PGNPs in nanopatterned films is elucidated with the variation of the molecular mass for the PGNPs and the initial film thickness before patterning. With a better understanding of the chemically identical system from Chapter IV, we investigate the phase behavior of high molecular mass PGNPs in a chemically dissimilar polymer matrix under topographic nanopattern confinement in Chapter V. We reveal that a reversible distribution between selective and no partitioning can be achieved by varying the TA-SL annealing temperature above and below the lower-critical solution temperature (LCST). Thermodynamic driving force for the reversible nanoimprinting-directed assembly is elucidated. Chapter VI provides a summary of my Ph.D. research.

II. BACKGROUND AND LITERATURE REVIEW

2.1 Nanoparticles and Their Applications

Nanoparticles (NPs) are a kind of small materials with sizes ranging from < 10 nm to hundreds of nanometers. Due to the recent advancement in synthesis, it can vary with different shapes (spherical NPs, rods, and platelets) and materials (metallic, quantum dots, metal oxide, and carbon-based materials). As the size of it is in the nanometer scale, it holds very interesting properties. For example, the II-VI group quantum dots are well-known for its high quantum efficiencies, which has been used as photovoltaics or light-emitting devices.[28,29] The magnetic nanowires have been reported to make the field-effect transistors.[30]

Another important way to utilize NPs is to use it as additives to other materials. Most of the time, it is added to bulk matrix with different chemistry or structures. This type of blends is referred to as nanocomposites.[3,31] The most widely used nanocomposite can be find in the polymer industry, where the nanoparticles are added into polymer matrix to alter the properties of the polymers for different applications. This type of blends is called polymer nanocomposites (PNCs). As early as the 1900's, the polymer scientists have found that adding zinc oxide and carbon black to rubber can increase the mechanical properties of it, which help increase the durability of tires.[32] In the membrane area, scientists have developed a system called "mixed matrix membranes", where the addition of inert nanofillers have been proved to increase both permeability and selectivity of the filtration due to the modification of system free volume from the NPs.[11] Adding nanoparticles to polymer matrix can also totally change the properties of it. For example, researchers found that adding conductive

NPs, like carbon nanotubes (CNT) or graphene, can increase the conductivity of the polymer film to make it high enough for electrostatic discharge and electromagnetic interference shielding.[33] Other applications include sensors, photonic devices, and flexible electronics. Table 2.1 listed some of the polymer nanocomposites and its application that has already been commercialized.[34]

Table 2.1 Examples of Nanocomposite Applications[34] (Reproduced with permission from Reference 34).

Polymer matrix	Nanoparticle	Property improvement	Application	Company and/or product trade name
Polyamide 6	Exfoliated clay	Stiffness	Timing belt cover: automotive	Toyota/Ube
TPO (thermoplastic polyolefin)	Exfoliated clay	Stiffness/strength	Exterior step assist	General Motors
Epoxy	Carbon nanotubes	Strength/stiffness	Tennis rackets	Babolat
Epoxy	Carbon nanotubes	Strength/stiffness	Hockey sticks	Montreal: Nitro Hybtonite®
Polyisobutylene	Exfoliated clay	Permeability barrier	Tennis balls, tires, soccer balls	InMat LLC
SBR, natural rubber, polybutadiene	Carbon black (20–100 nm: primary particles)	Strength, wear and abrasion	Tires	Various
Various	MWCNT	Electrical conductivity	Electrostatic dissipation	Hyperion
Unknown	Silver	Antimicrobial	Wound care/bandage	Curad®
Nylon MXD6, PP	Exfoliated clay	Barrier	Beverage containers, film	Imperm™: Nanocor
SBR rubber	Not disclosed	Improved tire performance in winter	Winter tires	Pirelli
Natural rubber	Silver	Antimicrobial	Latex gloves	
Various	Silica	Viscosity control, thixotropic agent	Various	
Polyamides nylon 6, 66, 12	Exfoliated clay	Barrier	Auto fuel systems	Ube

2.2 Polymer-grafted Nanoparticles

It is well-known that one of the prerequisites of those applications discussed earlier is the good or controlled dispersion of nanoparticles in the polymer matrix.[3] However, as the bare NPs are attracted by the van der Waals interactions between each other and the general tendency to decrease the surface area by aggregation, those bare NPs normally form clusters that brings non-uniformity to the whole properties of the materials.[3] One of the approaches to overcome those non-equilibrium disadvantages is to graft polymers to the NPs. Those type of NPs are called polymer-grafted nanoparticles (PGNPs). Recent advantages in the synthetic process facilitate the functionalization of NPs with polymer chains.[35–41] With variation of grafting density and the chemistry of grafting ligands, scientists have achieved enhanced distribution

and structures of the polymer nanocomposites, which opens more opportunities in advanced applications.[4–7,42–47] In the rest of this chapter, we will cover the recent development of the surface modification of PGNPs, the structures of PGNPs, and the up-to-date techniques to control the phase behavior/distribution of PGNPs in polymer matrix.

2.2.1 Synthesis of Polymer-grafted Nanoparticles

The surface modification of bare NPs is derived from the synthesis of hybrid polymer brushes onto the planar surfaces. The polymer chains can be added to the surface by either physical absorption, *i.e.* physisorption, or chemically functionalization.[48] In general, the chemically attaching approach is more widely used as the formed covalent bond is more difficult to be broken up compared to the physical adsorption, which makes the polymer brush more stable in the further processing and applications. The chemical modification can be divided into two different methods: the "grafting to" and the "grafting from".[40] **Figure 2.1** shows the schematics for these two different approaches. In the "grafting to" approach, the pre-synthesized polymers are directly grafted to the surfaces *via* tethering the functionalized anchor to the surface. The advantage for the "grafting to" is the well-control of the polymer ligands. However, the disadvantage for this method is the limited grafting density (σ), which is due to the entropic penalties arising from the limited free volume of the surrounded grafted polymer chains. Another type of the method is called the "grafting from" method, where the bulk free monomers react with the activated/initiated surface. The polymerization directly happens on the targeted surface. As the densities of the initiators are easier to be controlled, the "grafting from" method has better control

over the grafting density. By utilizing this method, densely grafted polymer brushes can be acquired as the smaller sized monomers have less entropic penalties from the surrounding polymer chains.[17]

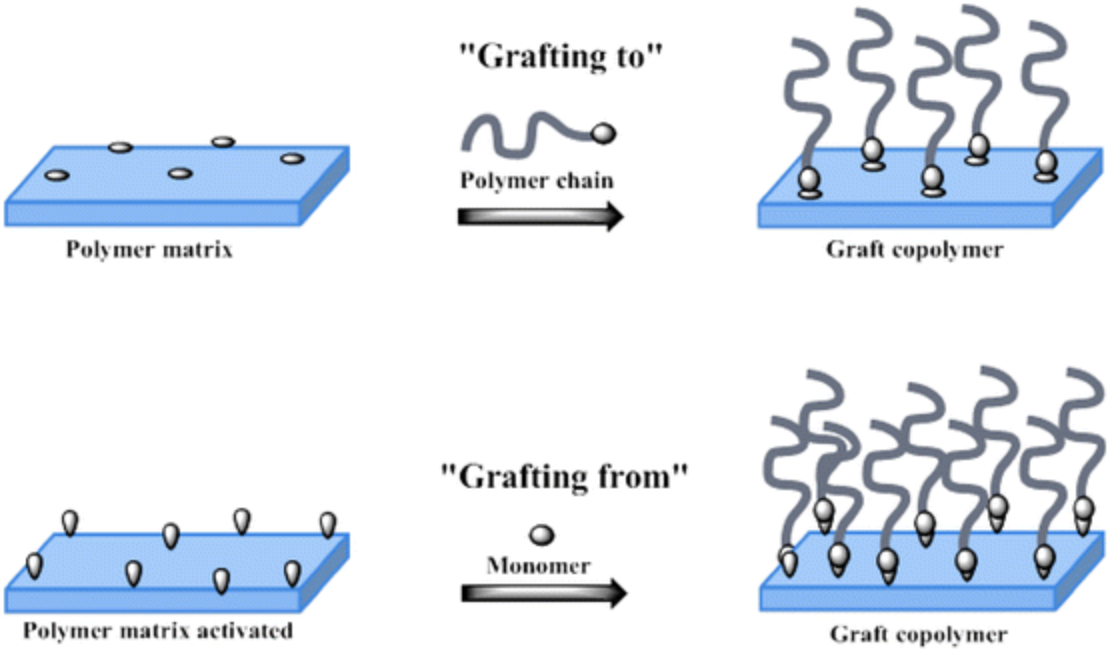

Figure 2.1 Schematic about the "grafting to" and "grafting from" polymerization on the planar surfaces.[40] (Reproduced with permission from Reference 40).

The "grafting from" method is also named as "surface-initiated polymerization" (SIP). One of the main approaches to have good-controlled SIP is called controlled radical polymerization (CRP).[16,49] CRP is a well-developed method, and can provide control over composition, grafting density, and length of the grafted polymer chains during SIP. There are several types of CRP, which includes reversible addition fragmentation chain transfer polymerization (RAFT), nitroxide-mediated polymerization (NMP), ring-opening metathesis polymerization (ROMP), and atomic

transfer free radical polymerization (ATRP). Among them, the surface initiated atomic transfer free radical polymerization (SI-ATRP) are the most widely used one.[50]

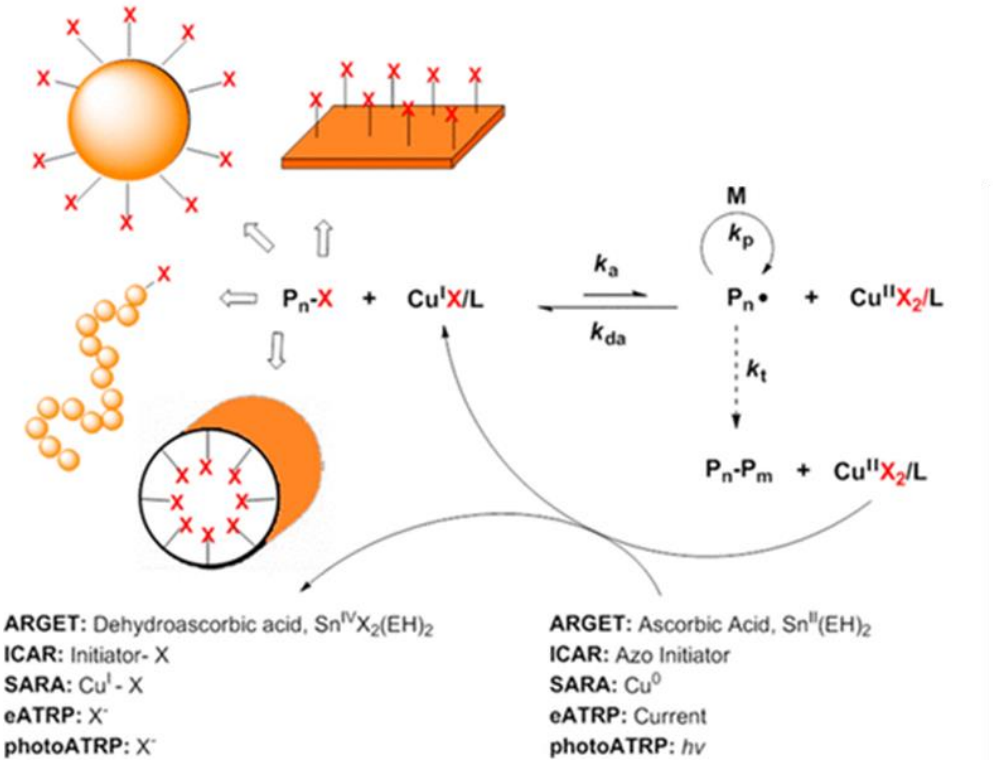

Figure 2.2 Illustration about the general SI-ATRP process.[37] (Reproduced with permission from Reference 37).

Figure 2.2 shows the typical SI-ATRP process. In the inset reaction, the P_n-X is the alkyl halide initiators/dormant species, which will react with the Cu^IX/L, the Cu^I halides with N-containing ligands (L), to form the free radicals $P_n^•$. This process is reversible, which will continuously providing $P_n^•$ to form the propogating polymer chains (P_n-P_m).[37] Generally, the SI-ATRP process includes four main processes: surface functionalization, initiation, propagation, and termination. The surface functionalization is among the most important factors during the whole process.

Normally, it requires multiple steps, which makes the whole process complicated and time-consuming.[15] Recently, Han *et al.*[15] invented a one-step synthesis process to prepare the functionalized surface on a organo-silica nanoparticles ($oSiO_2$) to further grow polymer chains on it through SI-ATRP. They symbolize the final product as C_y-$oSiO_2$-Br, where C_y is the composition of the hybrid inner nanoparticle core with y indicating the number of carbon atoms, and Br is the bromine functionalities, which is the X in **Figure 2.2** that will be used as the halide initiators to generate the free radicals in SI-ATRP. **Figure 2.3** shows more detailed information about preparing this hybrid organic nanoparticle initiators using the method.

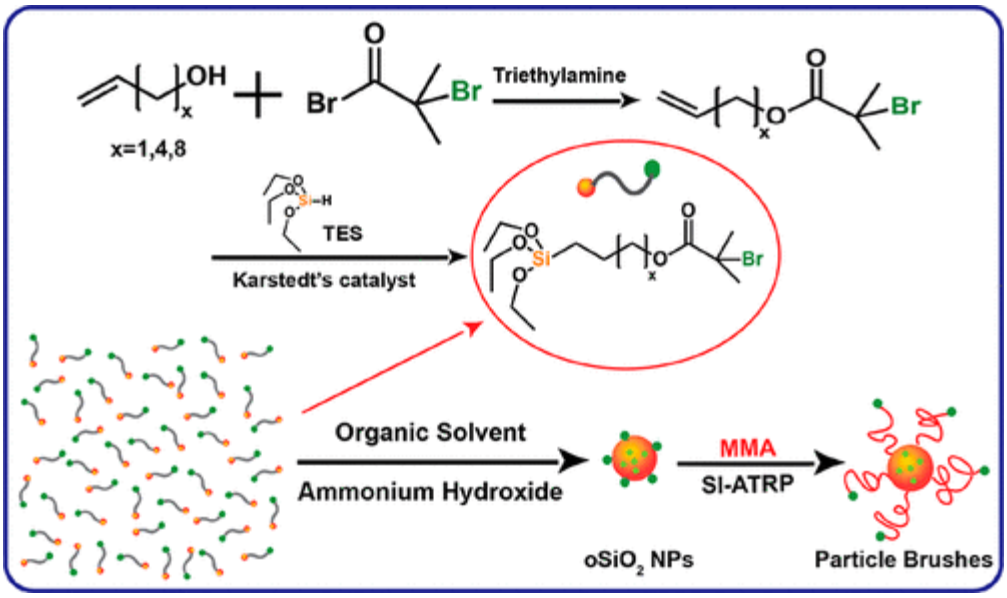

Figure 2.3 Scheme about the synthesis process for making polymethyl methacrylate (PMMA) grafted organo-silica nanoparticles ($oSiO_2$) using SI-ATRP.[15] (Reproduced with the permission from Reference 15).

2.2.2 Structure of Polymer-grafted Nanoparticles

Understanding the structure of the polymer-grafted nanoparticles (PGNPs) is the vital component to interpret and predict the behaviors and physical properties of

PGNPs. Generally, the structure of PGNPs depends on the grafting density (σ) and the chain length. The first and the most investigated case is the structure of linear polymer chains grafted onto the flat surface. We will start with that and then extend our discussion to curved and spherical surfaces.

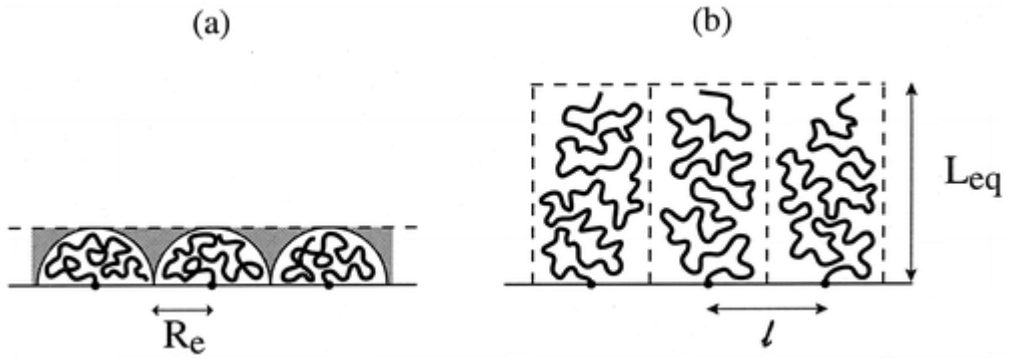

Figure 2.4. The structures of grafted polymer changes from "mushroom-like" structures (a) to "brush-like" structures as the grafting density increases.[51] (Reproduced with permission from Reference 51).

Structure of Linear Polymer Chains on Flat Surfaces. Let's first consider a linear polymer chain with *N* (degree of polymerization) monomers and the length for each monomer is a in the melt. The end-to-end distance can be calculated as $R_e = aN^{\frac{1}{2}}$. After taking the quality of the solvent into consideration, R_e can be represented as $R_e = aN^{\nu}$, where ν is the excluded volume parameter, which is a function of Flory-Huggins interaction parameter χ and can be calculated as $\nu = \frac{1}{2} - \chi$.[52] For a dilute good solvent condition, the radius of gyration (R_g) can be approximate as R_e. When the grafting density (σ) is sufficiently low, each polymer chain has enough free volume to move around and form a "mushroom-like" structure (**Figure 2.4.a**).[51] As the grafting density (σ) increases above the critical value ($\sigma^* = (aN^{\nu})^{-2}$), each polymer chain has

limited free volume to move around and has to be "stretched" to form "brush-like" structures on the surface (**Figure 2.4.b**).[51]

For the densely grafted polymer chains ($\sigma^{-\frac{1}{2}} < R_g$), the thickness of the brush layer (h_{brush}) can be estimated based on the Alexander[53] and de Gennes[52] model. They predict the outer polymer brush is like a "spring" where the spring constant is a function of k_BT with k_B as the Boltzmann constant and T as the temperature. It means that it costs k_BT energy to double the end-to-end distance of each polymer chain. By minimizing the total free energy of the system (F), h_{brush} can be estimated as $h_{brush} \sim N\ (v\sigma a^2)^{\frac{1}{3}}$. This estimation indicates that R_g is linearly related to the degree of polymerization (N): $R_g \sim N$, while for the ideal linear polymer chains, $R_g \sim N^{\frac{1}{2}}$. This predicts that for the high molecular mass (high N) polymer chains, the length of the densely grafted system will be much longer than the ideal linear system.

The above discussion hasn't considered the influence of the solvent quality on the structures of the linear polymer chains. Both theoretical and experimental studies have proved that the thickness of the polymer layer decreases when it is immersed in the poor solvent.[14] **Figure 2.5.B** shows the calculated polymer layer height as a function of solvent quality measured from neutron reflectivity (NR). The result (inset of **Figure 2.5.B**) show that the height decreases to over 50% when the film is immersed in the *d*-cyclohexane (the theta solvent for polystyrene) when compared to the film in *d*-toluene (the good solvent for polystyrene).[54]

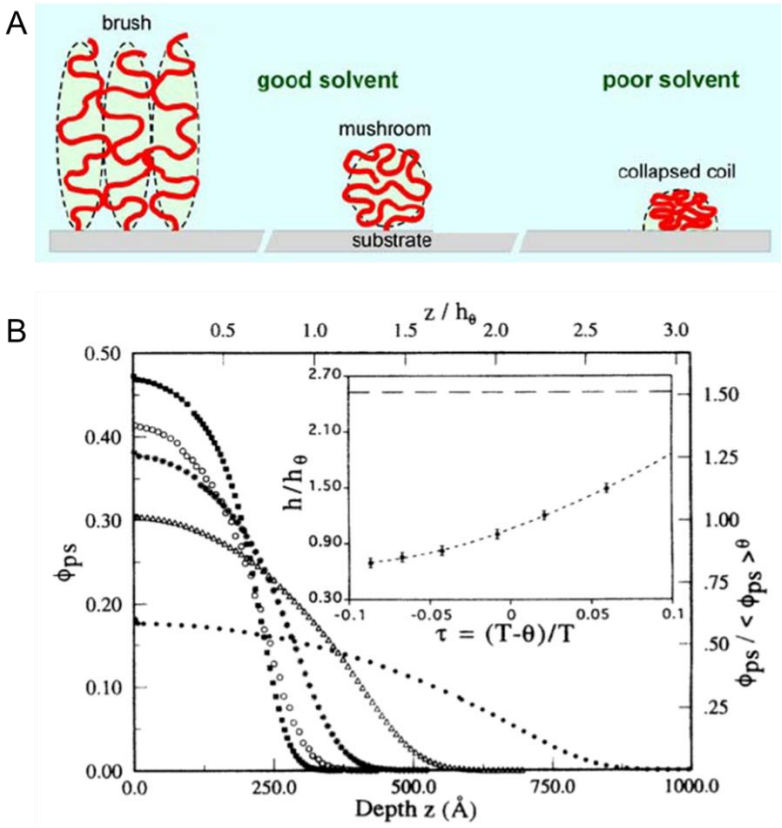

Figure 2.5 Influence of solvent quality on the structures of PGNPs.[14,54] (Reproduced with permission from Reference 14 and 54).

Structures of Polymer Chains on Curved Surfaces. With the understanding of the structures of linear polymer chains on the flat surfaces, we are now discussing the structures of polymer chains on curved surfaces. We will firstly start with small curvature. Wijmans *et al.*[55] investigated the brush height by a parabolic potential profile. Based on their conclusion, the brush height on the curved surfaces (*H*) can be calculated as

$$\left(\frac{H}{H_0}\right)^3\left(1+\frac{3H}{4\omega H_0}+\frac{1}{5}\left(\frac{H}{\omega H_0}\right)^2\right)=1, \tag{2.1}$$

where H_0 is the height on flat surfaces as discussed earlier, ω^{-1} is the relative curvature, which is the ratio of the H_0 to the radius of the curvature of the surface.

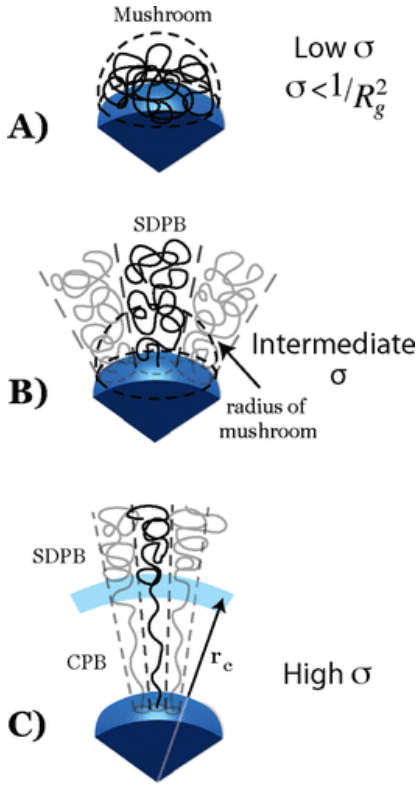

Figure 2.6 Schematic representation of grafted polymer layer structures on spherical nanoparticles as a function of grafting density (σ).[56] (Reproduced with permission from Reference 56).

Structures of Polymer Chains on Spherical Nanoparticles. Till now, we have already discussed the structures of polymer chains on both flat (planar) and small curved surfaces. This section will explain the structures of polymer chains on spherical nanoparticles. Daoud and Cotton develop the first model to study the influence of curvature on the structures of star polymers. They found out that the conformation of star-shaped polymers can be separated into three regions[57]. Ohno and his coworkers extend the Daoud-Cotton (DC) model to predict the structure of polymer grafted

nanoparticles (PGNPs)[56]. They found out that the conformation of PGNPs also depends on the grafting density (σ) as the planar and small curved surfaces. For lower grafted ($\sigma < 1/R_g^2$) nanoparticles, the brush formed a random coiled chain conformation ("mushroom-like" structures). In the intermediate grafting density, as the free volume between each polymer chain decreases, the polymer chain are slightly stretched and formed a regime named semi-dilute particle brush regime (SDPB). In the densely grafted nanoparticles, the conformation is separated into two regions. The inner side region is called the 'concentrated particle brush' (CPB) region, where the polymer chains are fully stretched due to the limited free volume, similar to the densely grafted polymer brushes on the planar surfaces. Due to the curved structure, the free volume for each densely grafted chain increases along the direction of the chain growth. When the chain length reaches above the critical value, the free volume for each polymer chain is large enough to form the SDPB region, which in turn establish a hybrid structure of CPB region near the inner nanoparticle core while SDPB near the outer brush region. Ohno *et al.* introduced the critical radius r_c to estimate the critical point from the center of the inner nanoparticles that separate the CPB and SDPB region. The r_c can be calculated as $r_c = 2r_0 v^{-1} a(\pi\sigma)^{\frac{1}{2}}$, where r_0 is the radius of the inner spherical nanoparticle core, v is the excluded free volume for each polymer chain, a is the length for each monomer.

Table 2.2 shows how the length of polymer chains scale with degree of polymerization and the reduced grafting density (σ^*) at different kinds of surfaces and

regimes based on the literature.[58] σ* is defined as $\sigma^* = \sigma a^2$, where a is the monomer length.

Table 2.2 Listed chain length as scaled with N and σ^*.[58] (Reproduced with permission from Reference 58).

Curvature	Behavior	Scaling with N, σ*	Chain Interactions
flat/spherical	mushroom	$N^{3/5}$	free chain in good solvent
flat	SDPB	$N^1\sigma^{*1/3}$	pairwise, excluded volume effects
flat	CPB	$N^1\sigma^{*1/2}$	higher-order, non-gaussian chains
spherical	SDPB	$(N\sigma^{*1/3})^{3/5}$	pairwise, excluded volume effects
spherical	CPB	$(N\sigma^{*1/2})^x$, $3/5 < x \leq 1$	higher-order, non-gaussian chains

Many experimental results have proven the existence of this hybrid CPB/SDPB regions and experimentally studied its scaling with different N and σ. Duke *et al.*[58] studied the brush height of polystyrene grafted silica nanoparticles with variation of degree of polymerization and grafting density in the bulk solution using dynamic light scattering (PS-SiO_2, d_{core} = 14 ± 4 nm, σ: 0.05 chains/nm^2 – 0.55 chains/nm^2, N = 40 – 1000). They reported that the scaling of h to N changes from $h \propto N^{\frac{4}{5}}$ in the CPB regime to $h \propto N^{\frac{3}{5}}$ in the SDPB regime. Choi *et al.*[4] investigated the brush height of PS-SiO_2 in the thin film state using transmission electron microscopy (TEM). **Figure 2.7** shows their result calculated from the interparticle distance between the PS-SiO_2. They found that the brush height scale as $h \sim N^{0.81}$ in the CPB region, similar to the situation reported by Dukes *et al.*[58] in the dilute bulk state. However, when it transfers to the SDPB region, $h \sim N^{0.52}$, which is smaller than the h

$\sim N^{0.6}$ in the bulk state. This is likely due to the collapse of the polymer chains in the dried films compared to swollen state in the bulk solution.

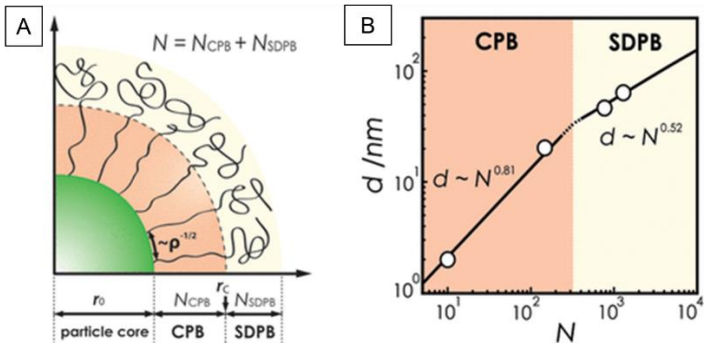

Figure 2.7 Schematic illustration about the CPB and SDPB regions on spherical nanoparticles.[4] (Reproduced with permission from Reference 4).

2.3 Phase Behavior of Binary Polymer Blends

The main objective of this dissertation is to study and control the phase behaviors of polymer-grafted nanoparticle blends. Before we moved to that topic, the preliminary research and conclusions about phase separation behaviors of binary homopolymer blends can be a good reference for our study. Generally, under different conditions (e.g. temperature and solvents), polymer blends can exhibit two different phase behaviors: miscibility and phase separation. The main equation used to explain the phenomena is

$$\Delta G_m = \Delta H_m - T\Delta S_m, \tag{2.2}$$

where ΔG_m is the free energy of mixing, ΔH_m is the enthalpy of mixing; ΔS_m is the entropy of mixing and T is the temperature.

Based on this equation, the Gibbs free energy of mixing consists of two part, the enthalpy of mixing and the combinatorial entropy of mixing. For the miscibility to occur, the following two conditions need to be met

$$\Delta G_m < 0 \text{ and} \tag{2.3}$$

$$\left(\frac{\partial^2 \Delta G_m}{\partial \Phi_i^2}\right)_{T,P} > 0, \tag{2.4}$$

where Φ_i is the volume fraction of component i.

When $\left(\frac{\partial^2 \Delta G_m}{\partial \Phi_i^2}\right)_{T,P} < 0$, the phase separation will occur even the ΔG_m is less than zero.

2.3.1 Flory-Huggins theory of binary polymer mixture.

In binary polymer mixtures, the free energy of mixing is mostly modeled by the Flory-Huggins theory. The mathematical expression, including both the entropy and enthalpy of mixing, is expressed as

$$\Delta G_m = kT\left[\frac{\Phi_1}{N_1} ln\Phi_1 + \frac{\Phi_2}{N_2} ln\Phi_2\right] + \Phi_1\Phi_2\chi_{12}kT, \tag{2.5}$$

where k is the Boltzmann's constant, N_i=degree of polymerization of component i, T=temperature, Φ_i=volume fraction of component i, χ_{12}=Flory-Huggins interaction parameter. The first two terms denote the combinatorial entropy of mixing while the last term describes the enthalpy of mixing. Based on the Flory-Huggin's expression, the combinatorial entropy of mixing for polymer mixtures is extremely small and will even vanish when $N_i \to \infty$. This indicates that the phase behavior of polymer mixtures is mostly governed by the enthalpy of mixing.

As mentioned before, when the second derivative of ΔG_m is less than zero, the polymer mixtures will phase separate into two phases. Assuming a symmetric system where $N_1=N_2=N$ and $\Phi_1=\Phi_2=0.5$, the condition for phase separation can be expressed as

$$\left(\frac{\partial^2 \Delta G_m}{\partial \Phi_1^2}\right)_{T,P} = kT\left[\frac{1}{\Phi_1} + \frac{1}{1-\Phi_1} - 2\chi N\right] < 0\,. \tag{2.6}$$

For the symmetric homopolymer blends, **equation (2.6)** can be simplified as $\chi N > 2$. Because of this, χN is commonly used as a measure for the driving force of polymer mixture's phase separation.

2.3.2 Phase diagrams: Upper and Lower Critical Solution Temperature (UCST/LCST)

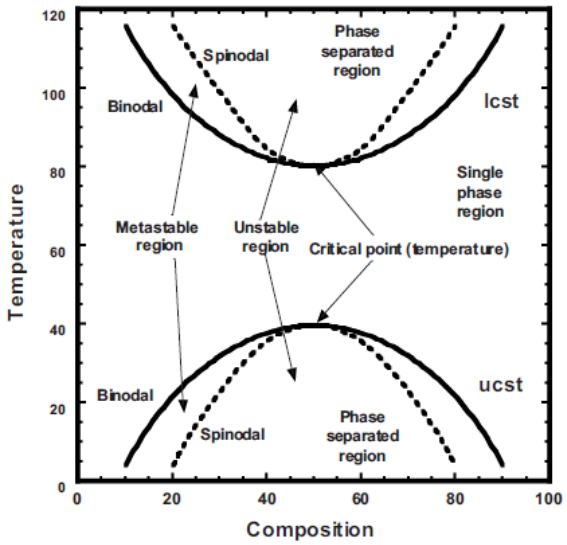

Figure 2.8 Phase diagrams for polymer blends. (Reproduced with permission from reference 59).[59]

Phase diagrams are used to describe the relationship between polymer mixtures' temperature and composition. In most cases, they can be explained by two different types: upper critical solution temperature (UCST) and lower critical solution temperature (LCST). **Figure 2.8** gives a detailed explanation of these two different phenomena. Both types have two curves, a binodal and a spinodal curve. The binodal curve is the curve that separates the single phase region and phase separated region. This curve is defined by the following equation

$$\Delta\mu_1^a = \Delta\mu_1^b;\ \Delta\mu_2^a = \Delta\mu_2^b, \tag{2.7}$$

where $\Delta\mu_i^j$ is the chemical potential of component i in phase j.

The spinodal curve divides the metastable and unstable phase separated region, which is described by

$$\left(\frac{\partial^2 \Delta G_m}{\partial \Phi_i^2}\right)_{T,P} = 0. \tag{2.8}$$

From **Figure 2.8**, UCST and LCST show two different phase behavior. In UCST system, increasing the temperature can change the phase behavior from phase separated region to the single phase region. However, in LCST blends, increasing the temperature will bring the mixtures from the single phase region to the phase separated state.

2.3.3 Phase Separation Mechanism

The bulk polymer blends' phase separation can be explained by two mechanisms: nucleation and growth (NG) and spinodal decomposition (SD). Nucleation and growth will occur when the phase separation happens in the metastable region in the phase diagram (**Figure 1.2.1**). It is often related to the crystallization from the solution. Spinodal decomposition happens when the phase separation is directly quenched into the unstable regions. This mechanism typically contains three different stages. In the beginning, the amplitude of the fluctuations will increase while the wavelength will remain constant. In the next stage, the diffusion will typically control the phase separation. The domain size will increase with the time in the following relation: $d \sim t^{\frac{1}{3}}$ .The last stage is mainly hydrodynamic-driven, and the

domain size linearly grows with the time: $d \sim t$. Chung and his coworkers[60] reveal the three stages of the spinodal decomposition with a PMMA/PSAN blend films (**Figure 2.9**).

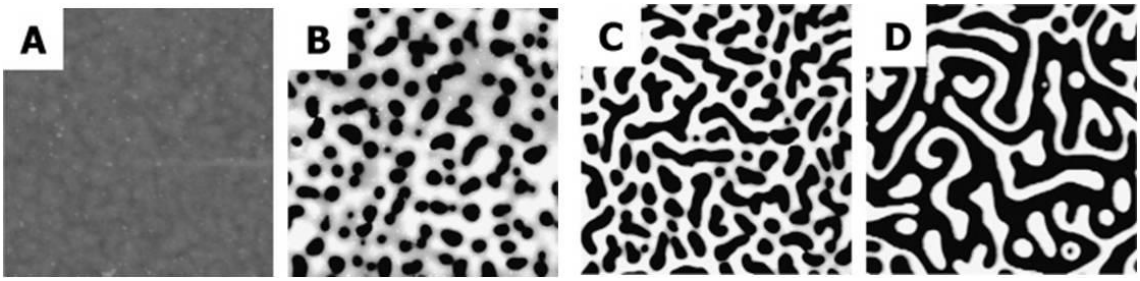

Figure 2.9 Evolution of phase diagrams at different stages of spinodal decomposition.[60] (Reproduced with the permission from Reference 60).

2.4 Phase Behavior of Polymer-grafted Nanoparticles in Homopolymer Matrix

With the development of the synthetic grafting techniques, scientists have a better control over the structures of polymer-grafted nanoparticles (PGNPs), which expedites the study of its phase behaviors and related applications. PGNPs in homopolymer matrix is the most popular system. The PGNPs acts as an additive/filler. Some people referred to this system as "Polymer Nanocomposites". Generally, the phase behavior of the PGNPs in homopolymer matrix depends on the following parameters: nanoparticle size (r_0), grafting density (σ), chemical compositions of the grafted and free chains, and the degree of polymerization of the grafted chains (N) and the free chains (P, from the homopolymer matrix). Both enthalpic and entropic (conformational and mixing) interactions between the polymer chains play important roles in the phase behaviors of PGNP/homopolymer system.

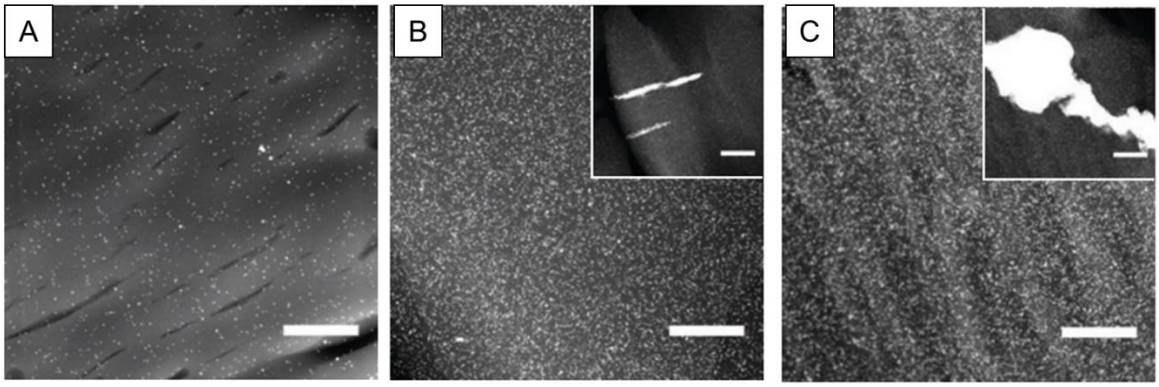

Figure 2.10 STEM images for phase behaviors of AuPS in PS matrix with different mass ratio. **a**, 0.3 wt% $AuPS_{10}$/PS. **b,** 1.0 wt% $AuPS_{10}$/PS, **c,** 3.0 wt% $AuPS_{10}$/PS. (Reproduced with permission from Reference 61). [61]

2.4.1 Phase Behavior of Densely Grafted Polymer-grafted Nanoparticles

As discussed in the previous sections, for the densely grafted PGNPs, the grafted polymer chains stretched out near the inner nanoparticle core, which "block" it from the polymer matrix. The phase behavior is then mainly controlled by the interaction between the outer polymer brush and the homopolymer matrix. For a "chemically identical system", where the grafted polymer chains have the same chemistry as the homopolymer matrix, the enthalpic interactions, a function of Flory-Huggins interaction parameter χ, equals to zero. This makes the phase behavior/miscibility only governed by the entropic interaction, which is related to the structures of PGNPs in the polymer matrix. There are two basic structures of PGNPs in the polymer matrix: wet brush and dry brush. For the small inner particle core ($r_0 < R_g$) PGNPs, when the $N > P$, the homopolymer chain (from the matrix) can interpenetrate in-between the grafted polymer chains, which swells it and form the "wet-brush" regime. The "wet-brush" regime is favorable for miscibility/homogenization. However, if $N < P$, the free homopolymer chain can no

longer interpenetrate to the grafted polymer layer (due to the entropic energy penalty), the grafted polymer layer ended "expelling" all the free homopolymer "outside" and forming the dry brush regime. The 'dry-brush" regime causes the PGNPs to aggregate to themselves and phase separate from the homopolymer matrix.[62] Ferreira *et al.*[63] reported that the transition from "wet-brush" to "dry-brush" happens when $\sigma > P/N^{\frac{3}{2}}$. Trombly and Ganesan[64] investigated the influence of curvature (the size of the inner nanoparticle core) on the critical point of transition from "wet-brush" to "dry-brush" region. They found that increasing the curvature (decreasing the size of inner core) enhances the miscibility of PGNPs with the homopolymer matrix. These theoretical predictions of transition from miscibility to phase separation has also been experimentally validated. Bansal *et al.* [65] studied the influence of molecular mass of the polystyrene matrix on the phase behavior of densely grafted PS-SiO_2 (σ ~ 0.57 chains/nm^2, N = 1500, d_0 = 14 ± 4 nm). They found that the polymer film changes from miscible (well-mixed) state to the phase separation state when P/N > 0.7. Meli *et al.*[66] investigated the phase behavior of polystyrene gold nanoparticles (AuPS) in PS matrix. As P/N decreases below 1, the system tends to favor the miscibility, which is the same as predicted in the theory. However, for the very small PGNPs ($r_0 \approx h \approx 1 - 2$ nm), that rule (P/N > 1 for phase separation) cannot be applied anymore. Oh and Green[61] investigated the phase behavior of AuPS (d_0 = 5 nm, N = 10) immersed in the PS (P = 50) matrix. They found that the AuPS is still in the miscible state with the PS matrix (**Figure 2.10**) even when P/N = 5. They concluded that the transition from the miscible to phase separation is influence not only by P/N but also by the size of the PGNPs.

2.4.2 Phase Behavior of Sparsely Polymer-grafted Nanoparticles

As the grafting density decreases, the inner nanoparticle core can no longer be "blocked" from the grafted polymer layer. Because of that, the interaction from the inner nanoparticle core, along with the grafted polymer layer and the polymer matrix, contributes to the phase state of the polymer nanocomposite films. Jayaraman and Schweizer[67] studied the phase behavior of lightly grafted nanoparticles in polymer matrix using polymer reference interaction site model (PRISM). They found that both "tether-induced steric stabilization" and "matrix-induced depletion-like attraction" influences the phase behavior. Akcora *et al*.[68] experimentally investigated the phase behavior of sparsely grafted AuPS (σ = 0.05, 0.01, and 0.1 chains/nm^2) in the PS matrix (molecular mass M_g = 142 kg/mol).**Figure 2.11** shows the morphologies under TEM. With the ultralow grafting density and low molecular mass for the grafted chains (σ = 0.05, 0.01 chains/nm^2, M_g < 60 kg/mol), the PGNPs form clusters of nanoparticles (**a, b, d, e**). As the molecular mass increase over 100 kg/mol, the PGNPs form strings in the film (**c, f**). As the grafting increases to 0.1 chains/nm^2, the PGNPs with low molecular mass grafting layer form the "sheet-like" morphology (**g**). This kind of structure disappears as the molecular mass increases (**h, i**). This is very interesting as the PGNPs with isotropic structure forms anisotropic phase separation. Akcora *et al.*[68] claims that this is a combination effect of the enthalpic core-core attraction (since the grafting density is low) and the entropic distortion from the grafted polymer layer and the matrix. The similar phenomena has been reported in the block-copolymer system, which is referred to as "microphase separation".

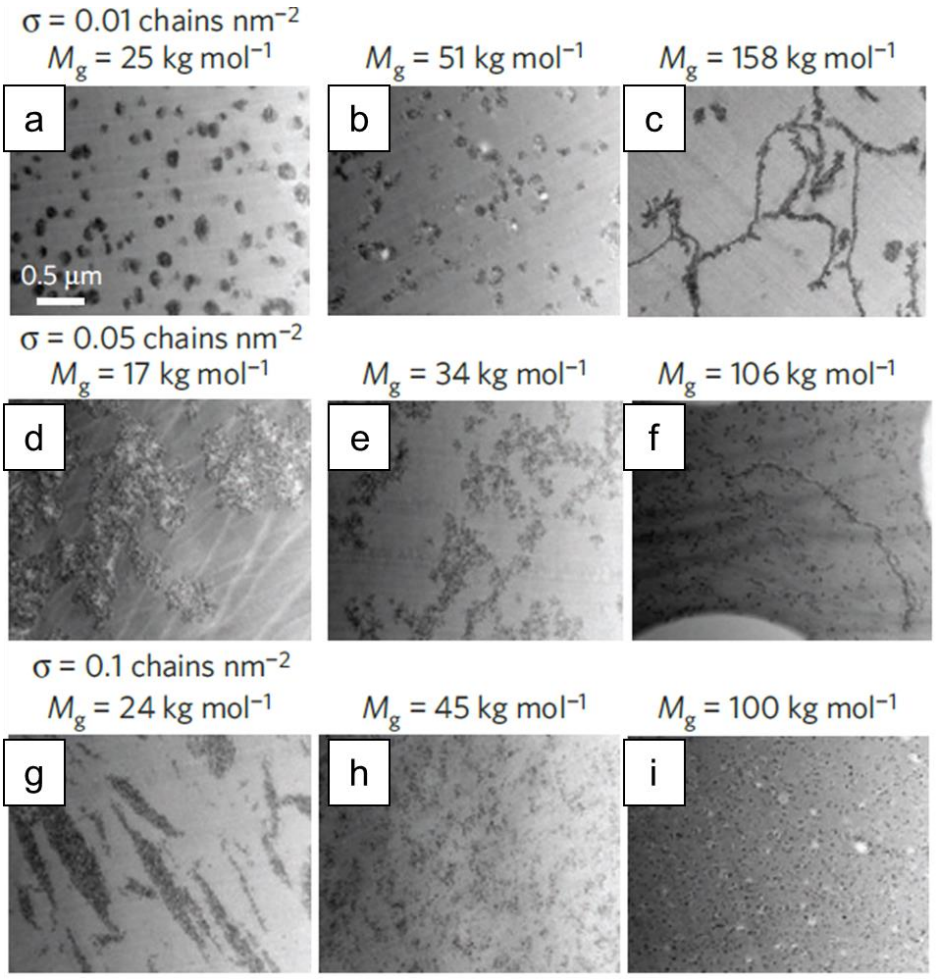

Figure 2.11 Phase morphologies of sparsely grafted PS-SiO_2 in PS matrix with various grafting density (σ) and molecular mass for the grafted polymer chains (M_g).[68] (Reproduced with permission from Reference 68).

2.4.3 Phase Diagrams for PGNPs/homopolymer Blends

Kumar and his coworkers[69] have summarized the morphologies/structures of PGNPs in homopolymer mixture to a phase diagram as shown in **Figure 2.12**. They conclude that the morphologies depends on σ, N, and the relative chain length ($1/\alpha = P/N$). When the product of σ and $N^{0.5}$ is low ($\sigma N^{0.5} < 2$), the morphologies changes from strings (S), to connected sheets (CS) and small clusters (SC) as N decreases. In the other hand, when the grafting density is high ($\sigma N^{0.5} > 2$), the PGNP/homopolymer

systems form either well-dispersion (WD) state or phase separation (PS) morphology determined by the value of *P*/*N*.

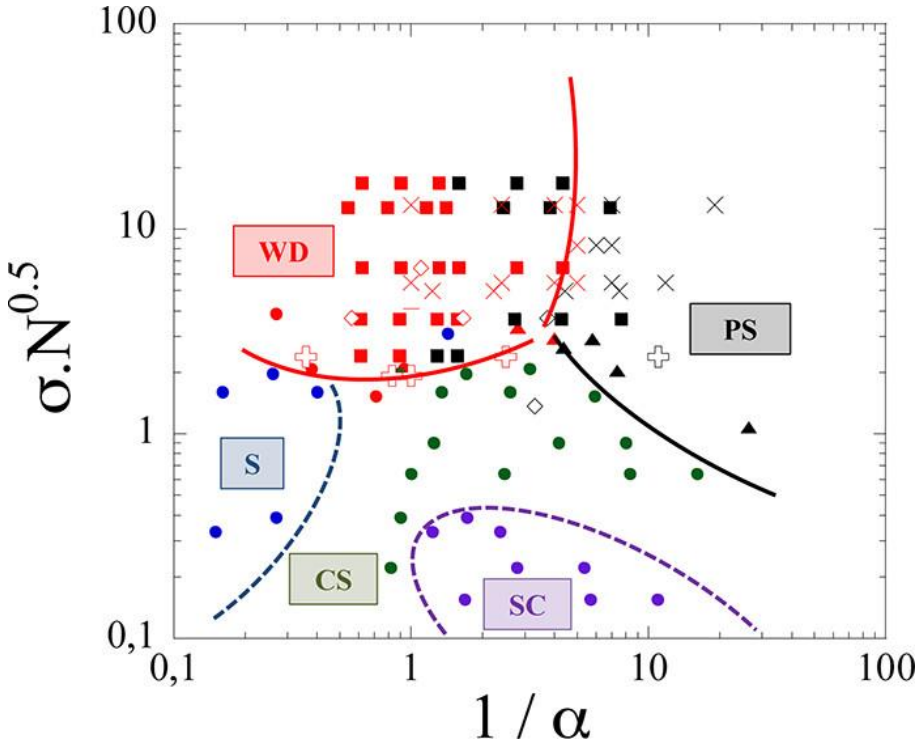

Figure 2.12. Summary of phase morphologies of PGNPs in chemical identical polymer matrix.[69] (Reproduced with permission from Reference 69).

2.4.4 Phase Behavior of PGNPs in Chemically Dissimilar Matrix

From the previous sections, we have discussed the phase behavior of PGNPs in chemically identical polymer matrix, where the entropic loss from the grafting polymer chain conformation is the vital factor governing the phase morphologies. In this section, we will cover the phase behavior of PGNPs in chemically dissimilar matrix, where the grafted polymer layer has different chemistry as the polymer matrix. The enthalpic interaction, a function of Flory-Huggins parameter χ, can no longer be neglected now. Borukhov and Leibler[62,70] theoretically investigated the phase behavior of this kind of system using the self-consistent field theory (SCFT). They quantified

the entropic for the matrix as related to $1/P$, while the enthalpic interaction as χP. This means that for the system with longer matrix polymer chains (large P), the enthalpic interaction dominates. However, for the system with smaller matrix polymer chains, the entropic force plays more important role. Due to the existence of enthalpic interaction, the PGNPs in the "dry-brush" region ($P > N$) can even well dispersed in the polymer matrix with the attractive interactions ($\chi < 0$). Martin *et al.*[71] investigated the phase behavior of deuterated polystyrene grafted silica nanoparticles (dPS-SiO_2) mixed in the poly(vinyl methyl ether) PVME matrix using X-ray scattering and neutron scattering. Due to the increasing "repulsive effective interactions" from the chemically dissimilar blends, the transition from the well-dispersed state to phase separation state is different than the "wetting-dewetting" transition from the chemically identical PGNPs/homopolymer system. Zhang *et al.*[21] studied the phase behavior of densely grafted polystyrene grafted gold nanoparticles (AuPS, σ = 0.7 chains/nm^2, $M_{n,PS}$ = 11.5 kg/mol, $r_{0,\text{gold}}$ = 1.21 nm) mixed in the poly(methyl methacrylate) (PMMA, $M_{n,PMMA}$ = 3.1 kg/mol) homopolymer matrix. **Figure 2.13.A** shows the transitions of morphologies as a function of mass ratio of AuPS to the PMMA matrix. As the value increase from 20% to 80%, it changes from the discrete domain to bicontinuous structure (50%), and in the end the inverse domain structure (80%), which is similar to the immiscible binary homopolymer mixtures. They also compared the phase separation kinetics of the AuPS/PMMA mixture to the corresponded PS/PMMA mixtures (**Figure 2.13.B** and **C**). They annealed the same system at two different temperatures: 140℃ and 180℃. The higher temperature provides more mobility for the polymers while introduces lower thermodynamic

driving force, which elucidates the role of thermodynamic driving force and mobility in the phase separation kinetics for both PGNPs/homopolymer and binary homopolymer blends. They fitted both plots to the power law, $q^*(t) \sim t^{-n}$, where q^* is the characteristic wavenumber, in the reverse relation to the interdomain spacing, and n is the exponent governed by different phase separation mechanism. When the films were annealed at 140℃, the AuPS/PMMA blends show three different n: 0.3 ± 0.02, 1.0 ± 0.01, and 0 (**Figure 2.13.B**). The first 0.3 region corresponds to the diffusive driven coarsening of bicontinuous structures, which can be explained by the Lifschitz-Slyozov (LS) law.[72] The second 1.0 region is caused by the hydrodynamic instability, while the last 0 region is induced by the pinning effect from due to the finite film thickness. However, for the parent PS/PMMA blends, only the hydrodynamic coarsening and the "pinning" region were shown, indicating faster kinetics compared to AuPS/PMMA blends. When the films were annealed at 180℃, a totally reverse trend between the AuPS/PMMA and the PS/PMMA blends was shown. For the AuPS/PMMA blends, it only shows the hydrodynamic coarsening and pinning mechanism. However, for the PS/PMMA, it showed all the three different mechanisms, including the diffusive driven coarsening region at the beginning. They concluded that the phase separation kinetics at this temperature is mainly caused by the diffusion instead of thermodynamic driving force.

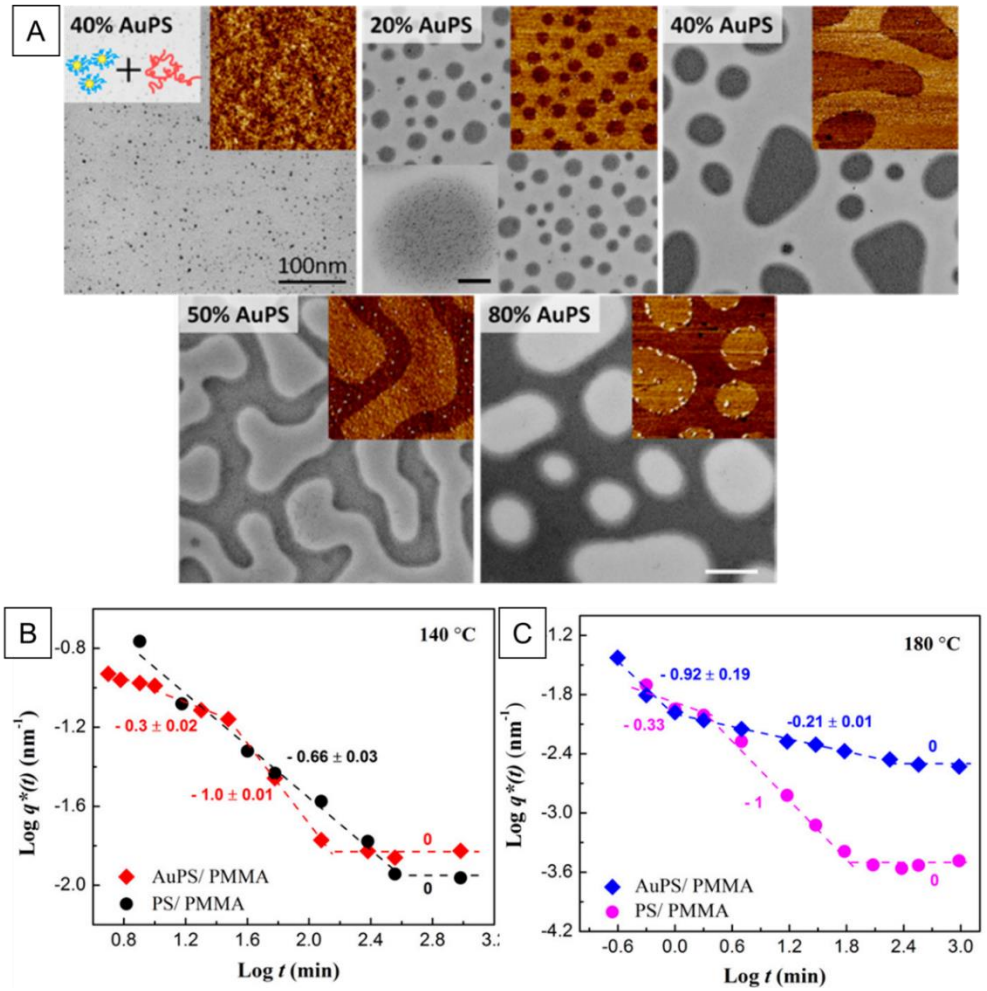

Figure 2.13 Phase behaviors of AuPS in PMMA homopolymer with different loading and comparison to the parent PS/PMMA homopolymer blends.[21] (Reproduced with permission from Reference 21).

2.5 Phase Behavior of Binary Polymer-grafted Nanoparticle Blends

The previous discussions are all focused on the phase behavior of PGNPs in homopolymer matrix. Will the phase behavior be different when the homopolymer matrix is replaced by another kind of PGNPs? Schmitt *et al.*[25] studied the phase behavior of PS-SiO_2/PMMA-SiO_2 ($r_{0,core}$ = 7.7 ± 2 nm, σ ≈ 0.5 chains/nm^2, N ≈ 350 for both PGNPs) blends. **Figure 2.14.I** shows the phase morphologies of this blend with variation of annealing temperature (140℃, 160℃, and 200℃) and volume ratio of

PMMA-SiO_2 (ϕ_{PMMA} = 0.25, 0.5 and 0.75). When the blend has less PMMA (ϕ_{PMMA} = 0.25), the PMMA-SiO_2 forms the discrete domains (dark color region in the AFM images, **A** and **B**). As the volume ratio increases to 0.5, it changes to the bicontinuous structures (**C** and **D**), driven by the spinodal decomposition. When the volume ratio increases to 0.75, inverse domain structures were formed (**E** and **F**). These variations of morphologies, induced by changing the annealing temperature and composition, indicates that the binary PMMA-SiO_2/PS-SiO_2 blends perform the same UCST phase behaviors as the related homopolymer blends and PGNP/homopolymer mixtures (**G**). Schmitt *et al.*[25] also investigated the influence of the $N_{PMMA\text{-}SiO2}$ and $N_{PS\text{-}SiO2}$ on the phase behaviors of the blends. With the smallest N (≈ 60 for both PGNPs), the system doesn't show any phase separation when it is heated at 140℃ (> T_g) for over 1 week (**Figure 2.14.II.A**). As N increases to around 200, the AFM phase image starts to show bicontinuous phase separation (**B**). When the N increases to around 350, the as cast film even showed the phase separation (inset in **C**), indicating the strong phase separating driving force even during the film casting.[25] This transition from the well-mixed state to the phase separation morphology with increasing N can be explained by the increasing enthalpic interaction potential (χN) between the two different PGNPs. As the discussion in **Section 2.3**, χN needs to be larger than a critical value (≈ 2 for symmetric binary homopolymer blends) to induce the phase separation. Although there is no theoretical or experimental discussion on the critical value for the binary PGNPs blends, it is reasonable to interpret that $N \approx 100$ is near the critical point. This transition of phase morphology also indicates the transition from more "hard-sphere-

like" properties for short chain PGNPs (in CPB region) to more "polymer like" behavior for longer chain PGNPs.

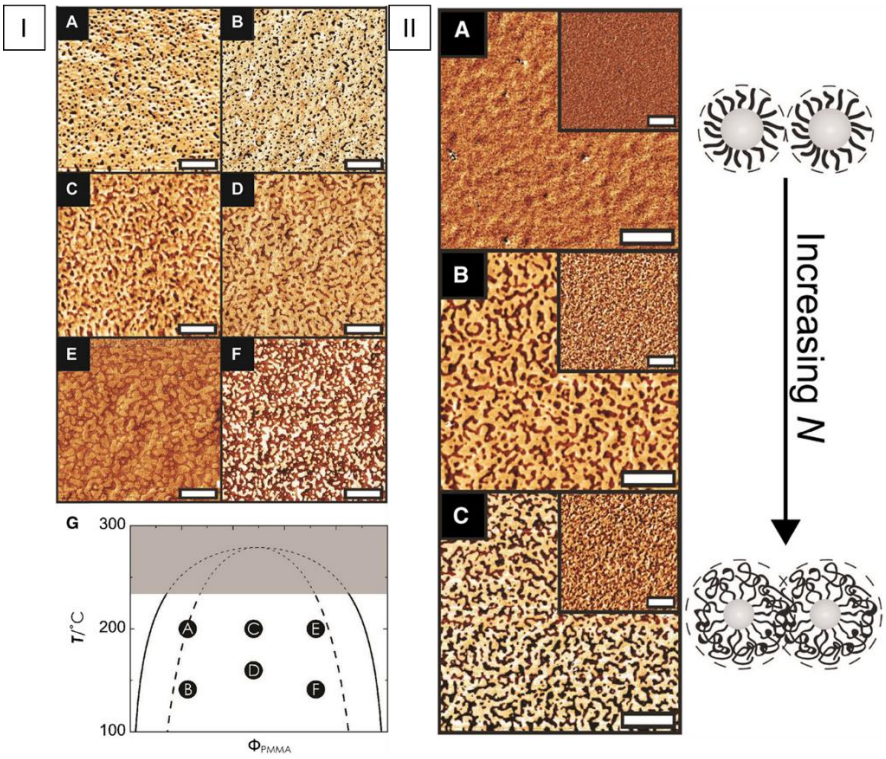

Figure 2.14 Phase behavior of binary PS-SiO_2/PMMA-SiO_2 blends indicating similar UCST phase behaviors as parent PS/PMMA homopolymer blends.[25] (Reproduced with permission from Reference 25).

Homopolymer blends or block copolymer films exhibiting LCST behavior can have reversible phase separation between the phase separation and well-mixed/homogenization by simply changing the annealing temperature (**Figure 2.15.A**).[73–75] This can be explained by the changing of interaction potential (χN) below and above the critical value (≈ 2 for symmetric binary homopolymer blends) since χ is related to annealing temperature. Can the similar reversible phase separation be achieved for a LCST PGNPs blends? Schmitt *et al.* studied the phase behavior of poly(styrene-r-acrylonitrile) grafted silica nanoparticles PSAN-SiO_2 and PMMA-SiO_2

blends. **Figure 2.15 (B-E)** shows the TEM images of PSAN-SiO_2/PMMA-SiO_2 blends annealed at different temperatures. When the film was annealed at 130℃ (< LCST ≈ 160℃), the TEM result shows a homogenous state (**B**). As the annealing temperature (T = 170℃) increases above LCST, the homogenous state changes to the phase separation state (**C**). When the same film was annealed back at the low temperature (*T* = 110℃), the phase changes back to the homogenous morphologies (**D, E**). The indicates that the binary PGNPs can also perform the similar reversible phase behaviors as other polymer blends.

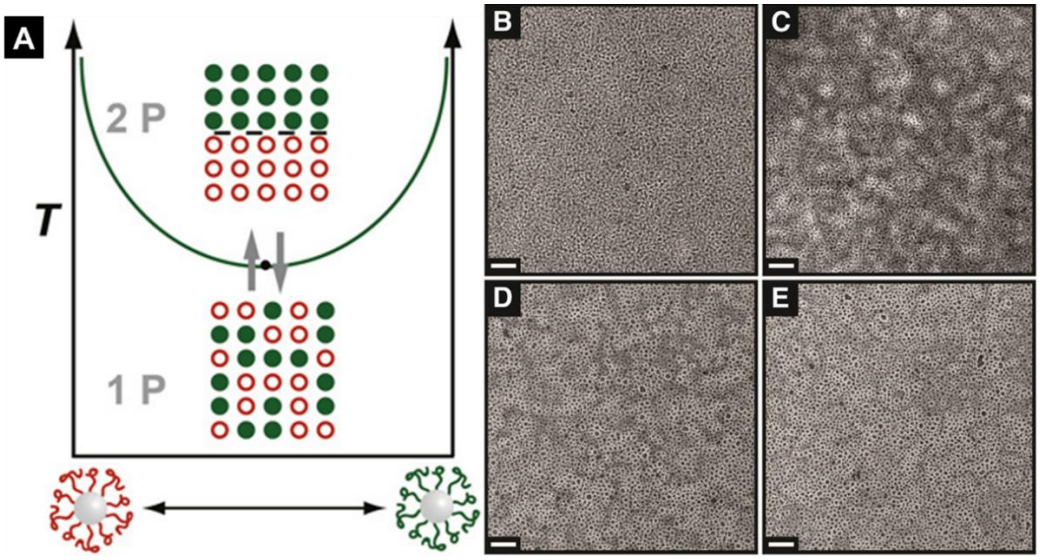

Figure 2.15 Reversible phase morphology alternation by changing the annealing temperature for PMMA-SiO_2/PSAN-SiO_2 blends.[25] (Reproduced with permission from Reference 25).

2.6 Controlled Organization of Nanoparticle Films

The controlled organization of the nanoparticles/PGNPs in the matrix (polymer nanocomposites) is the prerequisite for most of the applications, including biomedical, electronics, mechanical enhancement, optical detectors, and energy storage.[42,44,76–79] From the previous sections, we have discussed about the structures and phase

behaviors of polymer nanocomposites. In the following part, we will provide a brief overview about the state-of-art techniques in controlling the dispersions of polymer nanocomposite films. The methods can be categorized into two different directions: the "top-down" (external-in) and the "bottom-up" (internal-out) strategies.[80] Generally, the "top-down" method uses physical pattern or external fields to direct the nanoparticle dispersions. The "bottom-up" method alters the chemistry of the bottom substrates/templates and drives the organization of nanoparticles through mesophase assembly.

2.6.1 Controlled Nanoparticle Organization *via* External-in Method

Physical Pattern Induced Nanoparticle Organization. The physical pattern, with predefined structures like corrugations, holes, or trenches, can be used to guide the partitioning of bare nanoparticles or PGNPs. Mathur *et al*.[81] reported to use predefined corrugated silicon substrate to order the colloid PS spheres (d = 100 – 500 nm). They directly drop the solution of those PS spheres onto the corrugated substrate. During the drying process, those nanoparticles aggregate and form ordered structures in the lower region of the corrugated surfaces (**Figure 2.16 a-c**). Capillary interactions from the solution interface is the mainly driving force for the selective segregation of those PS nanoparticles. **Figure 2.16.d** is a cartoon illustrating the whole process, which can be divided into two processes. At first, the attracting capillary force makes the nanoparticles to aggregate and form the clusters. Then the ordering force becomes critical and moves the whole clusters to the "valley" or "trench" region of the corrugated surface.

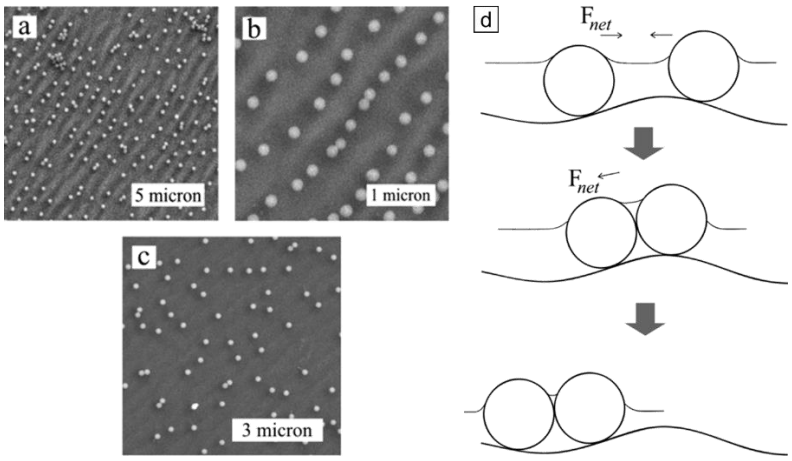

Figure 2.16 SEM images indicating the nanoparticles reside on substrates with large amplitude and explanation for the driving force for this selective segregation.[81] (Reproduced with the permission from Reference 81).

Zhang *et al.*[23] extend this ideal of using physical pattern to guide the ordering of PGNPs mixed in homopolymer matrix. Instead of making the substrate physically patterned, they applied the patterned elastomer to the film and use the capillary force to create the patterned polymer nanocomposite films. **Figure 2.17.A** shows their approach. Firstly, the AuPS ($r_{0,\,\text{core}} \approx 1.2$ nm, $\sigma \approx 0.7$ chains/nm^2, $M_{n,\,PS,\,grafted}$ = 11.5 kg/mol) was mixed with PS homopolymer ($M_{n,\,PS}$ = 3 kg/mol) to form a thin polymer film (thickness = 100 nm). Secondly, the PDMS with pattern transferred from commercial DVD (wavelength λ = 752 ± 6 nm, step height Δh = 119 ± 1 nm) was directly attached onto the film. Then the whole film with pattern on it was annealed above the glass transition temperature. As the wavelength is small, the capillary force in-between the patterned surface and polymer surface is large enough to drive the polymer film to fill into the empty space and form the patterned surface after topographic PDMS pattern was removed. They found that the PGNPs (black dots in the TEM images) in the more confined “trench” region (the region has lower height,

light color region in the TEM images) moved to the less confined "mesa" region (the region has higher height in the patterned polymer films, dark color "stripes" in **Figure 2.17.B**). They elucidated that the selective partitioning is driven by the entropy of the whole system, which can be easily varied by changing the initial film thickness (related to the "trench" height in the final patterned film) and the molecular mass of the homopolymer matrix (**Figure 2.17.B**).

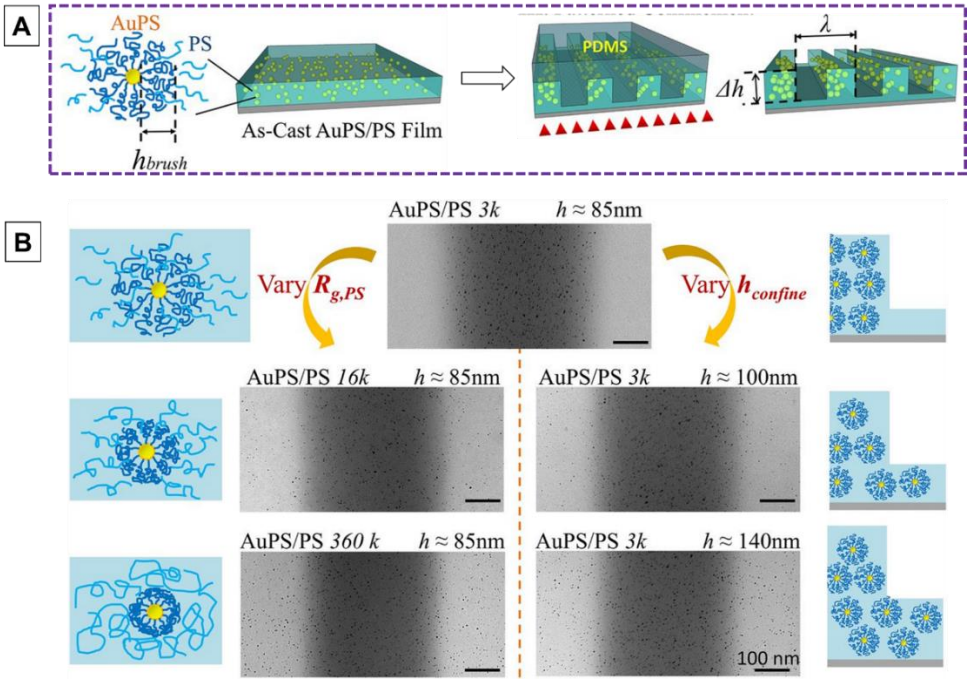

Figure 2.17 Schematic illustration of the topographic nanoimprint patterning induced selective segregation of PGNPs in homopolymer matrix.[23] (Reproduced with the permission from Reference 23).

Wang *et al.*[20] extended the same topographic patterning technique to a mixture of polystyrene grafted titanium nanoparticles (PS-TiO_2) and PS matrix. They found that the change of the entropy of the whole system by applying the topographic pattern can also induce the selective segregation of "clusters of PGNPs" to the less confined "mesa" region. Zhang *et al.* also investigated the influence of the topographic pattern

on the ordering of chemically dissimilar PGNPs/homopolymer system (AuPS/PMMA), where the enthalpic interaction between the grafted polymer layer and the polymer matrix cannot be neglected compared to the chemically identical system. As shown in **Figure 2.18**, the AuPS are also selectively segregated in the less confined "mesa" region. The difference (compared to the chemically identical system) is that all the AuPS bias near one side of the "trench" (**Figure 2.18.b**). They believed that it is due to the relatively unfavorable interaction between the AuPS and PDMS compared to the PMMA and PDMS. The differential interaction energy drives the AuPS to reside near the inner wall boundary of the "trench" region.[21]

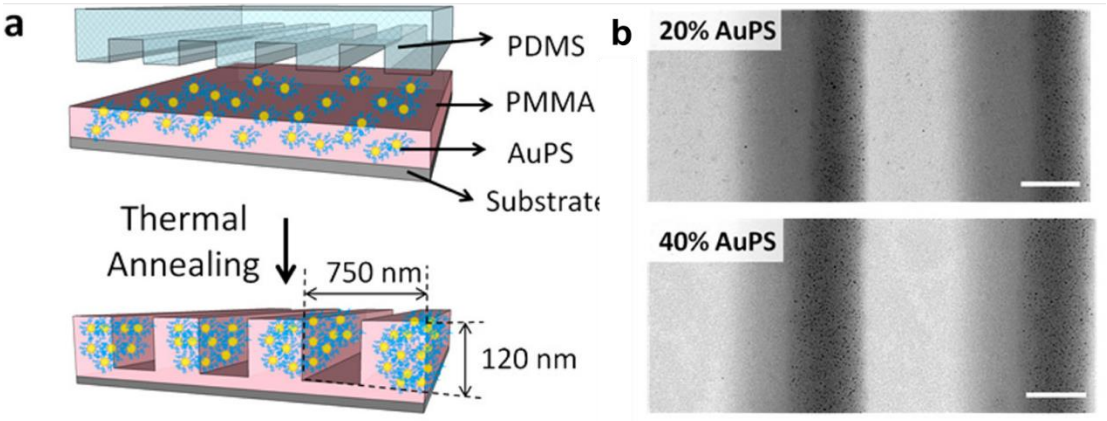

Figure 2.18 Schematic illustration of the topographic nanoimprint patterning induced selective segregation of PGNPs in chemically dissimilar homopolymer matrix.[21] **(**Reproduced with permission from Reference 21).

External Field Induced Controlled Organization of Nanoparticle Films. External fields, including the magnetic, electric, and shearing force, can be used to align the ordering of nanoparticles.[22,43,82–86] **Figure 2.19** shows some of the related findings. Yuan *et al.*[43] applied a magnetic field perpendicular to the flow coating direction of thin nanocomposite films (setup as shown in inset of **Figure 2.19.A**)

containing magnetic polymer grafted nanoparticles (MPGNPs). They found that those polystyrene end-grafted cobalt ferromagnetic nanoparticles have all been aligned along the direction of the magnetic field (**Figure 2.19.A**). Electric field can also be used to align the directions of nanoparticles. Gangwal *et al.*[83] applied low frequency alternating current (AC) electric fields on the Janus particles (**Figure 2.19.B**). As the electric field intensity is large enough to overcome the particle Brownian motion, the Janus particles form the aligned structures along the direction of the electric filed. The similar technique has been used to align both colloidal ellipsoids[84] (**Figure 2.19.C**) and two-dimensional crystals[86] (**Figure 2.19.D**).

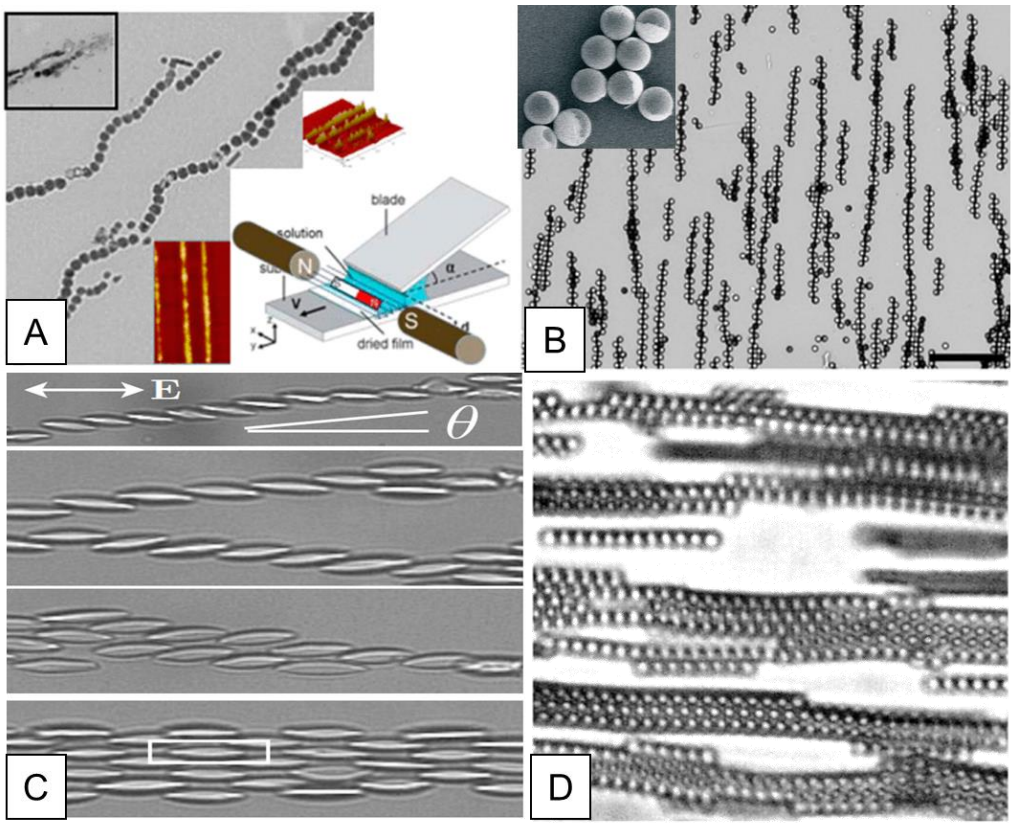

Figure 2.19 Magnetic field (**A**) and electric field induced alignment of nanoparticles (**B, C, D**). (Reproduced with permission from Reference 43, 83, 84, 86).[43,83,84,86]

Shear force can also be used to align the nanoparticles. Our group recently develop a facile method named dynamic zone annealing soft shearing (DZA-SS) to apply shearing force onto the polymer nanocomposites films and align the PGNPs.[22,82] The cartoon in **Figure 2.20** shows the schematic of the setup. The polymer nanocomposite film was directly casted onto the substrate (*e.g.* quartz). To generate the shear stress, a soft elastomer (*e.g.* PDMS) was attached onto the polymer film. The film (with the top elastomer) was then moved through the region with desired speed where two cold blocks "wrapped" around a hot wire. The sharp temperature gradient generated during this process (**Figure 2.20**) induce the strain stress, which is useful in aligning the PGNPs. Zhang *et al.*[22] studied the organization of AuPS ($R_{0,core}$ =1.21 ± 0.42 nm, σ = 0.7 chains/nm^2, M_n = 11.5 kg/mol) in PMMA (M_n = 3.1 kg/mol) using DZA-SS with different translation speed. As the translational speed increases from 1 μm/s to 60 μm/s, unidirectionally aligned PGNPs strings were formed in the finite confine nanocomposite film (**Figure 2.20**).

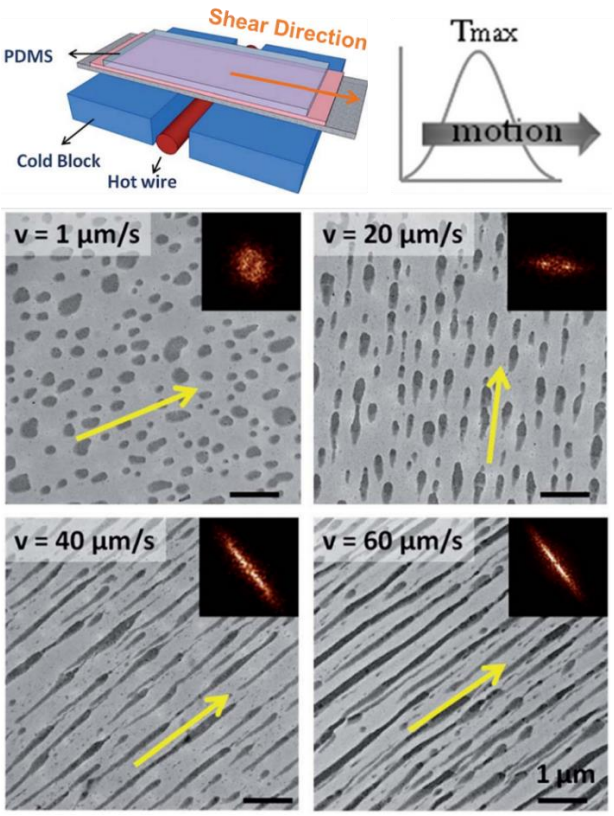

Figure 2.20 Schematic illustration about the DZA-SS process. TEM images show how the increased translational speed (*v*) align the ordering of PGNPs in polymer matrix.[22] (Reproduced with permission from Reference 22).

2.6.2 Controlled Nanoparticle Organization *via* Internal-out Method

Chemical Pattern Induced Nanoparticle Organization. Instead of the physical pattern, the enthalpic interaction between the nanoparticles and chemical patterned substrates can be manipulated for selective organization. In this section, we will cover two types of chemical patterns: blockcopolymer (BCP) and self-assembled monolayers (SAM).

Block copolymer is an ideal chemical pattern to guide the distribution of the nanoparticles. It has two chemically different polymer chain covalently bonded together. When the product of Flory-Huggins interaction parameter (χ) and the degree

of polymerization (N) is beyond 10.5, the block copolymer starts to "micro-phase separate". With the variation of the volume fraction of different blocks, the film can form different structures, including lamellae, cylinder, body-centered cubic spheres, and bicontinuous gyroid. Nanoparticles can then be added as a filler into those structures. With the variation of the chemistry of the grafted layer, grafting density, and the mass difference between the PGNPs and block copolymer chains, both the enthalpic and entropic interactions between the polymer brushes and the block copolymer microdomains can be tuned, which can lead to the selective ordering of the PGNPs within the block copolymer domains. Theoretically, both self-consistent filed theory (SCFT) and density functional theory (DFT) have been used to predict the behaviors of nanoparticles in the block copolymer matrix. For the large-sized nanoparticles, Thompson *et al.*[87] predicts that those nanoparticles will reside in the center of the block copolymer domain to compensate the loss in conformational entropy. For the smaller-sized nanoparticles, Huh *et al.*[88] predicts that the particles will cumulate at the interface between the block copolymer domain to maximize the translational entropy. Bockstaller *et al.*[89,90] experimentally investigated the phase behavior of aliphatic coated SiO_2 (SiO_2R_2, d_{core} = 21.5 ± 2.5 nm) and Au nanoparticles (AuR_1, d_{core} = 3.5 ± 1.0 nm) filled in the poly(styrene-b-ethylene propylene) (PS-PEP) copolymer ($d_{PS\text{-}domain}$ = 100, $d_{PEP\text{-}domain}$ = 80). **Figure 2.21** are the top-view TEM images indicating the distributions of AuR_1 and SiO_2R_2. The larger sized SiO_2R_2 segregates within the PEP domain, while the smaller sized AuR_1 resides at the interface of PS and PEP. This result is consistent with the theoretical predictions.

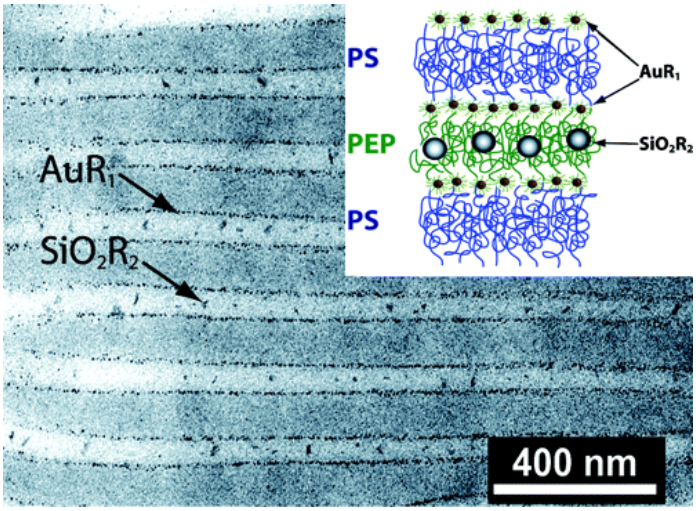

Figure 2.21 TEM images indicating the distribution of aliphatic grafted Au and SiO_2 in the lamellae PS-PEP copolymer domains as a function of particle size.[90] (Reproduced with the permission from Reference 90).

Jang *et al.*[91] revealed that the spatial distribution of PGNPs in block copolymer can be easily varied by changing the enthalpic interaction of the system. They synthesized the amphiphilic gold nanoparticles (AuNP) and grafted hydroxylated polyisoprene (PIOH) near the Au core and polystyrene shell (PS) near the outside and mixed it with poly(styrene-b-2-vinylpyridine) (PS-b-P2VP) copolymer. By varying the number of hydroxyl groups per chain (N_{OH}), degree of polymerization for PS (N_{PS}), and the grafting density ($\sum$), the distribution of AuNP can be switched from either PS or P2VP domain or at the interface of PS/P2VP (**Figure 2.22**). They elucidated that the variation of the distribution is due to the total enthalpic energy balance from hydrogen-bonding formation, the adsorption of P2VP chains on gold nanoparticles, and the enthalpic penalty of mixing PS to P2VP.[91]

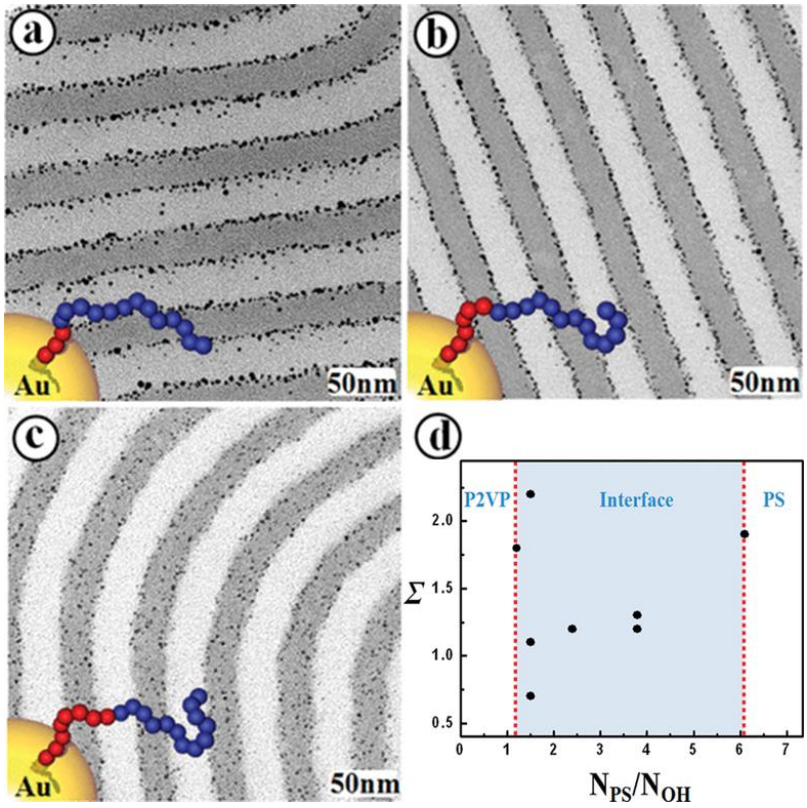

Figure 2.22 Tunning the distributions of AuNP *via* the variation of the hydrodynamic interactions between the NP and the copolymer domain.[91](Reproduced with the permission from Reference 91).

Another important method to order the nanoparticles is through changing the electrostatic interactions. One of the common ways is using the self-assembled monolayers (SAM). Nepal *et al.*[92] revealed that the orientation of the gold nanorods (AuNR), which is functionalized by grafting either mercaptopropane sulfonate (MS) or poly(ethylene glycol) (PEG), can be tunned by the width of the PS-P2VP pattern (**Figure 2.23**). When the width of P2VP pattern is comparable to the length of the AuNR, the nanorods can form either parallel or perpendicular orientations to the direction of P2VP pattern. This orientation is due to the electrostatic and hydrophobic selectivity to the substrate.

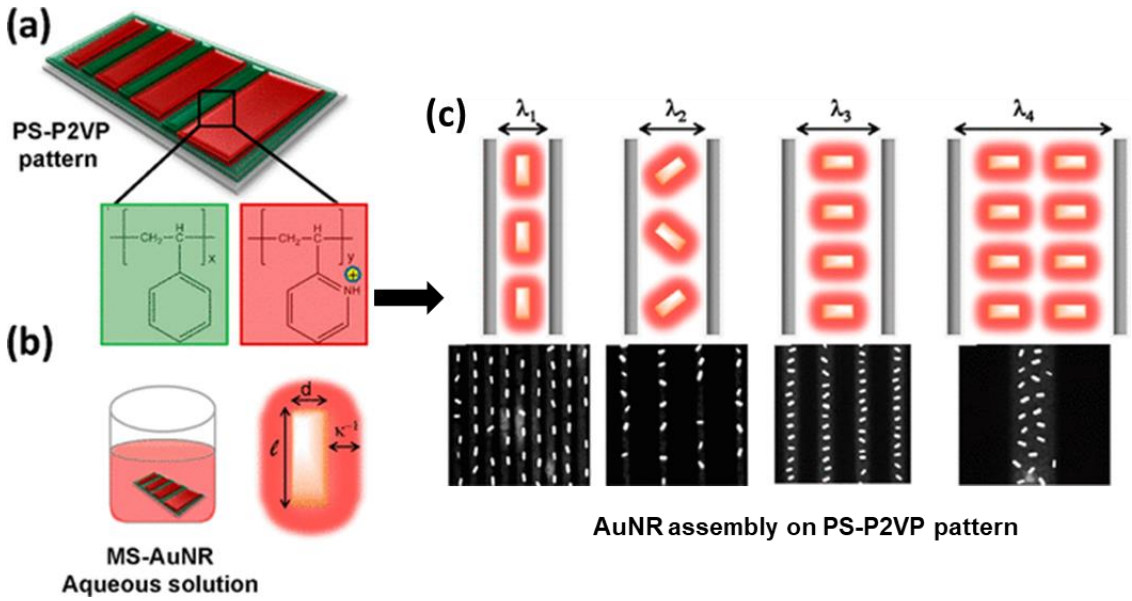

Figure 2.23 Control the orientation of AuNR vis the variation of pattern size.[92] (Reproduced with permission from Reference 92).

III. CONTROL OF THE PHASE MORPHOLOGY OF BINARY POLYMER GRAFTED NANOPARTICLE BLEND FILMS VIA DIRECT IMMERSION ANNEALING

3.1 Introduction

Polymer-grafted nanoparticles (PGNPs) have attracted significant attention in the past few decades as the physical properties can be modified from both the inner nanoparticle component and the outer polymer brushes.[1-11] Tsukruk *et al*.'s review illustrates the great potential of designing responsive colloidal systems from PGNPs.[97] Recent advances in synthesis have allowed for better control of grafting density, length, polymer and inorganic core compositions, and inner core sizes.[15,36,38,39,41,98,99] Theoretical studies have characterized the nature of the grafted polymer layers and their essentially equivalent many arm star polymers both in solution[100] and in the melt,[101] and these works have summarized highly relevant experimental observations about this type of nanoparticle in solution and in the melt state. Choi *et al*. have shown that by changing the grafting density of PGNPs, system properties can be altered between 'hard-sphere like' and 'star-polymer like' behaviors.[12] They also discovered that PGNPs could exhibit polymer-like crazing behavior with enhanced elastic and mechanical properties when the outer brush is in the semi-dilute polymer brush (SDPB) region,[4] creating opportunities for making hybrid nanomaterials. However, the field is currently dominated by polymer nanocomposite (PNC) materials due to their numerous envisioned applications that require a high concentration of inorganic nanoparticles and nanomaterials dispersed within a polymer matrix in a controlled manner. Therefore, research focused on pure PGNPs blend nanocomposites (PGNPs-

NC) is promised to hold much potential for developing nanocomposite materials with properties due to the high degree of dispersion of nanomaterials in a blend material with controlled macrophase-separation.

Recent work has shown that the phase separation morphology and the phase separation process of PGNPs in homopolymer matrix or pure PGNPs blends are similar in many ways to ordinary homopolymer blends so that the extensive methods and results for polymer blends can, to a large extent, be carried over to PGNPs blends and blends of PGNPs with polymers. Our work below qualitatively confirms this established pattern of behavior, but with quantitative differences of the phase separation kinetics. At the same time, we address the problem of processing PGNPs blends having high molecular mass grafted polymer layers whose thickness is comparable to the inorganic core of the PGNPs. Such materials inherently exhibit relatively sluggish phase separation dynamics, a behavior that can be undesirable in utilizing these materials in applications. We overcome these challenges using a solvent processing method that allows for tuning of both the solution viscosity and the thermodynamic driving force of phase separation of the PGNPs blends through the control of solvent additive.

Pioneering work by Kumar *et al*. [69] established that phase separation behavior in PNCs depends on the degree of polymerization of both the polymer matrix (P) and PGNPs (N) and the grafting density of PGNPs (σ). PGNPs with high grafting density and long-grafted chain length reside either in the phase-separated (PS) or well-dispersed (WD) state. However, PGNPs with a relatively lower grafting density and

short grafted chain length form a range of structures in the polymer matrix, including strings (S), connected sheets (CS), and small clusters (SC), due to the interplay of core-core attractions and brush-matrix interactions. Harton and Kumar *et al*. studied the high grafting density of PGNPs to show that the dispersion of nanoparticles in the polymer matrix is improved as the tangential spreading of brushes can alleviate the packing frustration.[102] Kumar *et al*. [68]and Karim *et al*.[20] also found that the chemistry of the inner core can also influence the dispersion of the PGNPs. For example, polystyrene grafted gold nanoparticles can be well-dispersed into the polystyrene matrix, while the polystyrene grafted TiO_2 nanoparticles can form large-scaled self-assembled morphologies. Dadmun *et al.* showed that the diffusion kinetics depends on the softness of the polymer brushes.[103] Zhang *et al.*[21] found that the phase separation process of the PGNPs in the homopolymer matrix is similar to ordinary homopolymer mixtures,[104] which shows a comparable coarsening exponent ($\approx$ 1/3 due to diffusive pattern growth and a late stage exponent near 1 caused by hydrodynamic instability). They also used polydimethylsiloxane (PDMS) as a soft pattern to guide the alignment of PGNPs. [21,23] The authors explained that the entropic forces created by applying the PDMS on the polymer nanocomposites could help guide the PGNPs into well-defined aligned nanostructures.[23] Wang *et al*. [20] extended this research into a directed assembly of 'clusters of PGNPs' (PGNPCs) and revealed their entropic localization within topographic printed patterns. Bhaduriya *et al*. [8,9] showed that the addition of PGNPs could also enhance the thermal stability of the nanoimprinted polymer films above the glass temperature of the nanocomposite.

Bocktsaller *et al*.[25] have extended the study to two chemically different PGNPs without any homopolymer matrix. Again it was found that these blends exhibited 'garden variety' phase separation in terms of morphology, although it was found that the coarsening kinetics of phase separation showed a reduced scaling exponent in these novel blends. This change in the coarsening kinetics of PGNP films made by spin casting was found to be robust to many samples, and we find a similar alteration below in our more complex DIA processing methodology. Notably, this change of coarsening exponent is not observed in polymer blends[60,105] and in blends of nanoparticles with a polymer matrix.[21] There would appear to be some special attribute of the PGNPs fluids that give rise to a qualitative change in the kinetics of the phase separation coarsening dynamics, but the general morphology and thermodynamic aspects of these blends otherwise appear to be perfectly 'normal'. Of course, the location of the critical temperature, critical composition, and mass dependence of the phase boundaries seem to be greatly altered in general by the chain grafting constraint, leading to the difference of the correlation length, initial phase separation scale, *etc*., in the PGNPs blends. Little theory currently exists to enable this variability of phase behavior in this type of 'blend' with PGNP structure, but we may qualitatively understand some patterns of this phase behavior from established empirical observations on ordinary polymer blends and extensions of the Flory-Huggins model to account for differences of monomer structure[106] and for the effect of polymer rigidity.[107] Even for ordinary blends, however, there is no validated quantitative theory for predicting the phase behavior of blends, and the prediction of blends of PGNPs phase behavior is a significantly more complex problem. Yatsyshin

et al. have recently attempted to address this problem computationally through coarse-grained polymer simulations.[108] The relatively sluggish dynamics of these blends and the general propensity to phase separate, common to most ordinary high molecular mass polymer blends, lead to technical difficulties in creating blend materials of desired particle organization. We address this issue using a method in which the polymer films are immersed in solvents having a composition that enables the manipulation of the film's glassy dynamics and the overall miscibility of the PGNPs.

In the present work, we focus on developing an efficient and reliable method to achieve reversible phase separation of polystyrene grafted silica (PS-SiO_2) and poly (methyl methacrylate) grafted silica (PMMA-SiO_2) blends. In this system, the relatively large PGNP size and mass of each particle brush, coupled with the weak temperature dependence of the Flory-Huggins interaction parameter, makes it challenging to achieve reversible and controllable phase separation by thermal annealing. Large PGNPs (59 nm and 128 nm hydrodynamic diameter in diluted THF solution in this study) can have higher intrinsic mechanical properties compared to the smaller nanoscale (< 20 nm to 30 nm diameter) PGNPs for more durability, but their sluggish thermal behavior prevents fundamental studies of interdiffusion and phase separation in the melt state. To overcome these issues, we apply a solvent-assisted annealing method termed direct immersion annealing (DIA) to help control PGNPs blend morphologies. DIA is a facile solvent annealing technique that was developed recently to investigate rapid phase separation in block copolymer films[109–111] and has shown comparable phase separation and self-assembly kinetics to the fastest block copolymer self-assembly techniques.[38–46] Unlike the traditional solvent vapor

annealing (SVA), DIA involves direct immersion of the binary PGNPs blend films into a tunable mixture of solvents to control the effective solvent quality, including a significant non-solvent fraction to prevent the dissolution of either PGNPs into solution. To our knowledge, a controlled phase-separation study of a binary PGNPs blend, including tests of reversibility from 2-phase to 1-phase state and progression in-between using direct immersion annealing, has not been previously reported. The situation is even more interesting because the brush can incorporate a different solvent mixture composition compared to the bulk reservoir composition by virtue of preferential wetting/solvation effects, which is known to occur in polymer brushes.[54,121–125] This can accentuate (enhance or diminish) its ability to phase separate from another PGNP polymer type that can concentrate a different solvent from the immersion mixture. In the physical chemistry literature, this rather general 'rule of thumb' for miscibility trends in multi-component solvents is termed Timmerman's rule.[126] The swelling of the PGNPs by a solvent can also modulate the interactions between the PGNPs, and impact the scale of phase separation in binary PGNPs systems, in ways hitherto not investigated in the literature, such as pinning of domain size and unconventional phase-separation kinetics, as reported in our present study.

We summarize some of the new results of the present chapter: 1) thermodynamically reversible single and two phase-separated states in a binary mixture of polymer grafted nanoparticles (PGNPs), 2) DIA driven mobility of large PGNPs not possible by thermal melt annealing, 3) complete tunability of degree of phase separation with solvent mixture quality and establishment of solvent compositional phase separation boundary, 4) the observation of unconventional phase

separation kinetics with a coarsening exponents consistent of a material with suppressed hydrodynamic interactions, 5) empirical control of the ultimate pinning scales of both the in-plane and out of plane scales of the phase-separated film through the control of the cast film thickness and choice of DIA solvent composition, and 6) relatively rapid phase separation which makes the method practically attractive for manufacturing applications, given their ability to form tough materials, especially with a large brush and core-size in this study.[12]

3.2 Experimental design

In this chapter, we investigated the phase behaviors of binary PGNPs blends casted on silicon wafer. We studied the influence of DIA annealing solvent on the morphologies of the dried films. Below is the detailed information about the materials we used and the experimental procedures.

3.2.1 Materials

The materials used in this study are binary mixture of polystyrene grafted nanoparticles (denoted as PS-SiO_2) and polymethyl methacrylate grafted silica nanoparticles (denoted as PMMA-SiO_2). Both of the PGNPs were synthesized using a surface-initiated ATRP method. They were prepared by our collaborators: Dr. Michael Bockstaller's and Dr. Krzysztof Matyjaszewski's group at Carnegie Mellon University. The average silica core size is $r_0 = 7.7 \pm 0.5$. The molecular mass for each grafted PS chain is M_n = 6.53 x 10^4 g/mol, and the grafted density of PS-SiO_2 is σ = 0.52 chains/nm^2. The molecular mass for each grafted PMMA chain is M_n = 3.50 x 10^4 g/mol, and the grafted density of PMMA-SiO_2 is σ = 0.57 chains/nm^2. The solution

used for both PGNPs dissolution (toluene) and preparing DIA mixtures (acetone, heptane, toluene) were purchased from VWR Inc.

3.2.2 Film preparation

Both PMMA-SiO_2 and PS-SiO_2 were dissolved in toluene (30 mg/mol) and sonicated in the water bath to ensure it is well dissolved in the solution. The polymer brushes were then mixed in the desired ratio and sonicated in the bath again to mix well. The samples were then flow coated on the bare silicon wafers that have been cleaned under the ultraviolet generated ozone (UV ozone) for 2 h. The casted films were then put into the vacuum oven and dried at room temperature overnight. The film thickness was measured by an interferometer (F3UV) using the Film metrics LSDT2 system.

3.2.3 Direct immersion annealing (DIA)

The samples were directly put into the DIA solution and caped to avoid the evaporation of the solvent into the air. After annealing the samples for the desired time, the samples were then dried by blowing air on them to avoid the influence of different evaporation rates of different solvents.

3.2.4 Characterization of polymer films

Blends of PGNPs are characterized by the atomic force microscope (Dimension Icon, Bruker) under tapping mode. Both surface topography and phase images are acquired from it.

Neutron reflectivity was conducted on the NG7 beamline at the National Institute of Standards and Technology Center for Neutron Research (NIST-NCNR).

The collimated neutron beam's wavelength is fixed at 4.76 Å, and the divergence was kept at 0.18 Å. The data were reduced and fitted using Ref1D and Reductus programs.[127]

Ultra-small angle neutron scattering was conducted on the BT-5 beamline at the NIST-NCNR. The wavelength is fixed at 2.4 Å. The sample size is 3 cm by 3 cm. 10 to 20 pieces of 500 nm thick film (cast on silicon wafter) were stacked together to increase the scattering volume. The data was analyzed and fitted using Igor.

ToF-SIMS analysis was conducted at Rice University. Negative depth profiles were performed using a TOF-SIMS NCS instrument, which combines a TOF.SIMS5 instrument (ION-TOF GmbH, Münster, Germany) and an *in situ* Scanning Probe Microscope (NanoScan, Switzerland) at Shared Equipment Authority from Rice University. A bunched 30 keV Bi_3^+ ions (with a measured current of 0.1 pA) was used as a primary probe for analysis (scanned area 90 × 90 μm^2), and sputtering was performed using Cs^+ ions at 1 keV with a typical current around 75 nA, rastered area (400 µm × 400 µm). The beams were operated in non-interlaced mode, alternating 2 analysis frames and 1 sputtering cycle followed by a pause of 2 s for the charge compensation with an electron flood gun. An adjustment of the charge effects has been operated using a surface potential and the appropriate extraction bias. During the depth profiling, the cycle time was fixed to 90 µs (corresponding to m/z = 0 a.m.u to 737 mass range).

3.3 Results and Discussions

3.3.1 DIA induced Reversible Phase Separation of PGNP Binary Blends

We investigated the phase behavior in a binary mixture of relatively large core-dimensions of polymer grafted nanoparticles (PGNPs) using a solvent mixture immersion method termed direct immersion annealing (DIA). The PGNPs consist of PMMA-SiO_2 (number averaged relative molecular mass M_n = 3.50 x 10^4 g/mol, grafting density σ = 0.57 chains / nm^2) and PS-SiO_2 (M_n = 6 .53 x 10^4 g/mol, σ = 0.52 chains/nm^2), with the SiO_2 core radius of ($r_0 = 7.7 \pm 0.5$, where ± 0.5 is the standard deviation) nm, dissolved by mass ratios as documented below from pure toluene solution, and cast as 100 nm to 400 nm thick films using a flow coater. The films were then dried overnight at room temperature in a vacuum oven and characterized by AFM. The as-cast films show nominal in-plane phase separation, presumably occurring in the late-stage solvent drying process during flow coating. Due to the large dimensions of the PGNPs, thermal annealing of cast films in a vacuum oven at elevated temperatures of 180 ^oC for extended times (≈ 20 h) showed almost no change of film morphology (or correlation length) (**Figure 3.1**). Quantitative analysis from the 2D Fast Fourier Transform (FFT) analysis (inset of **Figure 3.1**) and 1D Power Spectrum for the as-cast PS-SiO_2/PMMA-SiO_2 blends (A2) and after thermally annealing at 180 °C for 20 h (B2) confirmed the no evolution from as-cast structure by thermal annealing in terms of scale of phase separation, except for a sharpening of compositional contrast. In other words, this system is not amenable to a study of phase separation (or other phenomena such as thermal interdiffusion) by thermal annealing at the temperature on the order of ≈ 100 ^oC above the glass transition temperature (T_g).

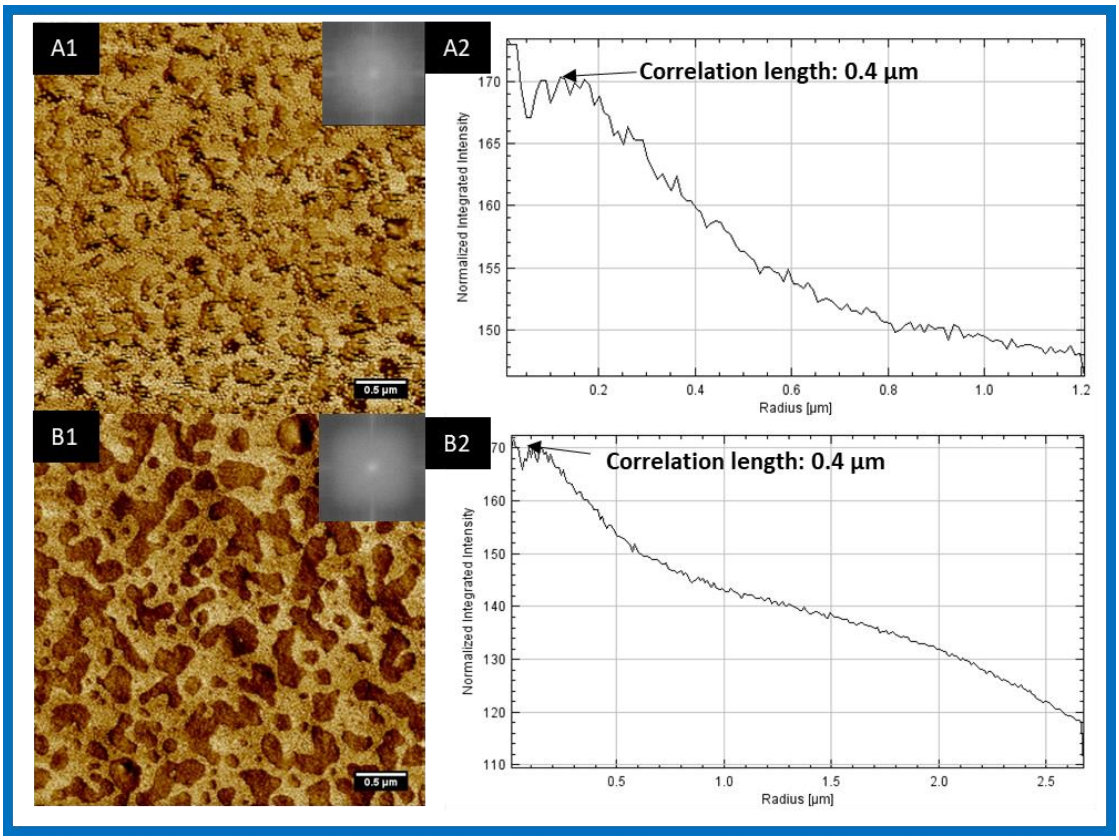

Figure 3.1. Atomic force microscopy (AFM) phase contrast images of as-cast (A) PS-SiO_2 and PMMA-SiO_2 blends and after thermally annealed at 180 °C for 20 h (B).

We are concerned about thermal degradation at temperatures much above that, therefore did not pursue that avenue. Instead, we examined DIA as a means of overcoming this kinetics problem. Notably, this also affects the thermodynamics of PGNP-brush/PGNP-brush interactions, because of solvent swelling of the brushes, with potentially differential internal solvent compositions by brush/solvent differential affinity. The precise nature of the internal solvent differential composition from the bulk solution will be the subject of another paper using small-angle neutron scattering and neutron reflection with deuterated solvent mixtures, but suffice to say, our past work on planar polymer brush in solvent mixture close to and far away from the

critical point of solvent/solvent phase separation demonstrates this effect clearly, *i.e.*, the brush can trap a solvent mixture composition significantly different from the bulk solvent mixture reservoir composition.[54,121] In the present case, the solvent mixture is fully miscible (1-phase) at all compositions.

Two distinct DIA solution mixtures were prepared to demonstrate the extrema of 2-phase and 1-phase behaviors of binary PGNPs blends, and the reversibility thereof between the two states. One solution (selective solvent mixture) consisted of a mixture of acetone and heptane in the ratio of 1:1 by volume fraction, wherein acetone is a more selective solvent for PMMA than PS, and heptane is the non-solvent for both PMMA and PS to suppress film dissolution.[110] The relative energy difference (RED) calculated from Hansen solubility parameter for PMMA in acetone is 0.6, while that for PS is 1.2,[128] noting that RED smaller than 1 indicates a good solvent while larger than 1 represents a poor solvent.[129] The other solution mixture (near neutral solvent mixture) contained toluene and heptane in the ratio of 1:1 in volume fraction, where toluene acts as a common good solvent for both PMMA and PS. The RED for PMMA in toluene is 0.9, while that for PS is 1.0.[128]

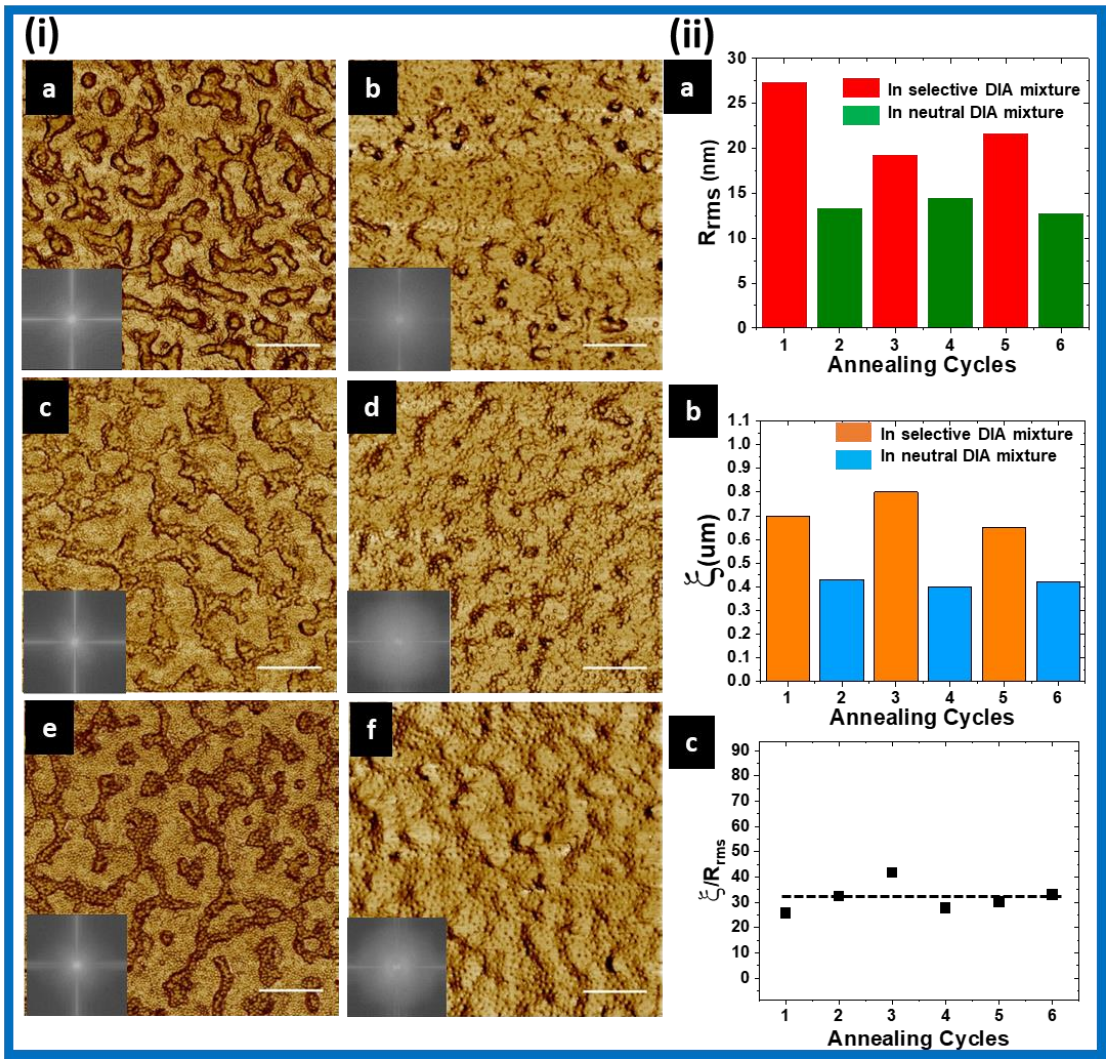

Figure 3.2 Illustration of reversible phase morphologies by using two different DIA mixtures. Scale bars in the AFM phase images correspond to 800 nm.

Figure 3.2 (i) shows the Atomic Force Microscopy (AFM) phase images of a PMMA-SiO_2/PS-SiO_2 film that was alternatively dipped and dried between the two different DIA solution mixtures for three cycles. The dark region in phase images corresponds to the PS-SiO_2 domains, while the light color area represents the PMMA-SiO_2 domains, confirmed by the increase of surface coverage of dark color region with the increase of mass ratio of PS-SiO_2 to PMMA-SiO_2 (**Figure 3.3**).

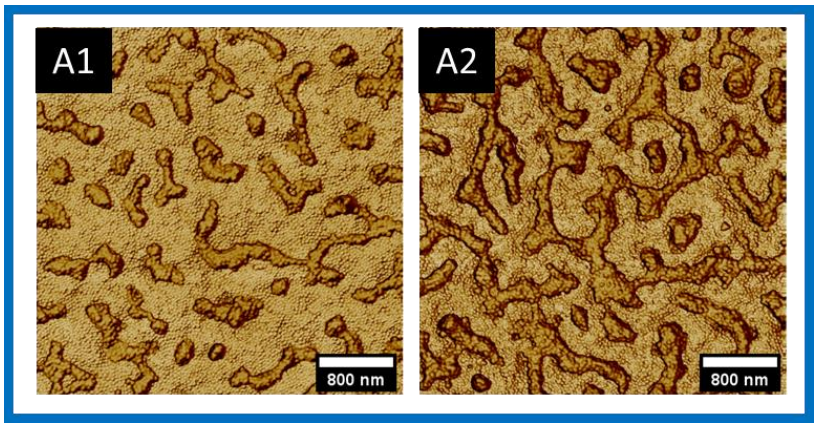

Figure 3.3 AFM phase images of 130 nm thick 1: 5 (mass ratio, A1) and 2: 5 (mass ratio, A2) PS-SiO_2/PMMA-SiO_2 blends annealed in acetone/heptane (1:1 by volume fraction) DIA mixture for 1 h.

Figure 3.2 (i) a,c,e shows dried phase-separated states where PMMA-SiO_2 rich and PS-SiO_2 rich domains are formed and re-formed by dipping the film (thickness = 100 nm) into the selective solvent mixture. In contrast, **Figure 3.2 (i) b,d,f** shows the reversal of phase-separated structures into near-homogeneous dried single-phase states by dipping the film into the neutral solvent mixture. We noted that surface segregation of PGNP components leads to some asymmetry near the surface and substrate interface in these near homogeneous structures, and there is still some minor residual phase-separated structure in the film interior, as shown later, resulting in shallow undulations of the film surface, as seen in **Figure 3.2**. Nonetheless, these figures indicate a high degree of rapid reversibility within 1 minute between phase separation (2-phase) and phase dissolution (1-phase) of the states over several DIA immersion alternating cycles, displaying quantitatively reproducible morphologies.

2D Fast Fourier Transform (FFT) images seen in the inset corresponding to the AFM images (in **Figure 3.2**) are used to characterize the systems' correlation length in

their respective states. For the more relevant phase-separated state, it corresponds roughly to the interdomain spacing between PS-SiO_2 and PMMA-SiO_2 domains, while for the quasi-homogenized phases, it is estimated from the remnant domain structures. The calculated correlation length from the 1D spectrum for each state is plotted in **Figure 3.2(ii). a.** It shows that for the 100 nm thick film, the correlation length stays at around 0.7 μm with a high intensity after the film is annealed in the selective solvent solution (acetone/heptane) for 1 min of DIA immersion time, in the pinning limit. In contrast, the correlation length decreases to 0.4 μm with relatively low intensity, similar to the as-cast film (**Figure 3.1**), after the film is annealed in the neutral solution mixture (toluene/heptane) for 1 min of DIA immersion time, following which there is no significant further homogenization. The root-mean-square surface roughness (R_{rms}) measurement from the AFM (**Figure 3.2 (ii).b**) indicates that the surface roughness is ≈ 20 nm of films annealed in the selective solvent mixture, which decreases to ≈ 13 nm when annealed in the neutral solvent mixture. Furthermore, the plateau value of aspect ratio (AR) of the phase-separated domains, defined by the ratio of in-plane correlation length to the out-of-plane R_{rms}, AR = ξ / R_{rms} ~ 35, is on the order of PS/PMMA surface tension to interfacial tension as a thermodynamic parameter. A previous study by Slawecki *et al.*[75] showed that in homopolymer thin film blend phase separation, the AR is given by a simple model: the ratio of polymer-polymer surface to interfacial tension. Our results show that the same kind of explanation can also be applied to the PGNPs blend system to predict the AR beyond the limit of initial time scales of evolution (≈ 1 min), as the AFM images of the domains do not evolve further if annealing is continued beyond the scale attained in 1

min. This kind of characteristic 'pinning' feature of phase separation domain size in binary PGNPs systems has also been observed in binary polymer blend ultrathin films.[104] However, the rapid kinetics of phase separation and dissolution behavior is distinctly different, as discussed in more detail.

3.3.2 One-phase and two-phase PGNP blend film morphologies

Since AFM is only a surface characterization technique, it cannot provide morphologies in the interior of the film. Neutron reflectivity (NR) is used to study the internal morphologies of the dried deuterated PMMA-SiO_2(dPMMA-SiO_2, M_n = 3.40 x 10^4 g/mol, σ = 0.76 chains/nm^2) and hydrogenated PS-SiO_2 (M_n = 6.53 x 10^4 g/mol, σ = 0.52 chains/nm^2) binary blends film, ordered in the 1-phase state under neutral solvent mixture. The NR experimental data (**Figure 3.4.a**) was fitted by a z-averaged depth model, whose structure is in strong agreement with the proposed 1-phase mixture (**Figure 3.4.c**). This structure includes a layer of PS brush near the airside and a layer of PMMA brush near the substrate interface due to the surface energy preference for each polymer type. The fitted scattering length density (SLD) *versus* depth plot (**Figure 3.4.b**) shows a PS-SiO_2 surface layer of around 30 nm thick. Beneath it is a homogeneous mixture of PS-SiO_2 and PMMA-SiO_2 with a thickness of about 60 nm, followed by a 20 nm thick PMMA-SiO_2 layer near the silicon substrate.

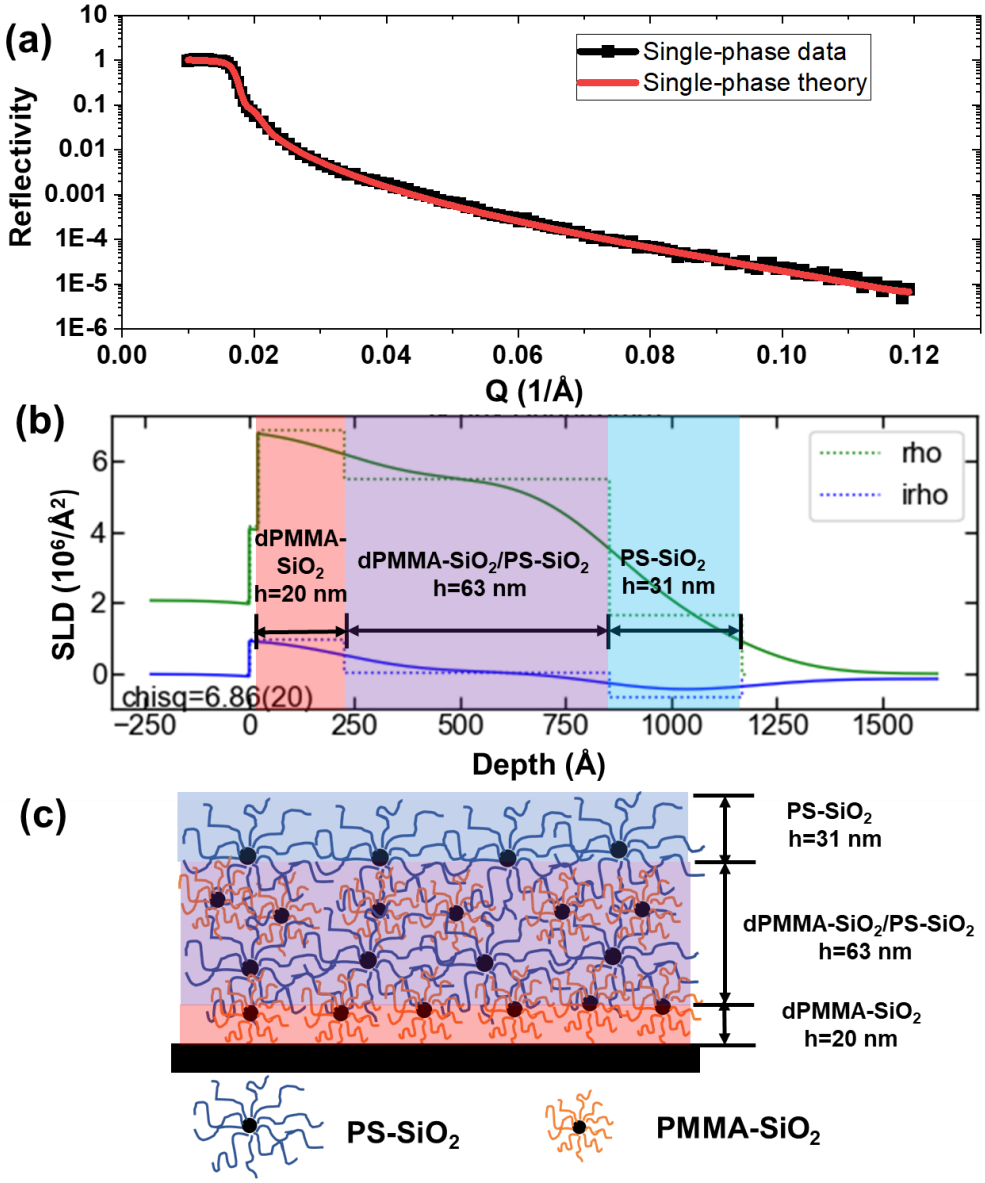

Figure 3.4. Neutron reflectivity data for dPMMA-SiO_2/PS-SiO_2 blends annealed in neutral good solvent (toluene/heptane) mixture for 1 min.

ToF-SIMS was also used to study the dried films' internal morphologies. It uses a cesium ion beam (Cs^+) as the sputtering source to etch the films and a pulsed bismuth ion beam (Bi_3^+) for collecting the mass spectrum through the depth. **Figure 3.5.a** shows the depth profile for both phase-separated (solid line) and homogeneous

state (dashed line). For the homogenenous material, our observations confirm our inferences from our NR measurement, albeit with a lower resolution, *i.e.*, a tri-layer structure exists due to the surface energy difference between the PS and PMMA blocks at the two boundaries. For the phase-separated profile, there are no significant z-depth fluctuations of either the PS and PMMA domains in the film, which indicates that the phase separation in-plane morphology is consistent throughout the film within the depth resolution of ToF-SIMS.

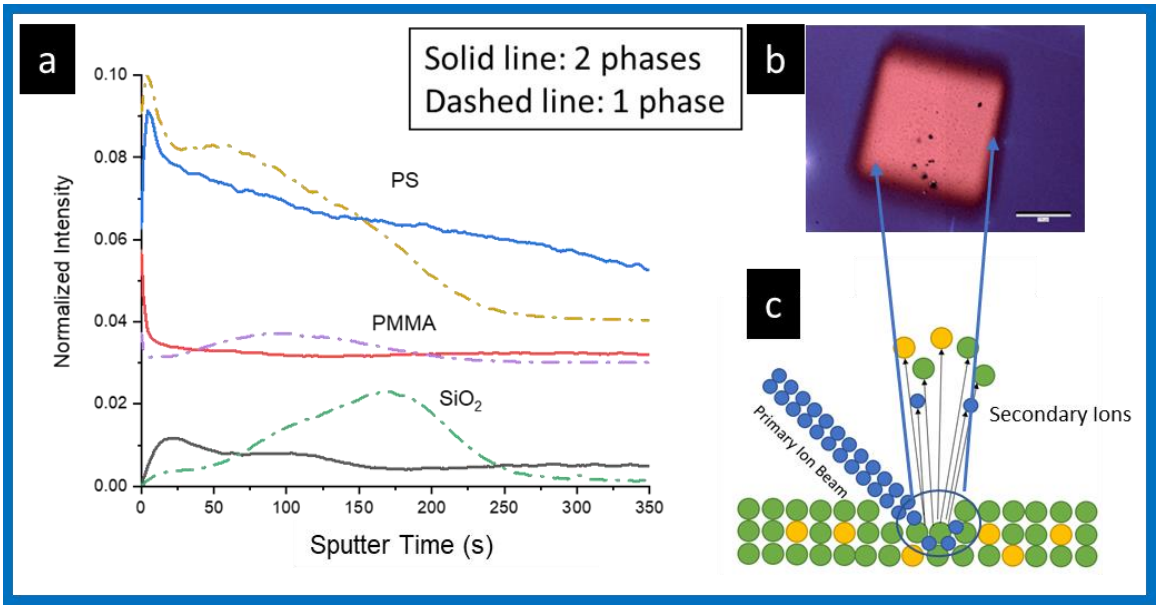

Figure 3.5. (**a**) ToF-SIMS in-depth profile for PMMA-SiO2/PS-SiO2 blends at different phases. (**b**) microscope images of the film after sputtering. (**c**) Schematic for ToF-SIMS analysis.

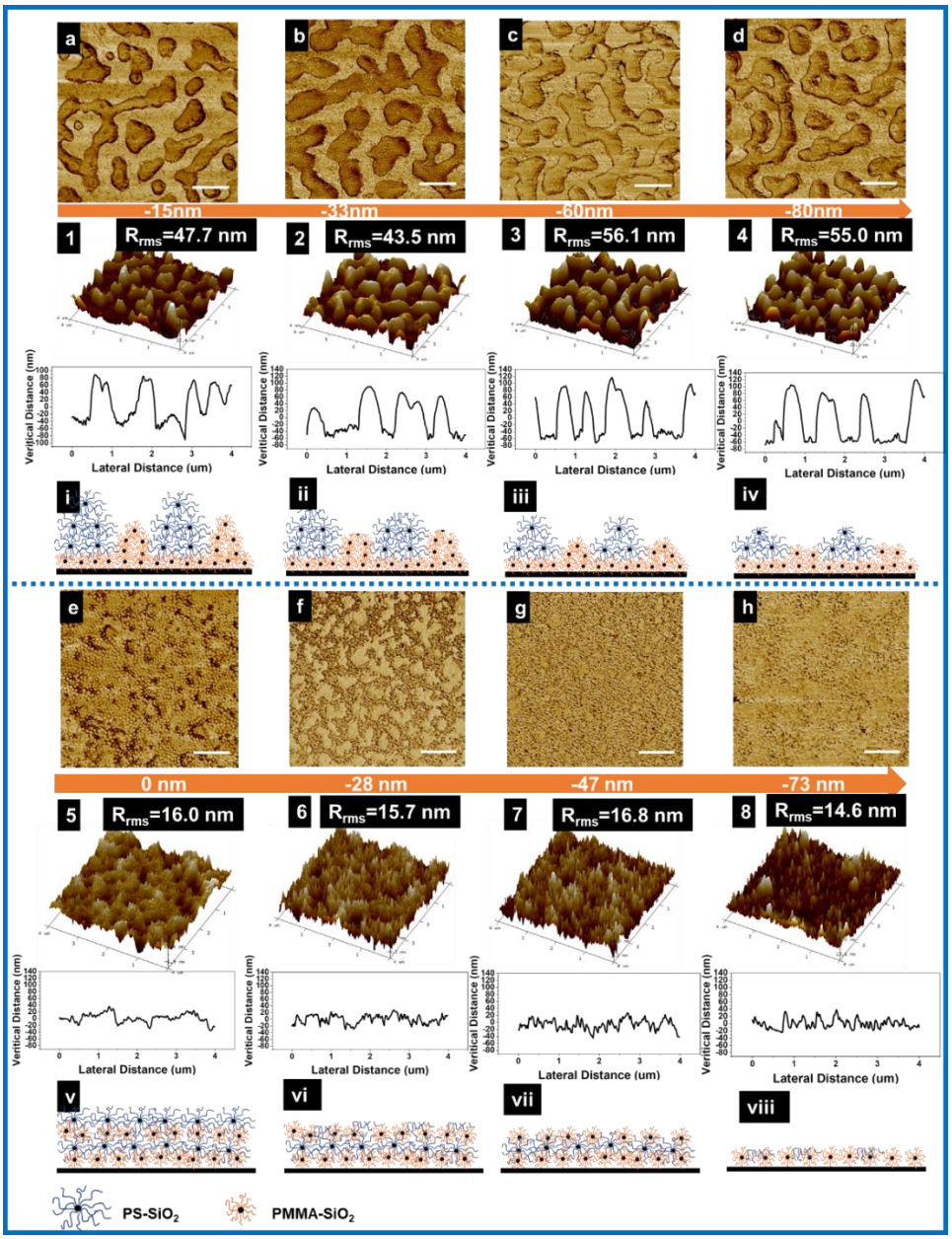

Figure 3.6 AFM phase and height images at different depths of the film for phase-separated and quasi-homogenized state. 0 nm indicates the surface. The scale bar is 800 nm.

The sputtering gun from ToF-SIMS has also been used to etch and reach specific surfaces at different depths of the phase-separated films, which can be applied to observe depth-dependent morphologies by AFM in the etched areas. This useful combination of ToF-SIMS and etching followed by AFM scan provides invaluable

information to characterize the morphologies at different in-depth locations. **Figure 3.6** shows the morphologies throughout the film depth using this combination technique for both 2-phase and 1-phase films.

Figure 3.6 a-d shows the surface morphologies of a ≈ 130 nm thick 2-phase film at different etched depths. The negative value indicates the distances from the surface. According to these figures, the phase images show phase separation morphologies, from the near-surface region (**a**, 15 nm) down to the substrate (**d**, 80 nm), with little variation of morphology or dimensions. Due to the etching process's apparent conformal nature, the surface height profiles are preserved in our observations through the etching process into the film. The corresponding height images (**1-4**) show a similar surface topography through the film, with the root-mean-squared surface roughness (R_{rms}) above 40 nm. The PS domains are the protruding phase. *In situ* AFM scan of the film immersed in the acetone/heptane shows an R_{rms} at around 28 nm, indicating the surface topography has already formed *in situ* during immersion in the selective solvent due to preferential solvent/PGNPs lower interfacial energy. During the drying process, this topography gets rapidly quenched and creates the surface roughness observed. It needs to be noted that the ToF-SIMS etching rate process may potentially have different sputtering yields for PS and PMMA, which leads to the increase of R_{rms} after etching (≈ 50 nm) in **Figure 3.6 1-4** compared to unetched films (≈ 30nm). Tanguy *et al.*[130] reports the ratio of the sputtering yield between PMMA and PS using Cs^+ at 250 eV is around 3, which means the PMMA gets etched out 3 times faster than the PS. Although the sputtering energy we use is

1keV, which decreases this difference. However, the sputtering yield ratio can never be 1, so the difference continues to induce roughening of the surface during the process. That's why we believe the increase of R_{rms} in **Figure 3.6 1-4** compared to the unetched films is due to this difference. Based on these pieces of information, a simple morphological model has been developed to describe the two-phase states of PGNPs blends (**i-iv**). The blue brush represents PS-SiO_2, while the orange brush corresponds to PMMA-SiO_2. **Figure 3.6 e-h** shows the in-depth phases when treated by the 1-phase inducing toluene/heptane composition. Based on the NR fitting profile (**Figure 3.3**), AFM, and ToF-SIMS images, it consists mainly of PS on the surface. After etching away 28 nm of the top film profile (**Figure 3.6 f**), the film shows some residual but well-distributed phase-separated structures containing both PS and PMMA. As the ion beam sputters more towards the substrate, the PMMA phase exceeds the PS phase, with the substrate surface almost entirely covered by PMMA-SiO_2, reflective of PMMA's well-known attractive interactions with the silica surface, and not affected much by its solvent swelling in the DIA mixture. The corresponded height images (**Figure 3.6 5-8**) indicate that the homogenized 1-phase state shows a minor variation in the surface roughness ≈ 16 nm for all images in **Figure 3.6 e-h**. This indicates that the overall structure induced from the 1-phase solvent mixture is a quasi-homogenized PGNPs blend state with surface segregation layers of PS-SiO_2 and PMMA-SiO_2 at air and substrate interfaces, and near homogeneous phase separation in the interior. Any incomplete homogenization is due to low mobility associated with the large size (> 50 nm dry, and even larger in DIA mixture) of the PGNPs, resulting in weak miscibility driving forces.

3.3.3 Thermodynamics analysis and reversible nature of the phase separation process

The free energy model developed by Flory[131] and Huggins[132] is known to describe the phase behavior of homopolymer melt blends, with the criteria $\chi N > 2$ for symmetric polymer blend phase separation to occur.[133,134] During the DIA process, we note that the effective interaction parameter, χ, varies in different DIA solutions. For polymers in selective solvents (or solvent mixtures with a preferential solvent for one PGNP brush polymer), Zeman *et al.*[135] found out that $\chi_{\text{polymer1-polymer2}}$ increases when $\chi_{\text{polymer1-solution}} \neq \chi_{\text{polymer2-solution}}$. Bank *et al.*[136] revealed that the same compatibility phenomena could persist after solvent removal from cast films, extending the compatibility phenomena to polymer films prepared from polymer solutions. Zeman[135] argued that the polymer-polymer interaction parameter is proportional to the square of the difference of two different polymer-solvent interaction parameters, which can be expressed as the following equation

$$\chi_{12} = \frac{(\chi_{1s}-\chi_{2s})^2}{(\delta_1+\delta_2-2\delta_s)^2}\frac{RT}{v}, \tag{3.1}$$

where χ_{ij} represents the Flory-Huggins interaction parameter between component *i* and *j*, δ is the Hansen solubility parameter, and 1,2 polymers while *s* indicates the solution. We adopt this simply semi-empirical approach to understanding miscibility in our PGNP blends. When polymer blends are 'annealed' in such a solution that is selective to one of the PGNP polymer blocks, χ_{12} increases and induces phase separation. Furthermore, the solvation of PGNP by the solvents provides intrinsic room

temperature mobility to the binary PGNP system to rearrange PGNP configurations to reflect the phase separation domain formation.

In contrast, when a neutral good solvent (or solvent mixture) is used, which can swell both polymers, the interaction between the polymer components is screened as a result of decreased interactions, to a first approximation, $\chi_{12,\,\mathrm{eff}} \approx (1 - \phi_{solvent})\,\chi_{12}$, where $\phi_{solvent}$ is the volume ratio of good solvent (for both polymers) in the DIA solvent mixtures, driving the blends to 1-phase state above a critical common good solvent composition. Although this applies to solvated homopolymer blends, it should qualitatively apply to solvated PGNPs blends as well, wherein the unfavorable brush-brush interactions are mediated by the neutral solvent.

As noted before, Timmerman's mixing rule allows for a natural rationalization of this phenomena.[126] We can treat the solvent in our DIA solution as 'additives' to the polymer films. The additive that is soluble to both components (good solvent for both polymer blocks) can help stabilize the film and make the film's phase homogeneous. In contrast, the additive that is more soluble to one of the components (selective solvent for certain blocks) will destabilize the system and cause phase separation.

3.3.4 Tunability of PGNP Interaction Parameter with Solvent Composition Control

So far, we have examined the interchangeability of extreme behaviors of the high degree of phase separation and homogeneous state. However, there is also much interest in the cross-over regime from 2-phase to 1-phase behavior. To systematically explore the tunability of χ and thereby phase morphology of PGNP blends *via* solvent

mixture composition changes in DIA, different amounts of neutral solvent (good solvent for PS and PMMA), *i.e.*, toluene, was added to a fixed volume ratio of acetone/heptane (1:2) DIA solution, to vary the $\chi_{\mathrm{PS-SiO_2/PMMA-SiO_2}}$. The mass ratio of PS-$SiO_2$/PMMA-$SiO_2$ in the film was kept at the same (2:5), and the film thickness around 100 nm, as before. **Figure 3.7. (i)** shows the phase images of these films annealed in the corresponding DIA composition after 1 min. With no toluene added into the DIA solution (acetone: heptane = 1:2 in volume ratio), the PS (dark color region) and the PMMA (light color region) PGNPs shows phase separation (**Figure 3.7.(i).a**). The surface coverage of PS-SiO_2 (dark color region) is calculated to be around 76 % (**Figure 3.7.(ii).a**), which also implies that PMMA-SiO_2 may have selectively segregated to the substrate due to preferential attraction of PMMA to the silica surface. When 3 % (by volume relative to the total volume) of toluene was added into the DIA solution (**Figure 3.7.(i).b**), the surface coverage of PS (dark color region) started to increase (**Figure 3.7.(ii).a**). Both the AFM phase images (**Figure 3.7.(i).a-e**) and calculated PS surface coverage values (**Figure 3.7.(ii).a**) show that more PS-SiO_2 is segregated to the surface as more toluene is added. When the toluene volume increases to 18.9 % (**Figure 3.7.(i).e**), the free surface is mostly covered with PS-SiO_2 (> 99 % **Figure 3.7.(ii).a**). **Figure 3.7.(i).f-g** (circled in red) shows the corresponding magnified AFM scans (1μm x 1μm) of the larger **Figure 3.7.(i).a-e** (4 μm x 4 μm) AFM images. With no added toluene to the DIA solution, both the inter-domain boundary between PS-SiO_2 and PMMA-SiO_2 grains, as well as the intra-domain (particle-particle PGNP boundary), is very apparent. However, the intra-domain boundary, especially between the PS-SiO_2, becomes progressively blurred

with increasing toluene content due to swelling of the PS grafted chains by the good solvent toluene and a reduced interaction parameter. Upon evaporation of the solvent, the swollen chains cannot fully collapse back and instead remain entangled, leading to the disappearance of boundaries between the PS-SiO_2. We can track this change quantitatively by measuring the inter-particle distances between PS-SiO_2 following DIA treatment, as shown in **Figure 3.7.(ii).b.** The interparticle distance increases from 67.6 nm (± 14.2 nm) to 79.6 nm (± 15.5 nm) with increasing toluene composition. In comparison, the interparticle distance of PMMA-SiO_2 remains invariant at 40.6 nm (± 5.4 nm). As the toluene also screens the interaction between PS-SiO_2 and PMMA-SiO_2, **Figure 3.7 (i). e** and **j** suggest that for the highest toluene fraction of 18.9%, during this swelling process, the (smaller sized) PMMA-SiO_2 potentially mix with PS-SiO_2 chains, similar to the model we proposed in the toluene/heptane mixture (**Figure 3.4.c**), causing a further increased surface coverage of PS-SiO_2 due to its surface segregation behavior arising from its lower surface energy. We believe that for the highest toluene volume fraction of 18.9% in **Figure 3.7 (i). e** and **j,** the situation corresponds very closely to the critical interaction parameter, χ_c**,** for phase separation of the PS-SiO_2 and PMMA-SiO_2 blends. More detailed future studies are required to develop this analogy with thermally reversible phase separation in traditional polymer blends.

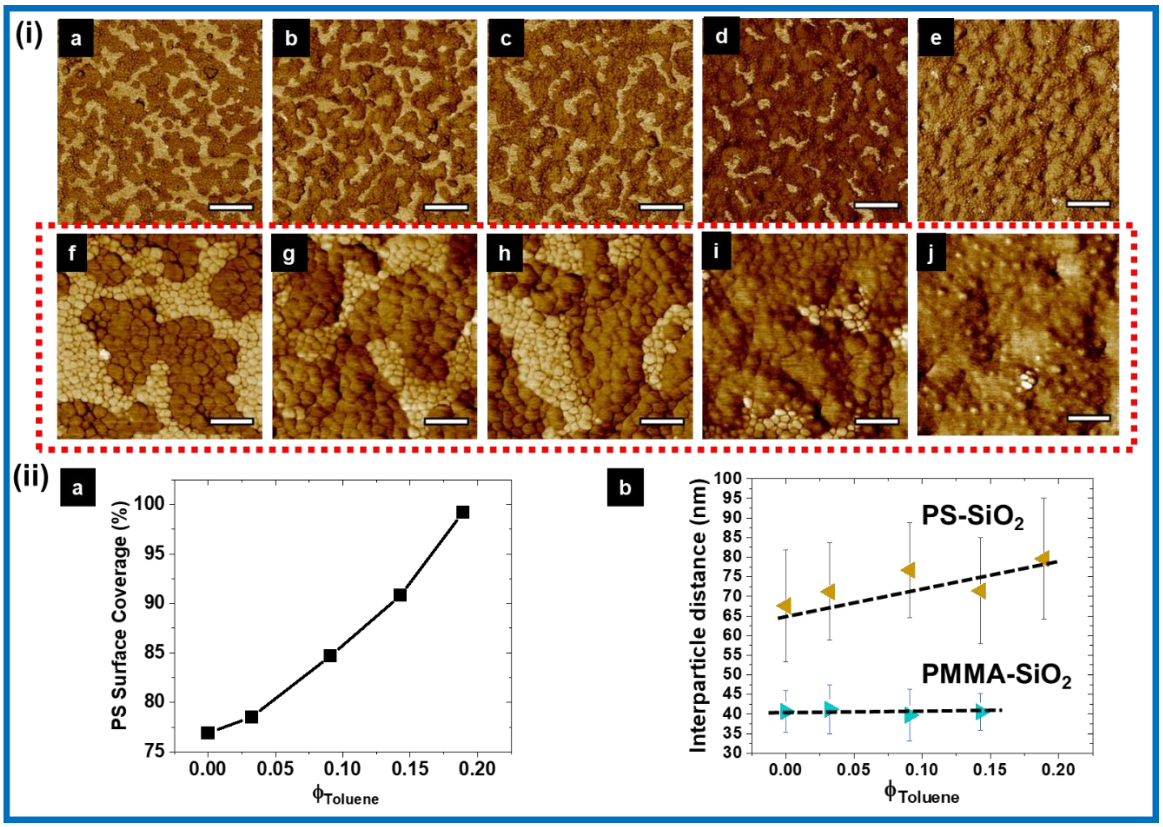

Figure 3.7. AFM phase images (4 μm x 4 μm) of PGNP phase separation as a function of volume ratio of toluene in fixed ratio acetone: heptane solution. The solid and dotted black lines are to guide the eye.

To study the inter-domain spacing of PGNP blends, we also performed ultra-small angle neutron scattering (USANS) on the films treated with different DIA solutions (with different volume ratios of toluene). Deuterated PMMA (M_n = 3.4 x 10^4, σ = 0.76 chains/nm^2)-g-SiO_2 was used here to have neutron contrast with the PS (M_n = 3.50 x 10^4, σ = 0.57 chains/nm^2)-g-SiO_2. The mass ratio of PS-SiO_2 to dPMMA-SiO_2 was 1:5, and PGNP blend film thicknesses were ≈ 500 nm on thin silicon substrates. About 10 to 20 stacked films were used for thru-transmission in USANS geometry for increasing USANS scattering intensity.

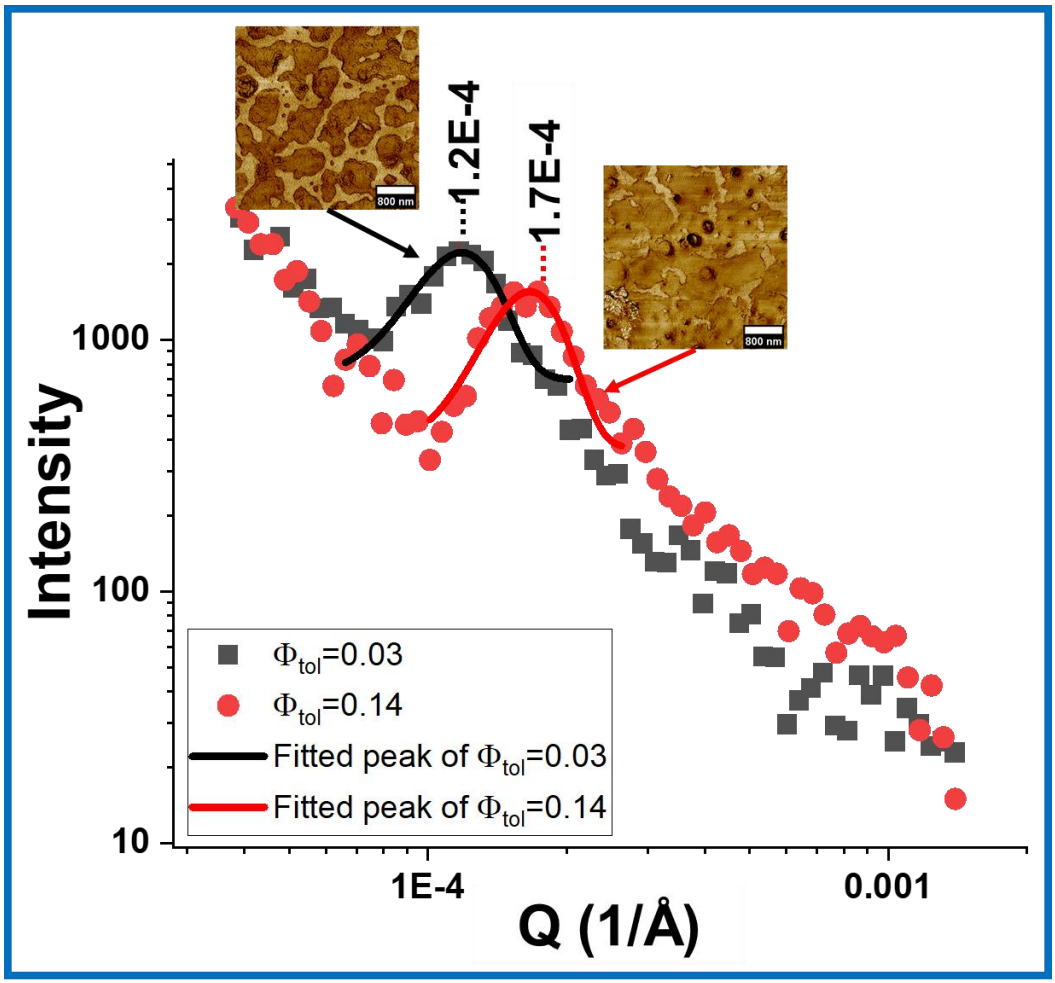

Figure 3.8. Correlating USANS and AFM phase images (calculated peak position inset) for the dPMMA-SiO_2/PS-SiO_2 blends treated by DIA solution with different toluene volume ratios.

Figure 3.8.a shows a peak in the USANS data at q^* = 1.2 x 10^{-4} Å $^{-1}$ (inset in the image), which corresponds to features of ≈ 5.2 μm in size, when the film is treated by an acetone/heptane/toluene mixture(1:2:0.1 in volume, ϕ_{tol} = 0.03). On the other hand, the peak shifts to q^* =1.7 x 10^{-4} $Å^{-1}$(**Figure 3.8.b**), which corresponds to about 3.7 μm in size when the film is treated by another acetone/heptane/toluene mixture (1:2:0.5 in volume fraction, ϕ_{tol} = 0.14) before it is pinned by limited in-plane surface mobility. This indicates that the film averaged inter-domain spacing between

dPMMA-SiO_2 decreases with higher toluene fraction in the DIA solution, as a result of a shift to a more 1-phase redistribution of the system. This trend is consistent with the AFM images at different depths created using the ToF-SIMS sputtering gun (**Figure 3.6 b** *vs*. **Figure 3.6 f**). The peaks were fitted using a Gauss model from OriginPro 2020 to obtain a fitted full width at half maximum (FWHM) for $\phi_{tol} = 0.03$ and $\phi_{tol} = 0.14$ sample of $5.4 \times 10^{-5} \pm 5.6 \times 10^{-6}$ and $7.1 \times 10^{-5} \pm 7.2 \times 10^{-6}$, respectively. The smaller FWHM (narrower the peak) value means longer range order, which is consistent with the embedded AFM images, showing an in-plane homogenization process with the increase of toluene's volume ratio in the DIA mixture.

3.3.5 Kinetics and Thermodynamic Aspect Ratio (AR) of PGNP blend phase separation

Experiments were next conducted to study the kinetics of the phase separation in PS-SiO_2/PMMA-SiO_2 blends with a mass ratio of 2:5. Two film thicknesses were investigated, 190 nm and 360 nm, to get better information on the development of film morphologies.

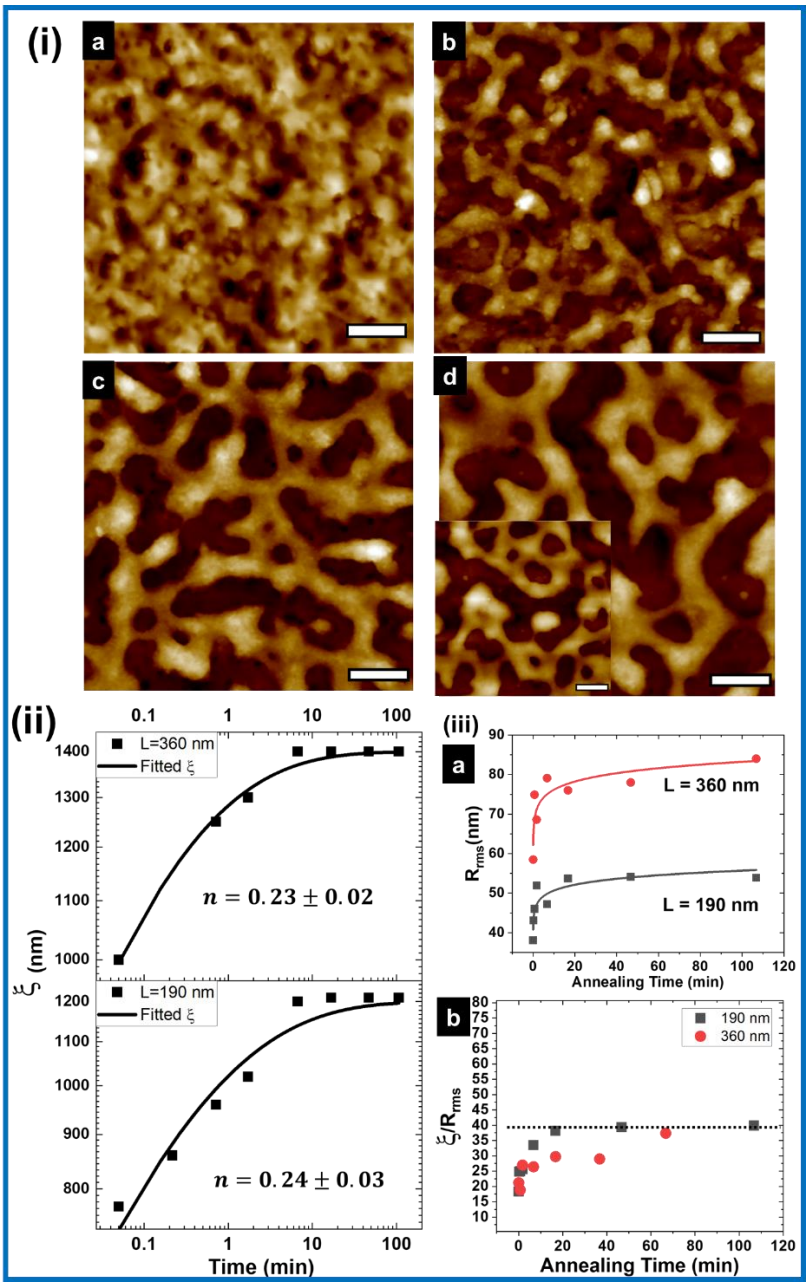

Figure 3.9. Time-dependent phase changes under direct immersion annealing. The scale bar of the AFM scan is 1 μm.

Figure 3.9. (i).a-d shows the evolution of the surface morphologies for the 360 nm thick film from the AFM height images. The light yellow region (the higher region in height images) corresponds to PS-SiO_2 as it selectively migrates to the upper (air upon drying) interface due to its lower surface/interfacial energy compared to PMMA-

SiO_2. When the film is annealed in the phase-separating DIA mixture of acetone and heptane (volume ratio: 1:1) for ≈ 3 s, (**Figure 3.9.(i).b**), the PMMA-SiO_2 and PS-SiO_2 start to phase separate into separate domains. As the immersion annealing time proceeds, the domains of PS-SiO_2 connect with each other for further growth into bicontinuous domains. After 45 s of annealing (**Figure 3.9.(i).c**), all PS domains connect and form a spinodal-decomposition-like morphology. Ultimately, the coarsening *via* this in-plane phase-separation of PS-SiO_2 domain stabilizes after 6 min of annealing (**Figure 3.9.(i).d**), with no further evolution of domains compared to 1 h later (**Figure 3.9.(i).d inset**). **Figure 3.9. (ii).a** shows the calculated correlation length (ξ), corresponding to the PS-SiO_2 characteristic domain size, calculated from the radially averaged 2D-FFT of AFM images of the 190 nm and 360 nm thick films, *versus* annealing time.

Because the phase separation pattern coarsening process ultimately saturates at a finite scale, the power-law growth of $\xi(t)$ due to molecular diffusion and coalescence processes associated with phase separation can only occur over a limited time period before this scale 'pins' to its asymptotic value at long timescales, ξ_∞. We may model this phenomenon in exactly the same fashion as diffusion-limited adsorption of polymers onto surfaces where the polymer surface concentration has been successfully modeled as a pseudo-first-order rate process with a time-dependent rate corresponding to the diffusion-limited rate of adsorption of polymer chains to the surface observable in short-time measurements.[137] Translating this argument to the present context, we model the time-dependent rate of growth of $\xi(t)$ as a pseudo first-order rate process in

which $\xi(t)$ obeys a power-law $\xi(t) \sim t^{n}$ at times much shorter than the 'pinning time' of the phase separation process. This model leads to a simple expression for $\xi(t)$,

$$\xi(t) = \xi_{\infty}(1 - e^{-Kt^{n}}). \quad (3.2)$$

The fitted exponent n for both film thicknesses is found to be $n \approx 0.23$ (**Figure 3.9. (ii).a)**, which is smaller than the normally reported value of 1/3 for fluid mixture phase separation.[60,104] A smaller coarsening exponent n, closer to 0.2, has also been observed in a previous, more controlled study of phase separation in melt blends of PGNPs.[25] We thus have evidence that the kinetics of phase separation in PGNPs blends can be appreciably different from 'ordinary' polymer blends. By contrast, we note that the coarsening exponent in blends of NPs (with and without grafted polymer layers) with a homopolymer gave a coarsening exponent near 1/3. [21,138] We mention that pinning of $\xi(t)$ at long times has also been observed in the liquid-liquid phase separation of certain micelle-forming liquids in which the micelle assembly and associated phase separation pinning occurs in the two-phase region,[139] and exactly the same equation and reasoning as in deriving Eq. (2) was used to model $\xi(t)$ in this complex phase separating fluid.

How do we understand this reduction in the coarsening exponent in the PGNP blend? Further studies will probably be required to fully establish this change in phase separation dynamics in this class of blends. However, we may offer a tentative explanation of this qualitative change of scaling of the phase separation coarsening. We think that an essential clue may be obtained from a recent simulation study of colloidal particle phase separation by Tateno and Tanaka,[140] both with and without

particle-particle hydrodynamic interactions (HI). In the case in which HI is included in the simulations, *n* for particle phase separation takes a value close to 1/3, but a definitely smaller value is observed in simulations in which HI is neglected, *i.e.*, Brownian dynamics simulations. Tateno and Tanaka interpreted this result as implying that Brownian dynamics 'fails even qualitatively' because it does not give rise to the 'correct' exponent value of 1/3. We note that the simulation observations of Tateno and Tanaka are consistent with earlier analytic calculations by Kawasaki and Ohta,[141] who found that the coarsening exponent should exactly equal 1/5 for liquid-liquid phase separation when the strength of the HI is taken to vanish, a condition that they designate as the 'solid' limit. Correspondingly, Kawasaki and Ohta[141] predicted *n* to equal 1/3 when HI interactions are fully developed. These theoretical results are entirely consistent with the simulation observations of Tateno and Tanaka on phase separating colloidal particles[140]. It has to be noted that the exponent *n* for the case without hydrodynamic interactions is not stated explicitly in Tateno and Tanaka's paper where the results for the coarsening scale of phase separation are given only in graphical form. Prof. Hajime Tanaka has communicated to us that an exponent value near $n = 0.2$ is consistent with the data given in this paper in the case where there is no hydrodynamic interaction.

PGNP fluids have an intrinsic property that might influence the strength of hydrodynamic interactions (HI) in these fluids. Apart from the 'solid-like' behavior arising from the 'dry layer'[101] corresponding proposed concentrated particle brush (CPB) region of densely grafted PGNPs[58], we propose instead that this emergent property of enhanced rigidity arises mainly from the relatively 'soft' properties of the

outer ‘semi-dilute particle brush (SDPB) region’[58] or ‘interpenetration layer’[142] of the polymer grafted layers that allows the PGNPs to fill space more efficiently, more like the bubbles in a foam than sand grains on a beach. This greatly enhanced molecular packing capacity of such ‘soft’ particles can make dense materials composed of such particles approach a limiting densely-packed ‘hyperuniform’state[143,144] in which the material properties become more similar in some ways to crystalline and quasi-crystalline materials than concentrated suspensions of spherical particles interacting through hard core repulsive interactions. The near ‘hyperuniform’ character of the PGNP mixtures might then be expected to lead to a suppression of HI, which are entirely absent in conventional solid materials. If such materials indeed resemble ‘solids’ from a hydrodynamic standpoint, as just hypothesized, then this would have the effect of changing the coarsening exponent to the value 1/5 predicted by Kawasaki and Ohta [141] rather than the ‘normal’ fluid mixture exponent value of 1/3. This argument seems to be entirely consistent with our observations, and this hypothesis merits further investigation. Lattice Boltzmann simulations of the ordering process of BCP materials indicate that the same HI mechanism influences the coarsening exponent in BCP ordering[145] so that this HI effect on the rate of phase separation is apparently a rather general effect. As noted above, *n* changes from about 1/5 to 1/3 with the absence and inclusion of HI in the particle mixture simulations of Tateno and Tanaka.[140] These simulation studies further show that the change of *n* arises from the role of HI in facilitating defect annihilation and that this change in phase separation kinetics due to HI is accompanied by subtle, but potentially observable, structural changes in the phase separation morphology.[60, 64] Recent

experimental work by Bilchak *et al.* have provided evidence for enhanced rigidity arising from the presence of the polymer grafted layer in rheological measurements, and qualitative evidence for strong interparticle interactions mediated from the grafted layers from imaging of the material, trends consistent with the expectations of emergent hyperuniformity.[146] We note, however, that the interpretation of observations for polymer grafted chains of variable mass must also take into account chain entanglement effects and alterations of the glassy dynamics so that the rheological measurements must involve a number of contributing factors that need to be better understood in PGNPs.

We note that HI also have a significant influence on how shear alters macrophase separation in fluid mixtures and microphase separation in block copolymer materials. Counterintuitively, the application of steady shear to fluid mixtures tends to diminish their miscibility, *i.e.*, the critical temperature increases with shear for UCST phase behavior.[147–150] The opposite trend arises in steadily sheared BCP materials, which are *solid* materials in their ordered state so that HI interactions are suppressed in the BCP material in its ordered state. Indeed, steady shear has been observed to cause the order-disorder transition temperature (ODT) to decrease in the common case in which BCP ordering occurs upon cooling,[151] an observation in complete opposition to sheared phase separating fluids. If one turns off the HI in the sheared fluid mixture calculations, then the critical temperature is then shifted by shear in the same way as BCP materials.[150] The presence of HI then controls the *sign* of the transition temperature shift under steady shear, and studies of the shift of the critical temperature under shear

could provide a clearer indication of the relative magnitude of HI in PGNP fluids in comparison to ordinary (Newtonian) fluids. [65-68]

To the contrast of the slow kinetics from the exponent, there is fast growth in pattern size as soon as the film is dipped into the DIA solution (**Figure 3.9.(i).b**). This fast pattern coarsening can be quantified by the large prefactor (*K*) in the power-law growth ($\xi(t) = K \cdot t^n$) describing the coarsening dynamics. The fitted prefactors for both thicknesses (**Figure 3.9.(ii).a**) is over 1000 nm/min$^{0.2}$, which is ≈ 10 times larger than those in homopolymer blends[60,104], blockcopolymer thin films[112] and pure PGNPs mixtures[25] using thermal annealing. Composto *et al*. reported that the power law for the discrete domain formation of homopolymer mixtures could be modified (*i.e.*, scaling prefactors) as a function of the polymer-polymer interfacial tension (σ), viscosity (η), and the film thickness (d) (**equation 3.3**)[60]

$$\xi(t) \sim (\sigma/\eta)^{1/3} d^{2/3} t^{1/3}. \quad (3.3)$$

The rate parameter *K* generally increases as the solution shear viscosity η decreases and, additionally, the rate of phase separation is further accentuated by film swelling.

Aside from the somewhat unconventional domain growth kinetics, we see domain size pinning and a fixed value of the aspect ratio (AR), the ratio of the surface roughness to the pattern scale, after long annealing times. These are typical trends that we have seen many times before in phase separating films.[21,104] **Figure 3.9.(ii).a** shows that the domains 'pin' at around 1.2 μm to 1.4 μm after 6 min of annealing. This is likely because the confinement from the film thickness impedes the rupture of

the bicontinuous PS-SiO_2 domains as the hydrodynamic forces are not large enough to overcome the increased viscoelastic stress, which in turn stops the formation of an array of well-ordered droplets.[105] Apart from the in-plane phase separation scale growth, the out-of-plane phase separation scale and surface roughness also grow rapidly under the DIA process. The as-cast film's surface roughness is only 10 nm for both 190 nm and 360 nm film (points not included in **Figure 3.9.(iii).a**). However, after 3 s of annealing, it quickly jumps to 38 nm (for 190 nm thick film) and 58 nm (for 360 nm thick film), and finally increases to 53 nm and 80 nm after 6 min. of annealing, respectively (**Figure 3.9.(iii).a**). This is induced by the PS domain dominating the air/film interface, which is caused by the PS domain's lower surface energy than the PMMA domain (γ_{PS} = 40.7 mJ/m^2 *vs.* γ_{PMMA}= 41.1 mJ/m^2). Previous studies of homopolymer blend phase-separation in thin films showed that the aspect ratio of longer time or pinned features, *i.e.,* AR ≈ domain width/domain height, roughly tracked the ratio of surface to polymer/polymer interfacial tension.[75] **Figure 3.9.(iii).b** shows the changes of AR (ξ / R_{rms}, correlation length over the surface roughness) as a function of time. It increases first and then stabilizes at 38, a value close to that in the previous section. This suggests that the model discussed in the previous section is potentially useful to interpret the semi-quantitively structural features of the DIA induced binary phase-separated 2-phase state.

The time-dependent study also helps us analyze the role of solvent immersion annealing on the particle brushes' phase separation. As the evaporation of the solvent during the drying process remains constant for different annealing time, it is safe to

conclude that the domain area's growth is mainly caused by the solvent immersion process instead of the solvent evaporation process. Indeed, this was also verified by *in situ* AFM solution studies (**Figure 3.10**).

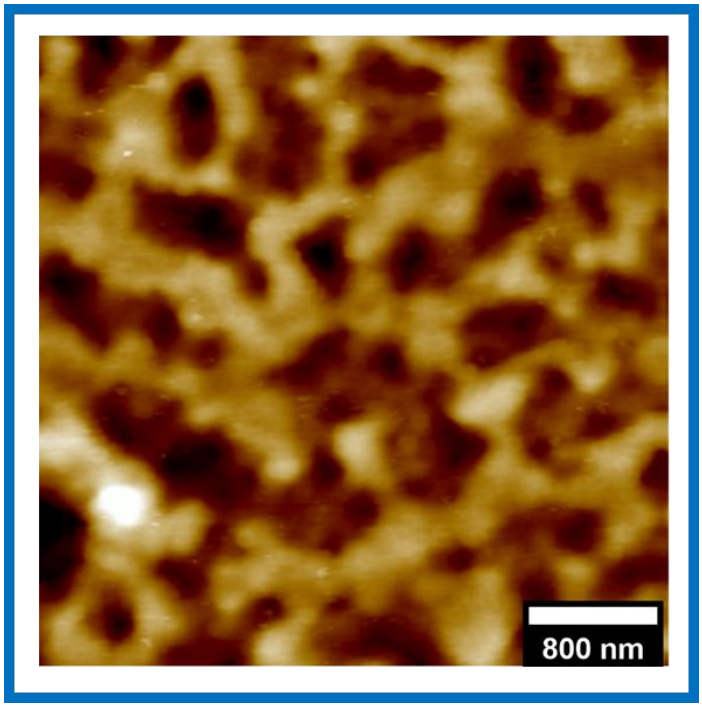

Figure 3.10. AFM height images of 130 nm thick PS-SiO_2/PMMA-SiO_2 (*mass ratio* 2:5) taken directly from acetone: heptane solution (1:1 in volume fraction), surface roughness, R_{rms} = 27.5 nm.

Finally, we want to finish by making some general comments about the rather special conditions under which we expect this unusual type of phase separation kinetics, and other special material properties that derive from the presence of the 'soft' polymer-grafted layer on the hard particle core of polymer grafted nanoparticles.

The 'soft' polymer layer of polymer grafted nanoparticles is probably *crucial* for observing the altered phase separation dynamics that we observe. Both computational and experimental studies have characterized the nature of the PGNPs in

solution[100] and in the melt.[101,152,153] These studies collectively indicate that the grafted polymer layers, both in solution and in melts of such nanoparticles, are not 'brush-like' in the literal sense of the polymer chains being stretched out in a geometrical form similar to the bristles of a paint brush. Rather, the polymer chains in these layers are closer in form to the 'random coil' shapes that individual flexible polymers adopt in solution, apart from a region near the grafting substrate. It is just this random coil aspect of the grafted polymer chains that gives rise to their entropy-driven segregation under confinement studied in previous studies by our group.[21,23] The highly fluctuating nature of the grafted polymer layer[100,154] for normally encountered grafting densities also has significant implications for molecular packing of this kind of nanoparticle in the melt.[155] The presence of a 'soft' deformable layer on the nanoparticle [See Fig. 2 of Barnett and Kumar's paper[156] for a helpful illustration of a polymer grafted nanoparticle melt generated through molecular dynamics simulation] gives rise to a strong interaction between the nanoparticle cores, leading to a 'jammed' state where the degree of jamming is quantified by the hyperuniformity index, h.[143,144,157]

h is defined as the ratio of $S(0)$, the static structure factor at low q, which is proportional to the isothermal compressibility and a measure of the capacity of the material to exhibit volume fluctuations at large length scales, to the magnitude of the first peak of $S(q)$, a measure of local interparticle density correlations, or informally 'jamming', at a scale on the order of the average interparticle distance. Thus, h could just as well be termed a 'dimensionless jamming index'. Simulation has shown that this jamming of the nanoparticle cores increases progressively with the mass of the

grafted chains at a fixed grafting density, at least over the chain lengths that could be investigated by simulation. However, the interparticle correlations between the nanoparticle core particles caused by the grafted chains must be ultimately lost as the mass of these chains approaches infinity (Note that the polymer grafting density is inherently dependent on polymer mass for polymer layers grafted from solution.). It is only in an intermediate 'window' of polymer mass and grafting density that we may expect the polymer grafted nanoparticle materials to approach a solid-like hyperuniform state in which $h \sim O(10^{-3})$.[143,144,158] There is evidently a 'sweet spot' corresponding to an intermediate polymer mass in which the jamming effect of the particle cores is maximized, even if strict hyperuniformity is not achieved. Fortunately, this 'jammed' condition corresponds to a polymer mass and grafting density regime that can be readily synthesized by grafting polymer chains onto inorganic nanoparticles in solution. We may anticipate many special mechanical, optical and acoustic properties to derive from materials in which nanoparticles are in this special jammed state.

Consistent with these general physical arguments, a stiffening of this class of materials compared to the homopolymer material characteristic has been found to be characteristic of polymer grafted nanoparticle materials.[26] Moreover, this stiffening effect disappears when the grafting chain length is short or the polymer grafting density too high. Bilchak *et al.* suggest that the non-monotonic variation in the mechanical[159] and gas permeability[146] of these materials derives from a transition from a jammed solid state at moderate chain lengths to a state similar to the pure polymer melt when the length of the grafted polymers becomes very long.

3.4 Conclusions

Binary PGNPs blend films follow a pattern of phase separation thermodynamics that is superficially similar to ordinary binary homopolymer blends. We can leverage our extensive knowledge about phase separation in blends to study this new class of blend materials. A fundamental problem with this class of mixtures is that they generally tend to have sluggish phase separation kinetics in the melt state, due to a combination of a large nanoparticle core coupled with a net high molecular mass grafted brush layer (cumulative Mw of individual grafted chains). This situation often applies for high molecular mass polymer blends, so we adopt the strategy of plasticizing the blend with a solvent mixture and controlling the polymer grafted nanoparticles' miscibility through control of solvent composition (DIA). In particular, we investigated the phase behavior of PMMA-SiO_2 /PS-SiO_2 blends at different DIA conditions. The application of this processing method allows us to control the phase separation morphology in a manner that otherwise would exhibit no morphological variation by thermal means. Using DIA, the PGNPs blends' morphologies can be reversibly changed from a 1-phase to a 2-phase state by simply altering the solvent mixture composition *i.e.* selective *vs.* neutral good solvent quality.

From a practical perspective, the DIA method is also relatively fast and suitable for real-world processing for materials fabrication. Phase separation or homogenization can often be achieved in seconds to minutes, despite a reduced coarsening exponent. This is due to the plasticization of the glassy grafted polymer layers by the solvent that profoundly influences the PGNP system mobility, resulting

in the rapid acceleration of the film domain growth dynamics in both directions of phase boundary crossing.

With this method of solvent annealing, we can exploit common features of phase separating polymer films: the late-stage pinning of the in-plane phase separation pattern scale at long times, and a corresponding constant ratio of the root mean squared roughness scale to the in-plane pattern scale, the so-called film pattern aspect ratio, AR. After DIA processing, we see the approach of the in-plane phase separation pattern scale and the AR to their long-time pinning values. This phenomenon is similar to phase separation in ultrathin binary homopolymer blend films and block copolymer films studied previously, but the timescale for this coarsening has been dramatically accelerated. The application of the DIA processing method should greatly facilitate the fabrication of polymer-grafted nanoparticle film materials for many applications.

Although many aspects of the thermodynamics of phase separation and dynamics are similar in polymer grafted nanoparticles to ordinary polymer blends, we find further evidence that the coarsening exponent for diffusive coarsening is different in this soft particle blend, an effect we attribute tentatively to suppressed hydrodynamics in this class of materials.

IV. FACILE ENTROPIC-DRIVEN SEGREGATION OF IMPRINTED POLYMER-GRAFTED NANOPARTICLE BRUSH BLENDS BY SOLVENT VAPOR ANNEALING SOFT LITHOGRAPHY

4.1 Introduction

Recent advances in polymer synthesis improved the control of the chemistry of the inner nanoparticle core and the encapsulating outer polymer layers of polymer grafted nanoparticles (PGNPs),[4,15,35,38,41,58] giving rise to an ever growing list of applications of these materials extending from electronics,[3,45,46,117,119,160] membranes,[3,27,118,146,156,161] to enhanced mechanical properties.[7,12,26] A critical requirement for fabricating these novel NPs and for their associated applications is the control of the PGNP dispersion and orientation in the system. For PGNPs dispersed in a polymer matrix, there are two different types PGNP bends encountered: blends for which the outer polymer brush of the PGNP has a different chemistry from the polymer matrix, and the case where brush layer of the PGNP and the polymer matrix has the same chemistry. For the chemically distinct system, extensive research has shown that these PGNP nanocomposites' morphologies can be controlled through variation of the Flory-Huggins interaction parameter χ, describing the strength of the polymer-polymer interaction strength.[21,24,166–168,69,112,116,120,162–165] Schmitt *et al.*[25] revealed that the morphologies of PGNPs having chemically different grafted layers could undergo upper critical solution temperature (UCST) phase behavior as in the corresponding homopolymer blends without NP cores. Wu *et al.*[24] demonstrated that varying the χ between the two different PGNPs via changing the annealing solvent of the direct immersion annealing (DIA) can reversibly alternate the morphologies

between phase-separated and homogeneous states. Zhang *et al.*[21] further found that imprinting topographic patterns on chemically different PGNPs/homopolymer blends led to a selectively partitioning of the PGNPs to the less confined 'mesa' region (thicker region of the patterned surface) due to entropic driving forces, but these studies were limited to relatively low mass grafted polymer layers because of the sluggish dynamics of the melts having high mass polymer-grafted layers. Below, we discuss a methodology that overcomes this limitation.

For chemically identical systems, it is well understood that entropic forces arising from architectural and flexibility differences between the polymer segments, the grafting density and length of the chains, along with the polymer nanoparticle core interaction strength can all influence the tendency towards phase separation and particle association in the melt and in solution. Akcora *et al.*[68] found that PGNPs can self-assemble into extended linear and branched polymeric structures in a chemically identical homopolymer matrix due to the balance of the energy gain from the approaching core and the entropic energetic cost of distorting the grafted polymer layers on the NPs. From the standpoint of the present work, this PGNP aggregation process is something that we seek to avoid since it normally implies a loss of control of particle organization.

Our group has recently focused on harnessing the general tendency of PGNPs to either self-assemble and associate or phase separate from each other in different kinds of matrix (homopolymers or PGNPs). In particular, we initially found that PGNPs dispersed in a matrix having a chemically identical nature as the grafted chains

allowed us to organize the PGNPs over large areas through the action of topographic confinement (PDMS pattern). It could also induce large scale patterning of the thin PGNP composite films through entropically-driven partitioning of PGNPs to the less confined 'mesa' region of the imprinted annealed films.[20,23] In particular, Zhang *et al*.[23] found that as the thickness of the 'trench' region (thinner surface region arising from the PDMS topographic pattern) decreases, the number density of the PGNPs in the 'mesa' region increases. In other words, the PGNPs in the 'trench' region get 'squeezed out' from the thin 'trench' thickness regions and migrate into the 'mesa' regions where the PGNP are less constrained (See Zhang *et al.*'s paper for a more extended discussion of this entropically-driven nanoparticle segregation process). Since the outer brush of the PGNPs has an identical chemical structure to the homopolymer matrix, Zhang *et al.* then concluded that entropic changes due to local confinement alone induced this selective nanoparticle partitioning. Notably, the PGNPs used in this previous study had a silica core radius of $R_0 \approx 1.2$ nm and a grafted chain mass, $M_{n,\,PS,\,grafted} = 11.5$ kg/mol.

Subsequent studies have revealed that the physical properties of PGNPs are sensitive to changes of inner NP core size and the molecular mass of the outer polymer layer.[26,101,146,169,170] Bilchak *et al*.[146] conducted rheology testing on PGNPs (with the diameter of the inner nanoparticle core: $D_0 = 14 \pm 4\,nm$, where ± 4 nm is the standard deviation) with different molecular masses and found that the *G'* plot starts to show a 'plateau' at low frequencies when the molecular mass decreases, indicating a transition to 'solid-like' structures. Lin *et al*.[170] revealed that the increased effective nanoparticle (NP) size will decrease the diffusion kinetics of PGNP to ≈ 100 times

compared to the prediction from Stokes Einstein law. Earlier we have demonstrated that for high molecular mass (M_n > 35 kg/mol) and large core radius ($R_0 \approx$ 7.5 nm) PGNP blends, annealed by direct solvent immersion annealing to increase PGNP mobility and repulsive interaction parameter, χ, the phase coarsening exponents decreases to ≈ 0.2, which was attributed to a suppression of the hydrodynamic interaction between these PGNPs resulting from the increased packing density of these materials.[24] There is also evidence that the entanglement interactions that can result from the greater interpenetration can lead to improved film toughness. We therefore investigate PGNPs with relatively high molecular mass grafted layers. As expected, this leads to greater inherent difficulties in processing these materials that may be overcome using methods such as solvent vapor annealing (SVA) to fully exploit the desirable properties of this class of materials.

4.2 Experimental Design

In this chapter, we investigated the distribution of high molecular mass polymethyl methacrylate grafted on silica nanoparticles (PMMA-SiO_2) in a low molecular mass PMMA-SiO_2 matrix. We studied the influence of topographic nanopatterning confinement on the segregation of PGNPs in the film. Below is the detailed information about the experiments.

4.2.1 Materials

The materials used in this study are PMMA-SiO_2 with variation of molecular mass for the grafted PMMA chains. All the PMMA-SiO_2 nanoparticles were synthesized using a surface-initiated ATRP method and prepared by our collaborators: Dr. Michael Bockstaller's and Dr. Krzysztof Matyjaszewski's group at Carnegie

Mellon University. For the smaller-sized PMMA-SiO_2, which is used as the matrix, the average silica core size is $r_0 = 1.5$ nm. The molecular mass for each grafted PMMA chain is $M_{n,PMMA,grafted} = 18.0\ kg/mol$, and the grafted density of it is $\sigma \approx 0.2\ chains/nm^2$. For the larger-sized PMMA-SiO_2 to study its organization, we used two different molecular mass to reveal the thermodynamic driving force for the selective partitioning under topographic nanopatterning confinement. The molecular mass for the first PMMA-SiO_2 is $M_{n,PMMA,grafted} = 43.7\ kg/mol$, while the other one is $M_{n,PMMA,grafted} = 26.7\ kg/mol$. The average core radius for both is $R_{0,core} \approx 7.5\ nm$, and the grafting density is $\sigma \approx 0.30/nm^2$. The solution used to dissolve the PMMA-SiO_2 is tetrahydrofuran (THF) and is purchased from VWR Inc. The solution used for solvent vapor annealing soft lithography (SVA-SL) is acetic acid. It was purchased from VWR Inc.

4.2.2 Film preparation

PMMA-SiO_2 was firstly dissolved in tetrahydrofuran (THF, VWR) solution (30 mg/ml) and sonicated in the water bath to ensure it is well dissolved. The PGNPs blends (mass ratio of $PMMA_{44K\text{-}15nm}SiO_2$/$PMMA_{27K\text{-}15nm}SiO_2$ to $PMMA_{18K\text{-}3nm}SiO_2$: 10%) were then sonicated in a water bath for 20 min to ensure good dispersion. The mixture was then flow coated into thin films of thickness *h* ranging from 70 nm to 140 nm on pre-cleaned (in ultraviolet generated ozone for 2 h) silicon substrates. The film thickness was measured by an interferometer (F3UV) using the Film metrics LSDT2 system.

Polydimethylsiloxane (Dow Corning, Sylgard 184) were crosslinked (curing agent mass: elastomer mass = 1:20) and cured at 120˚C for 12 h on commercial digital video discs (pitch $\lambda \approx 750$ nm, height difference $\Delta h \approx 120$ nm) or smooth glass slides to make the topographic pattern layers or smooth (non-patterned) layers (thickness ≈ 0.5 mm), respectively.

The samples for TEM measurements were prepared by directly cast the PGNPs blends films onto a thin (≈ 10 nm) poly(4-styrene sulfonic acid) (PSS; Sigma-Aldrich) layer that was pre-casted on the silicon substrates. After the SVA-SL/TA-SL processing, the multilayer films were then immersed into deionized water, where the top PGNPs blend films floated on the water surface while the bottom PSS layers dissolved in water. The PGNPs blends films were then transferred to copper grids (Ted Pella, 300 mesh Cu) for the TEM measurements.

4.2.3 Thermal annealed soft lithography (TA-SL)

The topographic PDMS pattern layers were directly put onto the polymer thin film and annealed in the vacuum oven for 24 h annealing. After the removal of the topographic PDMS pattern, the polymer films were then characterized by AFM and TEM.

4.2.4 Solvent vapor annealed soft lithography (SVA-SL)

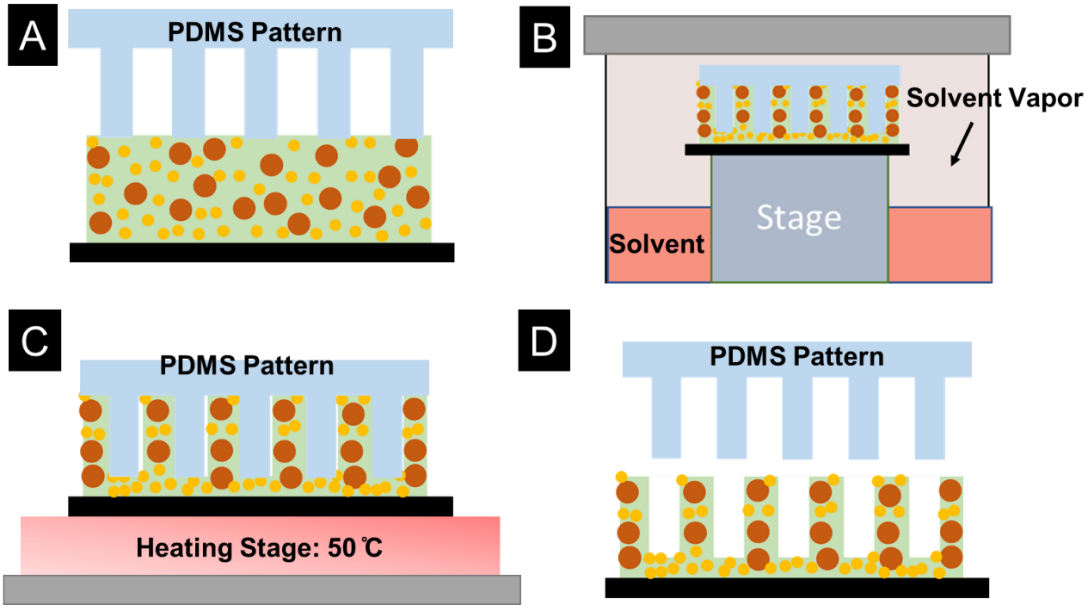

Figure 4.1. Cartoon of the solvent vapor annealed soft lithography steps.

Figure 4.1 shows the schematic illustration about the SVA-SL procedure. The polymer thin films with PDMS patterns were directly put in the acetic acid vapor. After the films were annealed for certain times, the films were then taken out from the solvent vapor and put onto a heating stage (50˚C) with the pattern still on it for 1 min. The patterns were then carefully removed from the surface and the films were characterized by AFM and TEM.

4.2.4 Method to calculate the partitioning parameter K_p

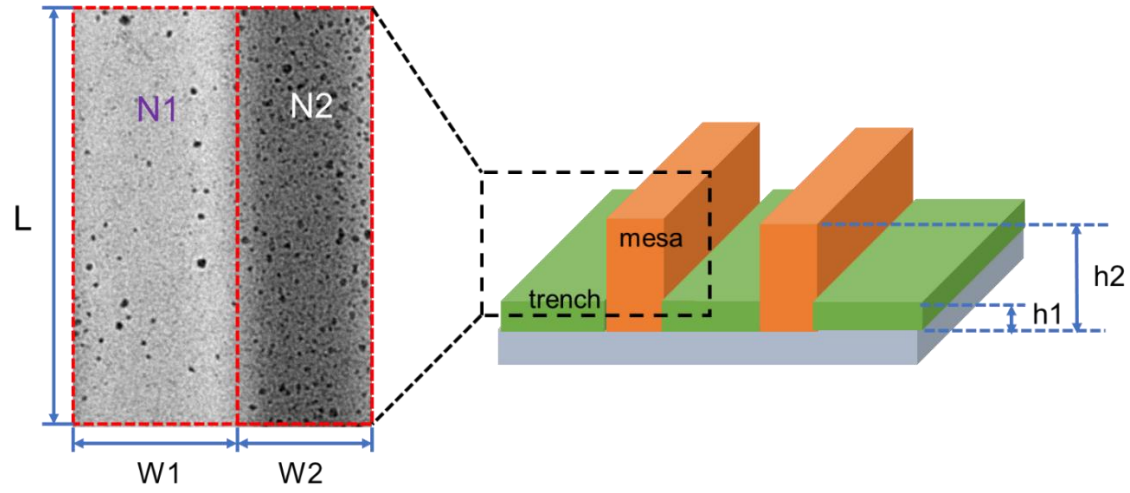

Figure 4.2. Illustration of the calculation of partition parameter K_p.

To quantify the extension of selective partitioning of high molecular mass PMMA-SiO_2 in the patterned film, we here introduce the partition coefficient parameter K_p. To illustrate the calculation of partition coefficient parameter K_p, we take the $PMMA_{27K}$-$_{15nm}SiO_2$/$PMMA_{18K}$-$_{3nm}SiO_2$ blends as an example (initial film thickness h = 83 nm). The number of larger-sized PGNPs in the trench (N1) and mesa (N2) are directly counted from the TEM images using ImageJ analysis. W1 and W2 are the widths of the trench and mesa measured using ImageJ analysis. The averaged h_1 and h_2 are calculated from the height difference between the mesa and trench (Δh) measured from the AFM height profiles. Multiple calculations have been taken in different locations to get the averaged K_p value of every single film. The equations for the calculation of K_p is

$$K_p = \frac{\rho_1}{\rho_2} = \frac{N_1 W_2 \, h_2}{N_2 W_1 \, h_1}, \tag{4.1}$$

where ρ_1 and ρ_2 are the number density of particles in trench and mesa, respectively. They can be calculated as

$$\rho_1 = \frac{N_1}{L\,W_1\,h_1} \text{ and} \tag{4.2}$$

$$\rho_2 = \frac{N_2}{L\,W_2\,h_2}. \tag{4.3}$$

h_1 and h_2 are the thickness of trench and mesa, respectively. They are calculated as

$$h_1 = \frac{h(W_1+W_2)-\Delta h W_2}{W_1+W_2} \text{ and} \tag{4.4}$$

$$h_2 = h_1 + \Delta h. \tag{4.5}$$

4.3 Results and Discussions

4.3.1 Distribution of PGNPs under topographic nanoimprinting pattern using thermal annealing soft lithography

We first investigate the selective partitioning technique applied to PGNPs having a high molecular mass grafted chains *via* thermal annealing soft lithography (TA-SL), similar to earlier work from our group by Zhang *et al.*[23] on lower molecular mass grafted chain and smaller core size counterpart of these PGNPs in a homopolymer matrix. We replace the smaller sized PGNP ($R_{0,core} \approx 1.5\,nm$, $M_{n,PS,grafted} = 11.5\,kg/mol$, grafting density $\sigma \approx 0.7/nm^2$) studied earlier with two different PGNPs having higher grafted chain molecular mass and larger inner NP core dimensions ($R_{0,core} \approx 7.5\,nm$, $M_{n,PMMA,grafted} = 43.7\,kg/mol$, $\sigma \approx 0.32/nm^2$; $R_{0,core} \approx 7.5\,nm$, $M_{n,PMMA,grafted} = 26.7\,kg/mol$, $\sigma \approx 0.30/nm^2$). We will refer to these two PGNPs as $PMMA_{44k}$-$_{15nm}SiO_2$ and $PMMA_{27k}$–$_{15nm}SiO_2$ below. The

homopolymer in Zhang *et al*. measurements are replaced by a PGNP ($R_{0,core} \approx 1.5\,nm$, $M_{n,PMMA,grafted} = 18.0\,kg/mol$, $\sigma \approx 0.2/nm^2$) having a relatively small size, which is referred to as $PMMA_{18k}$-$_{3nm}SiO_2$ in the discussion below. This asymmetric 'blend' of two different PGNPs, one higher molecular mass PGNPs with the lower molecular mass $PMMA_{18k}$-$_{3nm}SiO_2$ PGNP as the "matrix", are also referred to as the 27 K and 44 K PGNP blend systems below. The PGNPs are dissolved in THF solution and cast to different film thicknesses using a flow coater. The films were then dried at 50˚C in the vacuum oven overnight to remove residual solvent and then annealed at 180˚C in the vacuum oven for 24 h with a DVD topographical nanopattern in pre-cured PDMS (curing agent mass: elastomer mass = 1: 20) imprinted on it. The capillary force then drives rapid mold filling of the binary PGNP blend film systems into the PDMS pattern having a periodic topography, in particular, alternating 'mesas' (higher region) and 'trenches' (lower regions) with a pitch of $\lambda = (752 \pm 6)$ nm, where ± 6 nm is the standard deviation from multiple AFM scans.[23] **Figure 3** shows a schematic 'cartoon' of how we envision our experiment. The orange dot represents the PGNPs with higher core size and higher molecular mass, while the blue dots represent the smaller-sized PGNPs. Ideally, due to the entropic penalty arising from the confinement in the 'trench' region, the larger-sized PGNPs will be 'squeezed out' into the less confining 'mesa' regions.

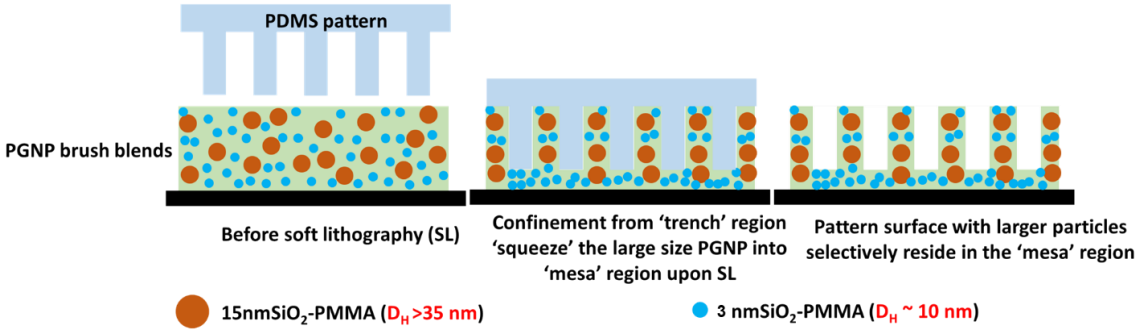

Figure 4.3. Cartoon of the proposed experiments of the selective partitioning of chemically identical high molecular mass PMMA-SiO_2 mixtures.

Figure 4.4 shows the top-view transmission electron microscopy (TEM) images of patterned surfaces with different initial film thicknesses *h* after being annealed in a vacuum oven for 24 h at 180 ℃. The black dots in the images (circled in red as examples in **Figure 4.4.A**) correspond to the larger-sized PMMA-SiO_2. The dark color strips on each image represent 'mesa' regions (the thicker regions on the patterned surface), as the thicker regions have a greater electron density than the thinner region from TEM images. According to Zhang *et al.*,[23] reducing initial film thickness decreases the 'trench' height and induces higher entropic penalties, driving larger-sized PGNPs into the 'mesa' region. However, in these disparate PGNP blends subject to melt annealing under the PDMS patterned imprint, as we decrease the film thickness from ≈ 100 nm to ≈ 70 nm for both systems, the trench regions still retain many larger-sized PGNPs, that are not segregated to the mesa region as expected. We employ the partition coefficient, K_p, implemented earlier by Ren *et al.*[23] to study the extent of the selective partitioning quantitively. K_p is defined as the ratio of the number density of larger-sized PGNPs in 'mesa' to those in the 'trench', with $K_p = 0$ implying that all the larger-sized PMMA-SiO_2 have segregated to the 'mesa' regions

as the best case selective partitioning result, while $K_p > 1$ demonstrates the reverse case wherein more larger PGNPs are segregated into the 'trench' region, and $K_p = 1$ indicates no selective partitioning at all. The calculated average K_p for both 27 K and 44 K PGNP systems are 0.86 ± 0.04 and 1.03 ± 0.14 (± 0.04 and ± 0.14 are standard deviations estimated from films having different initial thicknesses).

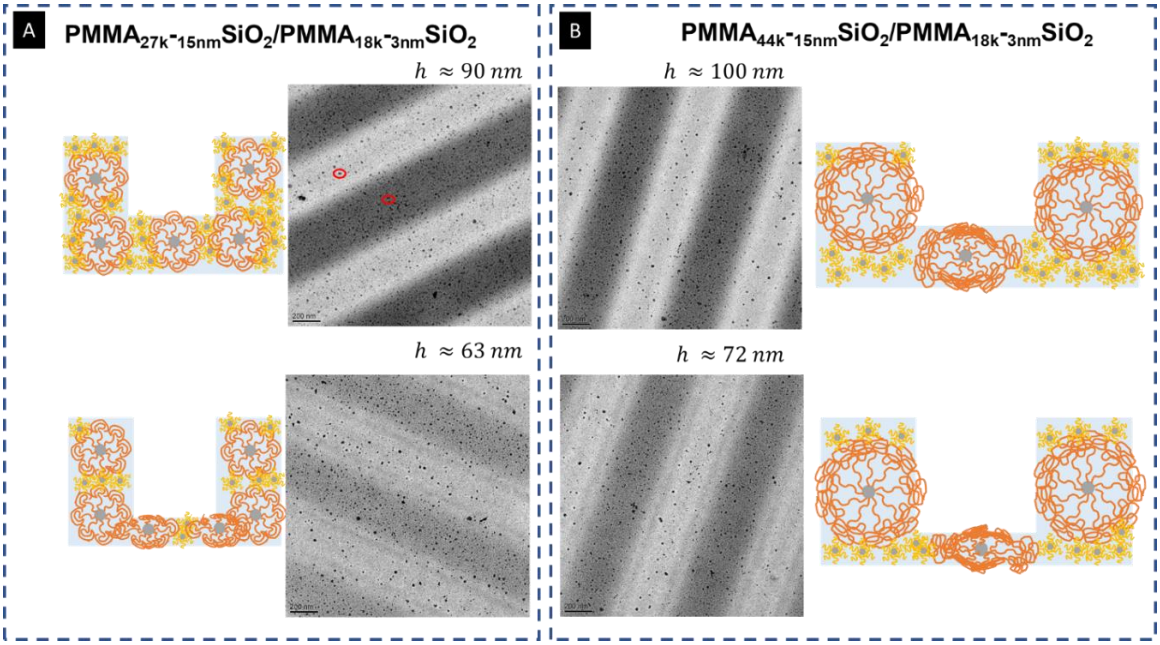

Figure 4.4. Top-view TEM images to study the segregation of larger-sized PGNPs (circled in red in **A** as examples) after the PDMS topographic pattern was removed by thermal annealing for 24 hours at 180˚C.

These results provide two important findings: (1) The selective partitioning for each system is poor by using thermally induced PDMS topographic patterning, regardless of the trench thickness. The 44 K system showed even poorer segregation than the 27K system, demonstrating no selective partitioning at all ($K_p \approx 1$). This means that the entropic penalty alone cannot drive the PGNPs to the mesa regions likely due to pinning as the molecular diffusivity of these large and entangled PGNPs is presumably too small to cross the activation barrier for particle displacement. In

contrast, earlier studies with smaller star-like PGNP systems could segregate as the entropic forces were sufficient to drive the selective segregation across a lower activation barrier.[23] (2) The selective partition for these larger-sized pure PGNPs blends cannot be enhanced by the variation of film thickness or using confinement effect by using the thermally-assisted method alone.

Why do the current PGNP blends show different behaviors from our earlier work? We believe it is due to the 'solid-like 'jammed state' ('hyperuniformity'[143,144,155,157,158] being a quantitative measure of this jamming) of these bulky PGNPs in the film, which also makes it difficult for the material to equilibrate so that equilibrium thermodynamics is not operative in governing the segregation of these nanoparticles. Earlier work from our group and others has shown that the relatively 'soft' outer polymer layer allows the polymer chains to interpenetrate and increase the packing density of these PGNPs. This layer is termed the "interpenetration layer" in Kumar *et al.*'s work.[101] Due to this enhanced packing of the PGNPs originated from their soft grafted layers, and associated near-hyperuniformity,[24,143,144,158] the properties of these PGNPs are closer in some ways to crystalline or semi-crystalline materials. Many theoretical studies have characterized similar 'jamming configurations' for the equilibrium layers both in the solution and melt state.[143,144,156,158,171,172] Barnett and Kumar [156] have provided a useful illustration of how the interaction between the deformable 'soft' outer polymer layer and the inner cores of the PGNPs induces a 'jammed' state between these particles that is similar in geometrical form to an emulsion of soft deformable emulsified droplets. Because of this 'solid-like' jammed condition of the PGNPs, the imprinted topographical pattern

simply cannot readily deform the outer polymer brush and ‘squeeze’ the PGNPs into the ‘mesa’ region. Instead, these PGNPs ‘pin’ in the ‘trench’ region, leading to limited partitioning. For some applications, this pinning effect might of the structure of the film be desirable, but we intended to observe the selective partitioning of the PGNPs in these materials with thicker grafted polymer layers so that this finding was initially unsatisfactory.

4.3.2 Distribution of PGNPs under topographic nanoimprinting pattern using solvent vapor annealing soft lithography

To address the general problem of sluggish dynamics in glassy and entangled polymer materials, and the general tendency of polymer materials’ thermodynamically driven propensity to phase segregate from entropic driving forces, we have developed a solvent-vapor annealing soft lithography (SVA-SL) method to anneal our patterned film under conditions where the PGNP dynamics are greatly enhanced and the tendency of the polymers to phase segregate is controlled *via* the control of the swollen brush structure via control of solvent quality. The swelling of the polymer brush should greatly enhance the dynamics with the grafted layers and should also increase the mobilities of the PGNPs through simple plasticization, and the solvent should also reduce the activation free energy barrier of segmental and PGNP mobility if the solvent is chosen judiciously.

Figure 4.5 shows the schematic illustration of the SVA-SL method developed in our laboratory. Unlike thermal annealing, where melt mobility induces mold filling, here enhanced mobility enabled by the solvent vapor of acetic acid allows rapid mold filling of PGNP films, while under a PDMS pattern for capillary forces to drive a

metastable equilibrium state within a reasonable annealing time (≈ 1 h). Acetic acid is a poor solvent (non-swelling) for PDMS,[173] and a good solvent for the PMMA brush,[174] which swells both large and small PGNPs of the blend film, and diminishes the densely packed state of these PGNPs compared to their melt mixed state. For the larger sized PGNPs ($PMMA_{44K}$-$_{15nm}SiO_2$/$PMMA_{27K}$-$_{15nm}SiO_2$), its effective entanglement with other PGNPs and deformability under the trench region is also apparently greatly diminished due to the swelling of the film. This allows them to be readily squeezed-out from trench region, which is assisted by the fact that solvent vapor also plasticizes these atypical blends and lowers the system glass transition temperature, T_g, thereby increasing their molecular mobility, especially relevant for the larger-sized PGNPs to have the center of mass motion. From a practical standpoint, we also realized that if the PDMS pattern is immediately peeled off after the film is removed from the solvent vapor, the residual solvent in the system will 'shear off' the blend film to some degree and damage the patterned surface. To avoid this problem, immediately after removal from the solvent vapor, we placed the film with the PDMS pattern intact on it onto a heating stage at 50˚C for 1 min to rapidly remove the residual solvent. **Figure 4.5 (III). B** shows the patterned surface created by the SVA-SL method. The AFM height profiles (**Figure 4.5 (III). C**) show no geometric difference between the dried thermal annealed soft-lithography (TA-SL) and SVA-SL patterned films, indicating that the SVA-SL method can produce patterned surfaces with rapid mold filling by capillary force with the same qualities and robustness of the TA-SL method.

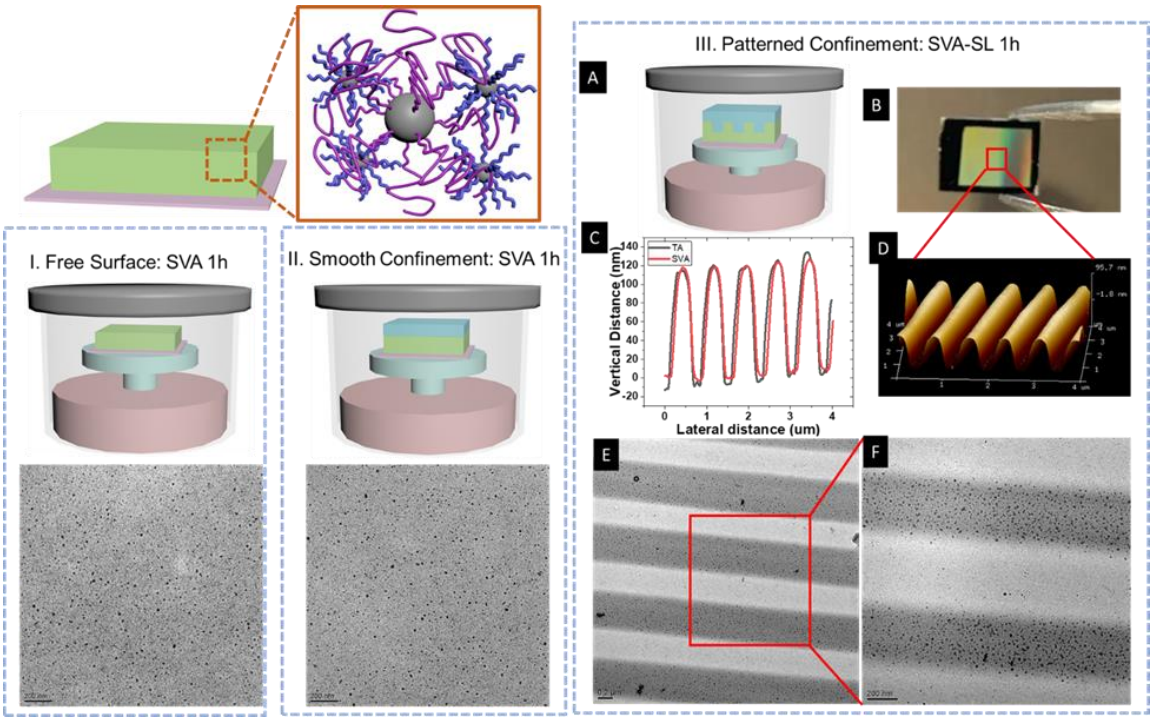

Figure 4.5. Sketch of the SVA-SL setup and top-view TEM results after 1 h annealing.

Figure 4.5 (III). E shows the TEM image of the 27 K PGNP system film ($h \approx$ 70 nm) patterned using SVA-SL after 1 h annealing. It is clear that almost all black dots (large-sized PGNPs) have selectively segregated to the 'mesa' region, which demonstrates that the topographic PDMS patterning can induce selective partitioning for these larger-sized PGNPs systems using the SVA-SL technique, a condition that cannot be achieved using the TA-SL method. Control experiments have also been conducted to study the phase morphology of the similar film under SVA without PDMS pattern (Free surface, **Figure 5 (I)**) and with only non-patterned PDMS elastomer (Smooth confinement, **Figure 4.5 (II)**). The corresponding TEM images show almost identical morphologies (well-distributed PGNPs blends) for both the free surface and smooth confinement, indicating that the chemistry of the topographic

PDMS does not affect the selective partitioning of these high molecular mass PGNP blends.

We then investigated the kinetics of the selective partitioning process. **Figure 4.6** (a)-(c) shows the top-view TEM images of ≈ 100 nm thick 44K blends that are annealed using SVA-SL with various annealing times. After 30 min of SVA-SL, there is still a large amount of (relative to the amounts in the 'mesa' region) the larger-sized PGNPs in the 'trench' region, indicating that the capillary driven selective partitioning is not completed within this short time frame. As the annealing time is increased to 1 h (**Figure 4.6. (b)**), the amount of larger-sized PGNPs in the 'trench' region decreases and is relatively identical compared to those annealed after 20 h (**Figure 4.6. (c)**). This indicates that the PGNP partitioning process is ultimately completed after 1 h of SVA-SL partitioning. The quantitative estimation of this progressive partitioning can be measured by tracking the partition coefficient, K_p (**Figure 4.6. (d)**) as defined previously. We observe that $K_p \approx 0.8$ after 30 min of annealing, decreasing to an equilibrium value of $K_p \approx 0.2$ after 1 h of annealing and does not evolve at longer times. Notably, an earlier kinetic study on smaller sized PGNPs in homopolymer mixture by Ren *et al.* indicates that the local enrichment is completed after 3 min of TA-SL at 120˚C.[23] We conclude that this relatively slower kinetics of the larger-sized PGNP system is due to the suppressed hydrodynamic interactions between these larger-sized PGNPs under SVA-SL conditions, as there remain some amount of 'jamming configurations of the PGNP grafted layers. Recent independent work has elucidated the novel phase separation dynamics of PGNPs blends having higher molecular mass grafted chains.[24] The development of localized enrichment of PGNPs

in ‘mesa’ region with extended SVA-SL annealing time also indicates that the selective segregation is mainly caused by the SVA-SL annealing, and not others parameters such as the constant time (1 min) of drying process at 50˚C, after the film (with PDMS pattern on it) is taken out from the SVA-SL container.

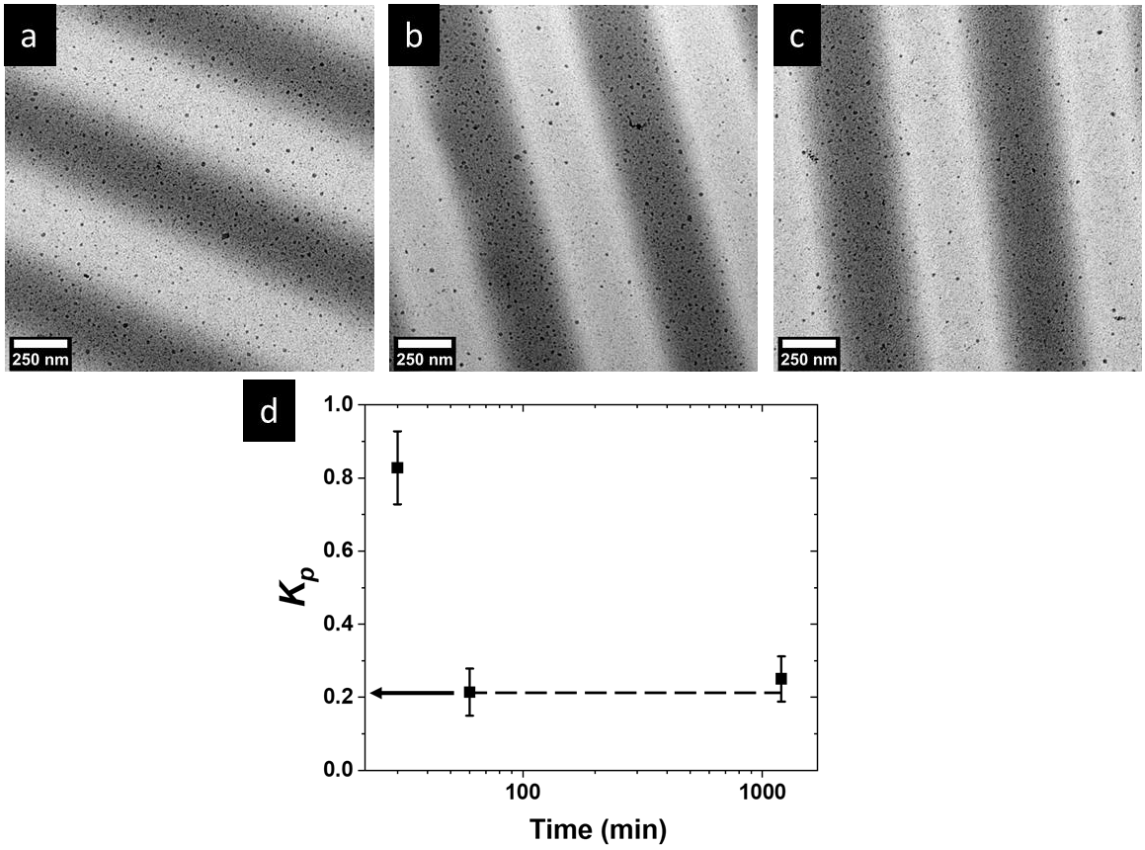

Figure 4.6. Kinetic study on the selective partitioning of the 44K PGNP system. (a) 30 min SVA-SL; (b) 60 min SVA-SL; (c) 20 h SVA-SL; (d) Calculated non-equilibrium partition parameter K_p as a function of annealing time.

4.3.3 Thermodynamic driving force for the selective partitioning

How can we explain this selective partitioning? Similar to Ren *et al.*’s system (PS-SiO_2/PS blends),[23] the attractive van der Waals interaction between PGNPs in our $PMMA_{27K/44K}$-$_{15nm}SiO_2$/ $PMMA_{18K}$-$_{3nm}SiO_2$ system is also negligible due to the dense grafting of PMMA shell on SiO_2. We then propose that the selective segregation of the

larger-sized PGNPs in 'mesa' region is caused by the loss of the conformational entropy coming from the topographic PDMS pattern. To support this hypothesis statement, we vary the degree of entropic confinement defined as, $h_{brush} / h_{confine}$. In this ratio, h_{brush} is the thickness of the outer PMMA layer of the $PMMA_{27K\text{-}44K}\text{-}_{15nm}SiO_2$, which is calculated as $d_{interdomain} / (2 - R_0)$ nm, where $d_{interdomain}$ is measured from the AFM images of pure dried PMMA-$_{15nm}SiO_2$ films (**Figure 4.7**) and R_0 is the radius of the inner SiO_2 core (≈ 7.5 nm). The $h_{confine}$ is calculated as $h_{confine} \equiv h_{trench} / (2 - R_0)$, where h_{trench} is the average height of the 'trenches', which can be calculated from the initial film thickness h and step height Δh from AFM measurement.

We note that both h_{brush} and $h_{confine}$ should be measured/calibrated under a solvent vapor condition (polymer chains are swollen) since the selective partitioning is proved to develop in the swelling state. However, our discussion below is based on a dried film state reference state due to the experimental difficulties of performing *in situ* TEM and AFM measurements with a PDMS patterned layer on top. Nevertheless, the general conclusion in the following discussion should still be correct and robust as the calculated partition parameter K_p is a ratio of the number density of larger-sized PGNPs (black dots) in 'trench' to 'mesa', which should remain the same upon drying after swelling induced entropic partitioning is completed. In addition, we have also shown earlier that no partitioning takes place during drying, and the extent of partitioning depends on SVA-SL annealing time only. The swelling condition has an effect on the value of $h_{brush} / h_{confine}$, which only shifts the x-axis of the **Figure 4.9** while the K_p values remain the same since it is dependent on the number density only.

The general trend of K_p (decreases with the increase of h_{brush} / $h_{confine}$, more detailed information in the later discussion) remains the same regardless of any solvent effect.

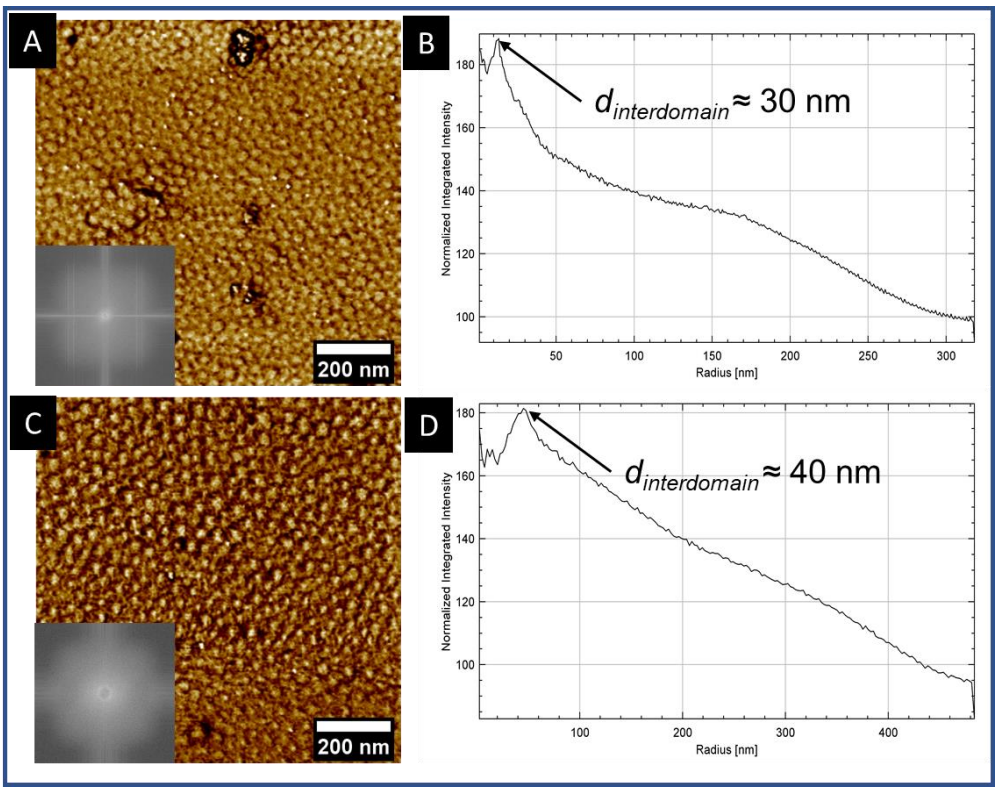

Figure 4.7. AFM phase-contrast images of as-cast $PMMA_{27K\text{-}15nm}SiO_2$ (**A**) and $PMMA_{44K\text{-}15nm}SiO_2$ (**B**) films with the corresponding 2D FFT images inset. (**C**) and (**D**) is 1D power spectrum for the interdomain distance.

Based on the above discussion, the influence of the entropic loss on the selective segregation can be studied and validated with the variation of h_{brush} / $h_{confine}$. We then chose both 44 K and 27 K PGNP blends to vary h_{brush}, and different film thickness to vary $h_{confine}$ as h_{trench} increases with the increase of initial film thickness h.

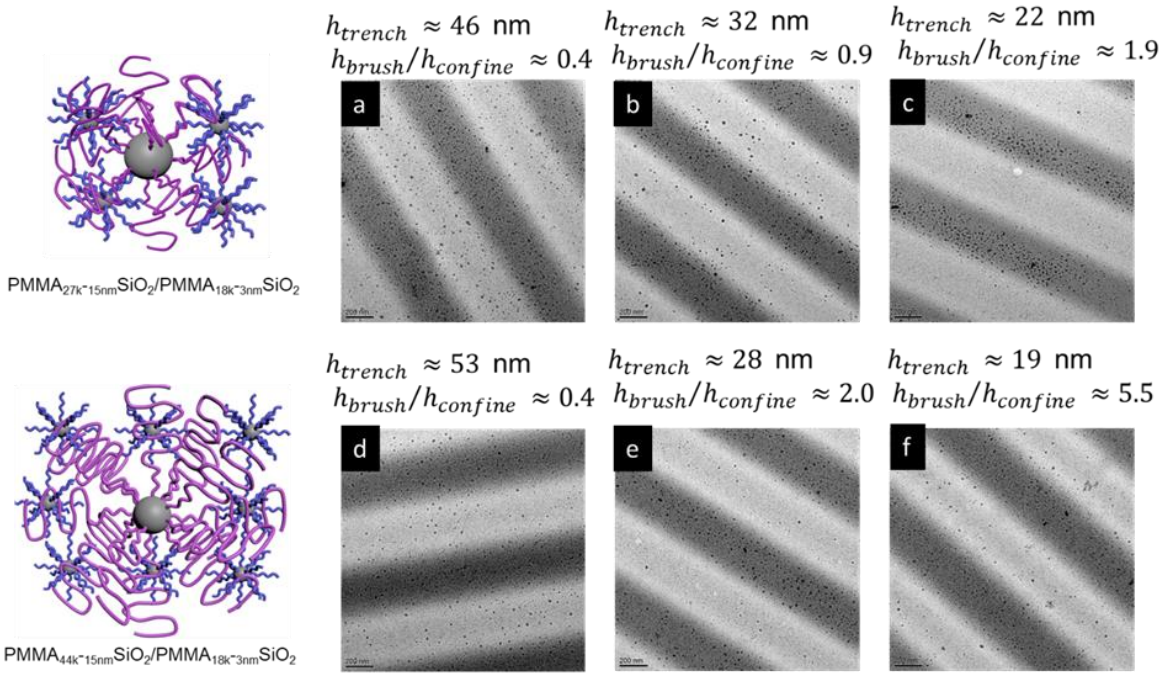

Figure 4.8. Top-view TEM results of the selective partitioning for both 27K **(a)-(c)** and 44K **(d)-(f)** blends as a function of confinement degree (h_{brush} / h_{confine}).

Figure 4.8 are the top-view TEM images of the patterned 27 K ((a), (b), (c)) and 44 K ((d), (e), (f)) films with different trench height (h_{trench}). For both 27 K and 44 K blends, the localized enrichment of the larger-sized PGNPs into the 'mesa' region increases as the trench height decreases, confirming selective entropic portioning using SVA-SL method. When the value of h_{brush} / h_{confine} is > 1 (≈ 2.0) for both systems, the larger-sized PGNPs in the 'trench' region encounter a high unfavorable entropic confinement from the topographic PDMS pattern, resulting in 'squeezing out' the larger-PGNPs to the less confining 'mesa' region, thereby minimizing the free energy and resulting in a lower of the partition coefficient K_p for both the systems, ≈ 0.2 for 44K blends and ≈ 0 for 27K blends. Interestingly, if the confinement is further increased for the 44K blends, the selective partitioning effect does not improve further.

Instead, the larger-sized PGNPs remain in the 'trench' regions (**Figure 8. f**) due to a 'pinning' effect arising from an 'over-confined' state.

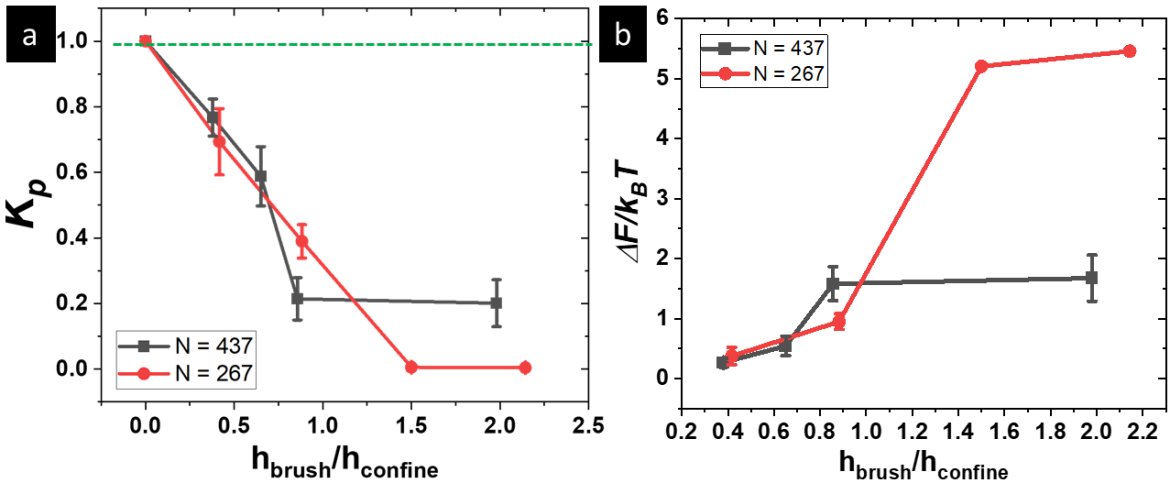

Figure 4.9. Confinement effect on PGNP partitioning. (**a**) Partitioning coefficient K_p and (**b**) free energy change ($\Delta F/ k_B T$) as a function of confinement degree ($h_{brush} / h_{confine}$). Both solid and dotted lines are to guide the eye.

Figure 4.9.a shows the changes of partition coefficient K_p as a function of $h_{brush} / h_{confine}$, which is used to quantitatively study the influence of the entropic penalty on the selective partitioning phenomena. For both molecular mass system, K_p decreases as $h_{brush} / h_{confine}$ increases, confirming the increase of local enrichment of the large-sized PGNPs into the 'mesa' region. For 27K blends, the strong confinement ($h_{brush} / h_{confine} > 1.5$) leads to the complete partitioning of $PMMA_{27K}$-$_{15nm}SiO_2$ into the mesa region ($K_p \approx 0$), as the entropic penalties for staying in 'trenches' should be substantial for this PGNP system. However, as the molecular mass increases, the strong confinement for the 44K blends ($h_{brush} / h_{confine} > 1$) doesn't lead to complete partitioning. Instead, K_p stabilizes at around 0.2, confirming the 'pinning' effect from the 'finite' confinement of the relatively large PGNP blends discussed above. This comparison indicates that selective partitioning results from the energy balance

between the entropic penalty and the 'pinning' effect from the finite film (trench) thickness. In other words, as the molecular mass increases above a critical value, complete partitioning cannot be achieved for the larger-sized PGNPs'. We then use a free energy model to quantify the entropic loss as a function molecular mass of both PGNPs' and the amount of the topographic confinement (h_{brush} / $h_{confine}$). Since we have a chemically identical system, the enthalpic part can be neglected, which simplifies the model to the following form: $\Delta F = -k_B T \cdot \ln(K_p)$, where k_B is the Boltzmann constant, K_p is the partitioning coefficient, and ΔF represents the free energy change of the system as one individual larger-sized PGNP moves from the confined 'trench' region to the less confined 'mesa' region. $\Delta F / \ k_B T$ can then be used to quantify the amount of entropic driving force from the topographic confinement. **Figure 4.9.b** shows that the entropic force increases with more confinement in the system for both PGNP blends. For the 27 K blends, when the confinement degree is relatively low (h_{brush} / $h_{confine}$ < 1), the entropic loss is generally small ($|\Delta F| \leq \ k_B T$). However, as the confinement degree reaches the strong confinement region (h_{brush} / $h_{confine}$ > 1), the entropic driving force dramatically increases ($|\Delta F| >> k_B T$), leading to the complete partitioning of the $PMMA_{27K\text{-}15nm}SiO_2$ into the 'mesa' region (as shown in **Figure 4.9 (a)**, **Figure 4.8 (c),** and **Figure 4.5.III (E),(F)**). However, due to the finite confinement effect in the trench region for the 44 K blends, the total free energy change is relatively small ($|\Delta F| / k_B T \approx 2$) even in the strong confinement region (h_{brush} / $h_{confine}$ > 1.5), leading to relatively reduced partitioning compared to the 27 K blend system.

4.4 Conclusions

High molecular mass PGNPs systems have attracted significant attention for their potential for enhancing mechanical properties of polymer thin films. However, the interpenetration of the outer polymer brush layer leads to a low mobility 'jammed' state. In this chapter, we introduced a method termed solvent vapor annealed-soft lithography (SVA-SL) to induce the selective partitioning of these high molecular mass PGNPs into less confined 'mesa' regions in the topographically patterned films. This effect cannot be achieved readily using traditional thermal annealed soft lithography (TA-SL). We investigated the local enrichment of the larger-sized PGNPs into the 'mesa' region as a function of the degree of confinement (h_{brush} / $h_{confine}$) and molecular mass of the PGNPs. For both of the systems, the degree of the selective partitioning, quantified using partition coefficient K_p, decreases as the degree of confinement (h_{brush} / $h_{confine}$) increases, while the entropic driving force, quantified using the free energy model $|\Delta F|/ k_B T$, increases dramatically as the system reaches the strong confinement state (h_{brush} / $h_{confine}$ > 1.5), supporting the inference that the entropic penalties in the 'trench' state that drive the selective partitioning of these blends that is controlled by film topography. We also note that the limit of the degree of partitioning is a function of PGNPs' molecular mass. As the molecular mass approaches a 'critical' value (44 K PGNP system investigated here), the 'pinning' effect from the 'ultra-confined' 'trench' regions impede the selective partitioning, even when using the SVA-SL method. This effect could have its applications in which the stability and uniform distribution of the PGNPs within the film of the imprinted patterns is highly desired.

V.REVERSIBLE PARTITIONING OF POLYMER-GRAFTED NANOPARTICLES BLENDS UNDER TOPOGRAPHIC CONFINEMENT

5.1 Introduction

Precise control of nanoparticles organization over large area is one of the important research direction of the current state-of-art electronical devices, including the circuit fabrication, sensors, and quantum dot display. Many different methods have been developed to achieve the controlled nanoparticle spatial distribution, including the application of shear stress, chemical template, electric or magnetic field, blockcopolymer template, and the self-assembly of nanoparticles. Recent research from our group reveals the usage of topographic confinment to induce the selective ordering/partitioning of polymer nanocomposite films. Zhang *et al*. reveals that the entropic driving force arising from the togographic PDMS pattern can drive all the low-molecular weight polymer-grafted nanoparticles (PGNPs) to selectively partitioned in the less confined 'mesa' region (higher region of the patterned film) in both chemically-identical[23] and chemically different[21] homopolymer matrix. Wang *et al*.[20] demonstrates that this entropic-driven selective partitioning can also be applied to 'clusters' of PGNPs in homopolymer matrix. However, all the above process is a 'one-way ticket', where the nanoparticles can only be directed to form long-range ordered domains while the morphology cannot be re-dispered into a well-dispersed state. We here proposed to use a polymer blends with lower-critical solution temperature (LCST) to achieve the reversible control of the long-ranged orderred *vs.* re-dispersed state. In this type of blends, when the annealing temperature is above the LCST, the enthalpic

driving force will drive the polymer blends to phase separate. However, when the annealing temperature is below the LCST while still above the glass transition temperature (T_g), the Flory-Huggins interaction parameter (χ) will decrease and make the product of χN smaller than the critical value (≈ 2 for symmetric homopolymer blends) and lead to the re-dispersion of the polymer blends.

5.2 Experimental Design

In this chapter, we investigate the influence of the topographic nanopattern confinement on the distribution of polymethyl methacrylate grafted nanoparticles (PMMA-SiO_2) as the filler into the chemically dissimilar polystyrene acrylonitrile (PSAN) homopolymer matrix. We varied the annealing temperature above and below the LCST of the PMMA-SiO_2/PSAN system and used top-view transmission electron microscopy to study the influence of enthalpic and entropic interactions on the partitioning of PMMA-SiO_2. Below are the detailed information about the materials and experimental method.

5.2.1 Materials

The PGNPs used in the system is PMMA-SiO_2, which is synthesized *via* surface initiated atomic transfer radical polymerization (SI-ATRP). PMMA-SiO_2 nanoparticles are prepared and provided by our collaborators: Dr. Michael Bockstaller's and Dr. Krzysztof Matyjaszewski's group at Carnegie Mellon University. The average silica core size is $R_{0,core} \approx 7.5$ nm. The molecular mass for each grafted PMMA chain is $M_n \approx 43.7$ *kg/mol*, and the grafting density is $\sigma \approx 0.32/nm^2$. The PSAN homopolymer is purchased from Polymer Source Inc. and used as obtained. The molecular mass is $M_n \approx 33.0$ *kg/mol*. Poly(4-styrenesulfonic acid) (PSS) solution is

used for floating the polymer nanocomposite films for top-view transmission electron microscopy (TEM) characterization. It was purchased from MilliporeSigma as 18 wt.% in dionized water. The weight average molecular mass is $M_w \approx 75$ kg/mol. Tetrahydrofuran (THF) is used for dissolving the polymers. It was purchased from VWR Inc. and used as obtained.

5.2.2 Film preparation

PMMA-SiO_2 and PSAN was firstly dissolved in tetrahydrofuran (THF, VWR) solution (30 mg/ml) and sonicated in the water bath to ensure it is well dissolved. The mass ratio of PMMA-SiO_2 to the PSAN matrix is set as 10%, 30%, and 50%. The mixtures were then sonicated in a water bath for 20 min to ensure good dispersion.

Flow coater was used to make the PMMA-SiO_2/PSAN thin film with film thickness ≈ 100 nm. The film thickness was measured by an interferometer (F3UV) using the Film metrics LSDT2 system.

To prepare the films for TEM measurement, PSS (diluted to 1 w.t.% using methanol) solution was firstly casted onto the silicon wafer to form a 10 nm thick water-soluble layer. As soon as it is dried, the PMMA-SiO_2/PSAN mixtures were directly casted on it using flow coater with the final film thickness to be around 140 nm. After the films were processed using the topographic nanoimprinting method, the films were then immersed into the deionized water. The PSS layer dissolves immediately, which makes the top PMMA-SiO_2/PSAN layer float on the water surface. The floated films were then picked up from the water onto the copper grids (Ted Pella,

300 mesh Cu). The transferred films were then placed onto the Kimwipes and left overnight till they are fully dried.

5.2.3 Topographic nanoimprinting patterning

To conduct the topographic nanoimprinting patterning or thermal annealing soft lithography (TA-SL), an elastomer with a pre-defined pattern must be prepared. The patterned was made by pouring the polydimethylsiloxane (Dow Corning, Sylgard 184) onto commercial digital video discs (pitch $\lambda \approx 750$ nm, height difference $\Delta h \approx 120$ nm). The crosslinking ratio of the PDMS is curing agent mass: elastomer mass = 1:20. It was firstly vacuumed to remove the air bubbles in the PDMS solution and cured at 120°C for 12 h to make the topographic pattern layers. After the PDMS pattern was made, it was cut into the specific sizes to fit the dimensions of the polymer films. The inner side that has DVD pattern transferred to was directly attached to the polymer films. The film, together with the PDMS pattern, was then directly heated in the vacuum oven above the glass transition temperature of the polymer. As the polymer gained mobility in the melt state, the capillary force coming from the free volume between the PDMS pattern and the polymer surface drive the materials to fill into the empty space. After the temperature decreases to the room temperature and the top PDMS pattern is removed, a patterned polymer film is formed.

5.3 Results and Discussions

5.3.1 Reversible partitioning of nanoimprinted polymer nanocomposite films

We investigated the distribution of polymer-grafted nanoparticles (PGNPs) in a homopolymer matrix as a function of annealing temperature. The PGNPs are

polymethyl methacrylate grafted on silicon dioxide (PMMA-SiO_2). The number averaged molecular mass for each polymer chain are $M_n \approx 43.7$ *kg/mol*, with a grafting density of $\sigma \approx 0.32/nm^2$ and a SiO_2 core size of $R_{0,core} \approx 7.5$ nm. The homopolymer matrix is polystyrene-acrylonitrile (PSAN) with the number averaged molecular mass of $M_n \approx 33.0$ *kg/mol*. The PGNPs and homopolymers are first dissolved in THF solution separately and mixed later with desired mass ratio. The mixture is then cast to different film thickness using a flow coater. The casted films were then dried at 50˚C in the vaccuum oven for 12 hours to remove any residual solvent. **Figure 1** shows the proccess of the experiments. The casted films (mass ratio of PMMA-SiO_2 : PSAN = 1: 9) were first annealed at 180˚C for 48 hours (> LCST) with a topographic pattern on it. The pattern was created by transfering from the commerical DVD template (with a pitch λ = 750 nm) using a pre-cured polydimethylsiloxane (PDMS) pattern (curing agent mass: elastomer mass = 1: 20). The samples were then divided into two different groups. In the first group, the topographic PDMS pattern was removed and the films were then characterized under the top-view transmission electron microscopy (TEM). For the second group, the films were then annealed at 130˚C for another 48 hours with the PDMS pattern still on it. The pattern was then removed and those films were also characterizated using the top-view TEM. **Figure 5.1** shows the TEM results for both films annealed at 180˚C and those annealed first at 180˚C and then at 130˚C. The dark color strips represents the ‘mesa’ region of the patterned surface as it has higher electron density than the ‘trench’ region. The black dots show on the AFM represents the SiO_2 core, which can be used to track the distribution of the PGNPs in the films. It is very clear that in the film annealed at 180˚C (the top image), most of the PGNPs are

distributed in the higher 'mesa' region. However, when the film at this state was annealed back at 130℃ (the bottom image), the PGNPs re-disperse back to the 'trench' region, indicating the reversible distribution of those PGNPs in the pattern film *via* simply changing the annealing temperature.

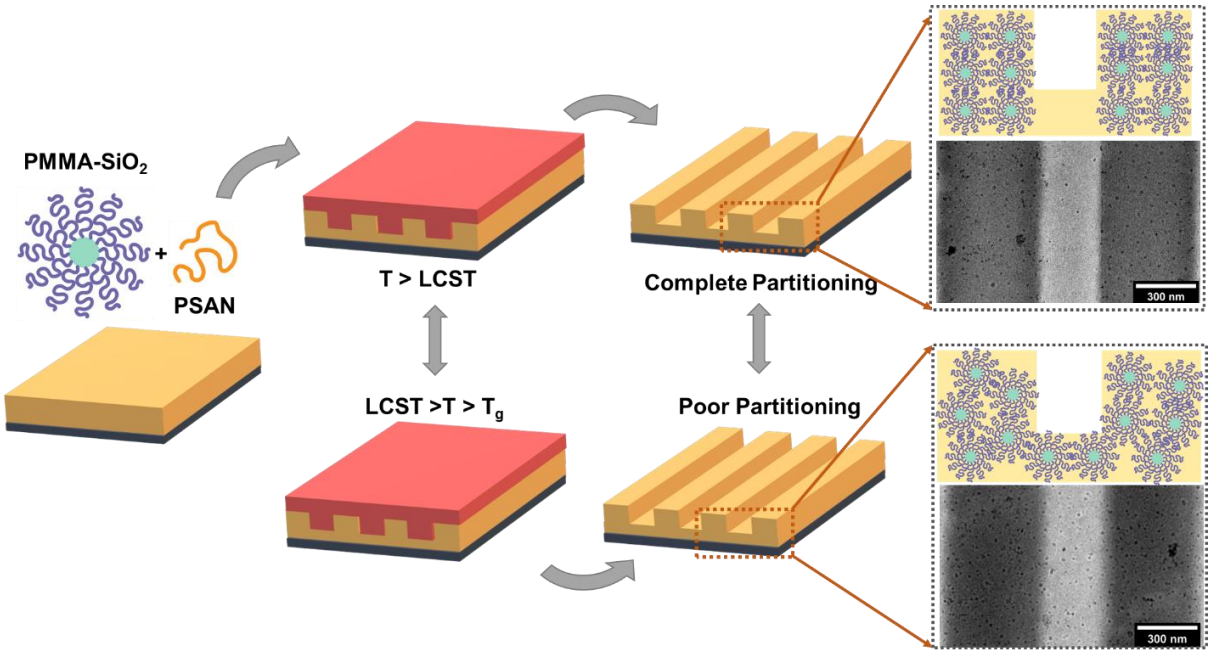

Figure 5.1. Illustration of the thermal-induced reversible selective partitioning of polymer nanocomposites.

5.3.2 Thermodyanmic investigation on the reversible partitioning process

How should we explain this reversible partitioning process? Flory-Huggins theory revealed that the phase behavior of polymer mixtures are determined by three different parameters: the interaction parameter χ, the degree of polymerization N, and the composition of the blends ϕ. For a symmetric (ϕ = 0.5) binary homopolymer mixture, the polymer blends phase separate when χN > 2. Although there is no theorical or experimental conclusion about the threshold χN value for polymer nanocomposite films, it is commonly agreed that the phase behavior of polymer

nanocomposites can be tunned with the variation of χN. For the blends with fixed value of N, the control of the phase behavior is achieved by changing the χ. For most of the polymer system, the χ is a function of annealing temperature (for thermal annealing) and the properties of the solvent (for solvent annealing). Karim *et al.*[75] studied the phase behavior of deuterated polystyrene (dPS) and poly(vinyl methyl ether) (PVME) blends as a function of annealing temeprature. They found that the blends phase separate at 170℃ due to an increased value of χ, while become homogenous at 130℃ as the χ reaches near zero. Similarly, Schmitt *et al.*[25] reported the same reversible phase behavior of a PGNP/PGNP blends (PMMA-SiO_2/PSAN-SiO_2). They found the film form phase separation at 170℃ and homogenization at 110℃. Recent work from our group found that the interaction parameter can be simply tunned by changing the chemistry of the annealing solvent for PMMA-SiO_2/PS-SiO_2 blends.[24] We found that by using the selective solvent for the mixture, as χ increases, the PGNP blends form phase separation. However, when the same film annealed in the common good solvent for both PGNPs, as the χ decreases below the threshold value, the phase separated film changes back to homogeous state. In conclusion, for both homopolymer and PGNP system, the phase behavior can be easily tunned by changing the interaction parameter χ. In another word, the enthalpic driving force can be changed by changing χ. In our topographic pattern scenario, when the film was heated at 180℃, the positive enthalpic forces increase as χ increases. This enthalpic force cooperate with the entropic driving force and move the PGNPs in the trench region to the mesa area. However, when the films were annealed at 130℃, as the enthalpic force decreases, it overcomes the entropic forces that induce the selective partitioning and

drive those PGNPs to redistribute back to the trench region to form the evenly distributed homogenous phase. To conclude, similar as what we proposed in the introduction section, the change of the enlthapic forces between ‘inducing phase separation’ and ‘inducing homogenization’ drives the topographic patternd PGNP nanocomposites films to have revesible PGNP organization between the ‘selective partitioning’ and ‘evenly distributed state’.

5.3.3 Kinetic study on the reversible partitioning process

We then investigate the kinetics of this reversible process. For the direction of the ‘selective’ partitioning, where the PGNPs are gradually segregated from the ‘trench’ region to the ‘mesa’ region, the films were annealed at 180℃ with the PDMS pattern on it for different annealing time. For the direction of the ‘re-dispersion’ of the partitioning, where the PGNPs are expecetd to re-disperse evenly to both ‘trench’ and ‘mesa’ region of the pattern film, the films were first annealed at 180℃ for 48 hours and then annealed back at 130℃ with the pattern on for different amount of annealing time. **Figure 5.2** shows the TEM images of the reversible partitioning process as a function of annealing temperature and time. When the films are annealed at 180℃ (above the LCST), as the annealing time increases from the 1 h (**Figure 5.2.A**) to 24 h (**Figure 5.2.C**), the PGNPs in the ‘trench’ region (the black dots in the light color strips) gradually move to the less confined ‘mesa’ region (dark color strips). After all of the PGNPs in trench region move to the ‘mesa’ region (180℃ for 48 h), the films were then annealed at 130℃ (with the pattern on it) for different amount of time to track the re-dispersion process. After 8 h of annealing at 130°C (**Figure 5.2.E**), the PGNPs started to re-disperse back to the ‘trench’ region. As the annealing time

increases to 24 h (**Figure 5.2.D**), considerable amout of PGNPs have segregated back to the 'trench' region. The gradual change of the amount of partitioning in both 'selective' and 're-dispersed' directions indicate that the reversible partitioing process is thermodyanmically favorable.

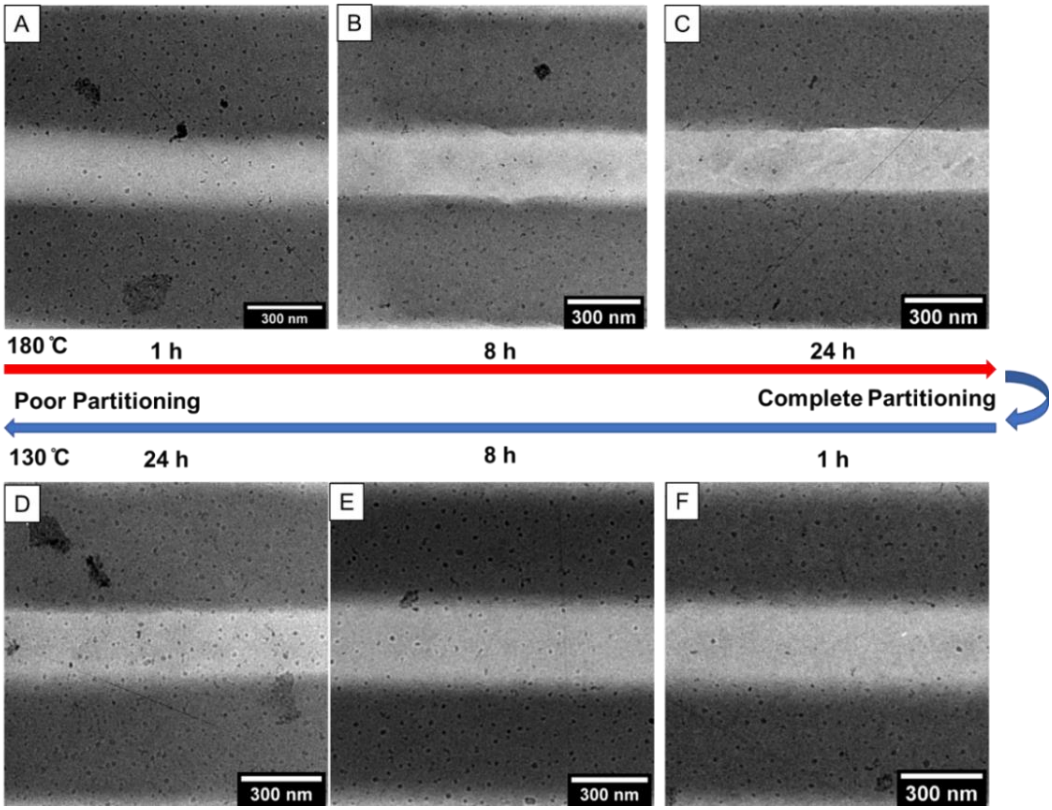

Figure 5.2. Top-view transmission electron images (TEM) showing the gradual change of the partition of PGNPs in the patterned films from more selectively partitioned (**A**, **B**, **C**) to more well-dispersed state (**D**, **E**, **F**).

To quantitatively study the kinetics of the reversible process, we here introduce a partitioning parameter (K_p) to quantify the extent of partitioning. The K_p is defined as the ratio of the number density of the PGNPs in the 'trench' region over those in the 'mesa' region, with K_p = 1 indicates even-distribution throughout the patterned film, < 1 indicates more PGNPs in 'mesa' while >1 indicates more PGNPs in the 'trench'

region. **Figure 5.3** shows the changes of K_p as a function of time when the films were annealed at 180˚C (**Figure 5.3.A**) and then at 130℃ (**Figure 5.3.B**). In the direction of selective partitioning (**Figure 5.3.A**), the K_p gradually decreases from ≈ 1.0 and stabilized at ≈ 0.2 after 48 h of annealing at 180℃, indicating a thermodynamically favorable selectively partitioning process. It has to be noted that in a recent research from our group, the partition parameter K_p for the same PGNPs in a chemical identical polymer matrix using solvent vapor annealing soft lithography (SVA-SL) also stabilized at ≈ 0.2. We concluded that this 'failure' to achieve complete partitioning ($K_p \approx 0$) is due to the 'jamming' configurations of these high molecular mass PGNPs. In the direction of reverse partitioning (**Figure 5.3.B**), K_p increases from 0.2 to ≈ 0.6 within approximately 5 hours of annealing. It continues to increase and finally stabilizes after 24 h of annealing.

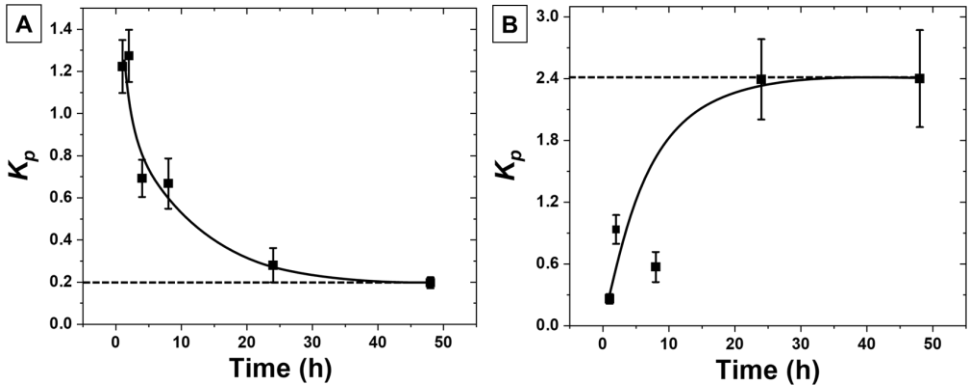

Figure 5.3. Changes of partitioning parameter K_p as a function of annealing time for 180℃ (**A**) and 180℃ (48 h) to 130℃ (**B**). The solid lines are used to guide the eye. The dashed lines are used for stabilized points.

5.3.4 Parameters influence the reversibility of the partitioning of the nanoimprinted nanocomposite films

We then investigate the influence of the mass ratio of PGNPs to the homopolymer matrix on the reversible partitioning process.

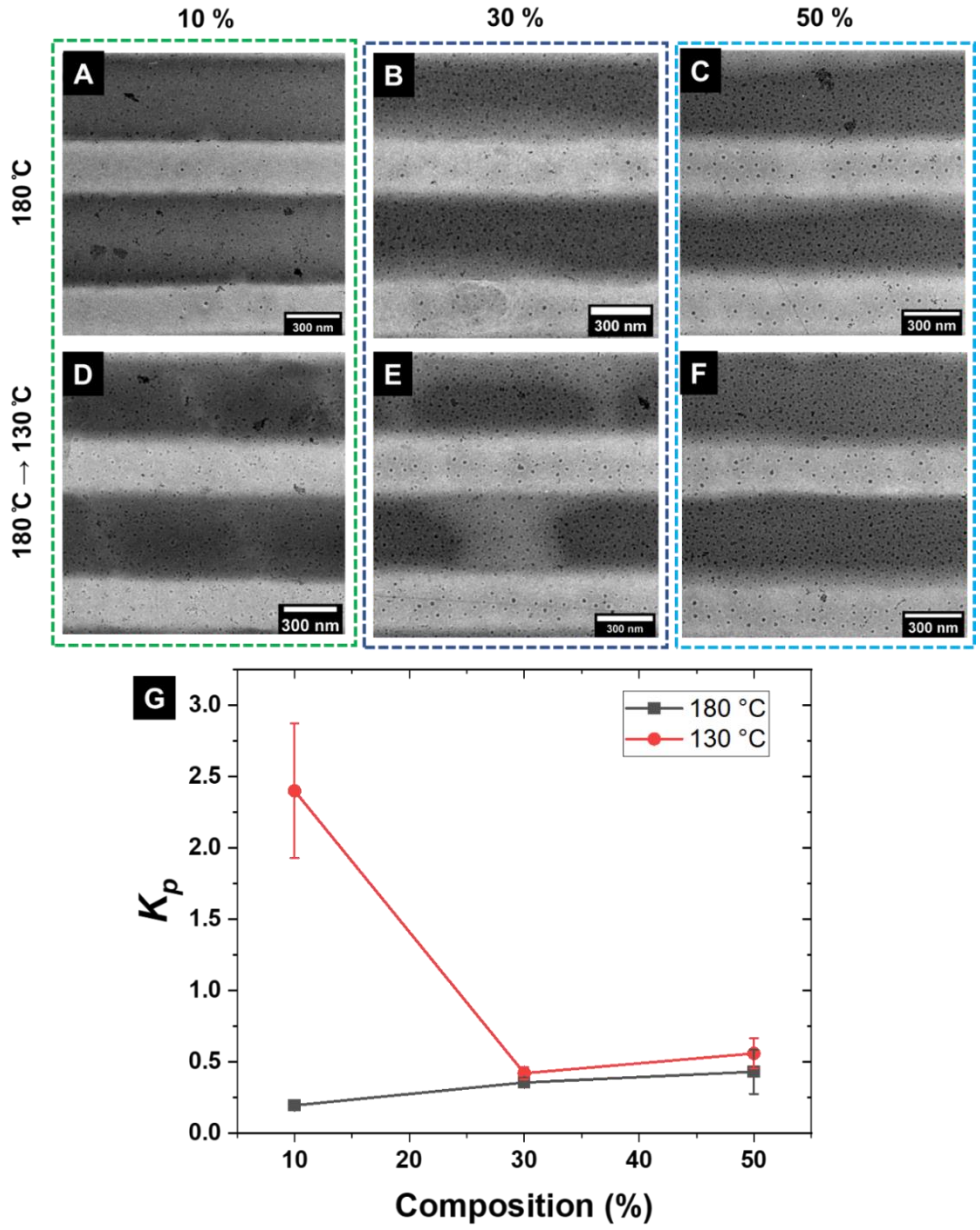

Figure 5.4. Top-view TEM images of the distribution of PGNPs in the nanopatterned films as a function of the mass ratio of PGNPs and annealing temperature.

Figure 5.4 shows the top-view TEM images of the distribution of those PGNPs as a function of the mass ratio and annealing temperature. For the 10% (mass ratio to the homopolymer) blends, most of the PGNPs move from the more confined trench region to the less confined mesa region when the film was heated at 180℃

(**Figure 5.4.A**), with a calculated partition parameter of 0.20 ± 0.03 (**Figure 5.4.G**). The large-sized PGNPs then move back and are evenly distributed in the patterned film, with a partition parameter of 2.40 ± 0.47 (**Figure 5.4.G**), indicating a strong reversible partitioning process. When the mass ratio of the PGNPs to the homopolymer matrix increases to 30%, the pattern annealed at 180℃ still shows selective partitioning of the PGNPs to the mesa region (**Figure 5.4.B**), with a calculated partitioning parameter of 0.36 ± 0.03 (**Figure 5.4.G**), indicating a poorer selective partitioning process than the 10% mixture. However, the extension of partitioning doesn't show big difference when the film annealed back at 130℃ for 48 h from the TEM images(**Figure 5.4.E**). The partitioning parameter is 0.42 ± 0.04 (**Figure 5.4.G**), indicating no reversible partitioning for this type of blends. The same phenomena happens on the blends with 50% mass ratio of PGNPs. When the film heated at 180℃ for 48 h, the PGNPs in the 'trench' region can still be 'squeezed' to the less confined 'mesa' region via the entropic driving force coming from the topographic pattern. The partitioning parameter is 0.43 ± 0.15. However, when it is heated back at 130℃, the TEM images show identical amount of PGNPs residing in the trench region. The partitioning parameter is 0.56 ± 0.11, confirming no strong indication of reversible partitioning compared to the 10% (mass ratio) blends. Why does the increase of the mass ratio of the PGNPs in the homopolymer matrix lead to the suppression of the reversible partitioning process? We believe it is due to the increase amount of the entanglement between the PGNPs. Due to this increase of entanglement between the PGNPs, the entropic and enthalpic driving force cannot be large enough to overcome the thermodynamic penalty from both the entanglement and

the ultra-confinment from the topographic pattern, which leads to poorer extension of PGNPs partitioning in the ‘mesa’ region than the less concentrated (mass ratio) system. When the film annealed at 130℃, the enthalpic driving force needs to overcome both the entropic penalty created from the topographic pattern (from the less confined ‘mesa’ to more confined ‘trench’ region) and the entanglement between the PGNPs. As some of the PGNPs have still been ‘squeezed’ from the ‘trench’ region to the ‘mesa’ in the selective partitioning process, the entanglement between the PGNPs in the ‘mesa’ even increased, which increases the entropic penalty for the PGNPs to reside from the ‘mesa’ back to the ‘trench’ region. This explains why the system with higher mass ratio of PGNPs cannot have the same reversible partitioning as the lower concentrated blends.

It is difficult for us to quantify the amount of entanglement between the PGNPs in the previously discussed conditions. However, a lot of theoretical and experimental research from other groups support our explanations. Dukes and his coworkers[58] found that the outer polymer brush forms two different regions: concentrated particle brush region (CPB) and semi-dilute particle brush (SDPB) region. The CPB region is near the inner nanoparticle core, where the polymer chains are stretched and is due to the less free volume. The SDPB region is near the outside where the polymer chains have more free volume to move around. Similarly, Midya and his coworkers develop a ‘two-layer’ model, a dry layer (similar to CPB) and an interpenetration layer (similar to SDPB), to describe the geometry and explain the physics of the polymer brushes. The ‘interpenetration’ terminology provides a more straightforward explanation about how the outer polymer region will ‘interpenetrate’

to each other and form a more 'packed' state with increased amount of entanglement between the polymer chains. One of the great advantages of the interpenetration of the polymer brushes are the enhanced mechanical properties of those materials. Ethier and his coworkers[6] compared the mechanical properties of polymer-grafted nanoparticle (PGNP) monolayers to the homopolymer thin films (with identical molecular mass). They found that both the simulation and the tensile testing show that the entangled PGNP film shows more uniform craze structure and significantly higher strain at break, while the short chain and unentangled showed no craz structure, which is similar to the homopolymer thin films. This indicates that the entanglement between the PGNPs is the critical factor that increase the whole mechanical properties of the PGNP thin films. Schmitt *et al.*[7] found that the fracture toughness of PGNP films will be significantly increased as the degree of polymerization goes over a critical 'threshold value', which is also related to the increased amount of the entanglement between the polymer brushes. Midya *et al.*[26] found that the entanglement between the PGNPs can also be increased by descresing the grafting density. With the identical molecular mass, the PGNPs with sparse particle brush shows higher elastic modulus than the dense particle brush. They concludes that the enhanced mechanical properties are mainly contributed by the SDPB region. Recent experimental work from Bilchak *et al.*[175] revealed a sluggish effect in PGNPs. They studied the rheology of poly (methyl acrylate) grafted silica nanoparticles (PMA-SiO_2, 14 $\pm$ 4 SiO_2 core diameter, σ = 0.43 chains/nm^2) as a function of polymer mass (M_n). When the M_n decreases to 77 kDa (a system close to the PS-SiO_2 in this paper), the G' plots show a plateau at low frequency, indicating the transition to 'solid-like' behavior. When the M_n continuously decreases to 27 kDa (a

system close to the PMMA-SiO_2 in this paper), the inner SiO_2 core dominates the dynamics, and the material is 'clearly solid-like'. This experimentally proves the existence of the increased amount of viscosity in PGNPs, and it is reasonable to expect similar rheology results from our systems.

5.4 Conclusions

Polymer-grafted nanoparticles (PGNPs) have gained extensive research interest due to its great potential in advanced applications, including the sensors, flexible electronics, conductivity, and thermal stability. One of the preliminary requests for those applications are the controlled distributions of PGNPs in the matrix. Recent research from our group shows that the entropic driving force from the topographic nanoimprint patterning or the thermal annealing soft lithography (TA-SL) can be used to induce the selective partitioning for PGNPs mixed in a chemically identical homopolymer matrix. However, the selective partitioning induced from TA-SL of a nanopatterned film cannot be redistributed to the even-distribution state, which decreases the reusability and limit the applications of a single nanopatterned polymer nanocomposite film. In this chapter, we developed a new system to have reversible partitioning of PGNPs in a chemical dissimilar homopolymer matrix. For the LCST PGNPs/homopolymer mixtures, both the positive enthalpic driving force (phase separation) between the grafted polymer chains and the polymer chains, along with the entropic driving force from the topographic nanoimprint confinement, induce the PGNPs to selectively segregated in the less confined "trench" region when the system was heated above the LCST. However, when the same nanopatterned films were heated below the LCST while still above the T_g, the negative enthalpic driving force

(for homogenization) can overcome the entropic penalty from the topographic nanoimprint confinement, which drives the selectively segregated PGNPs to redistribute evenly throughout the whole nanopatterned films. Kinetic study shows that the reversible partitioning process happens within 24 hours of annealing. Interestingly, as we increase the mass ratio of PGNPs to the homopolymer matrix from 10 % to 30% and 50%, the reversible partitioning process disappears. For the system with higher mass ratio, the total entropic penalty increases as the entanglement between the PGNPs increases due to more “confined” space, which makes the negative enthalpic driving force not large even to overcome the whole entropic penalty and leads to the failure of reversible partitioning. In conclude, we revealed a new nanopatterned system for reversible partitioning under topographic nanoimprint patterning. We elucidated the kinetics and the thermodynamic driving force for the reversible process. We also explored the boundary conditions for the reversible partitioning method.

VI. OVERAL SUMMARY

Understanding and controlling the phase behaviors of polymer-grafted nanoparticles (PGNPs) remains an important task in the polymer physics area since it is the pre-requisite for the related advanced applications, including flexible electronics, sensors, and conductivity. In this dissertation, we focus on the phase behavior of densely grafted high molecular mass PGNPs, which has great potential in enhancing both the mechanical and thermal stabilities of polymer nanocomposite films. We incorporate this kind of PGNPs into polymer matrix, with the purpose of controlling the phase behavior/PGNPs distribution through the interactions between the grafted polymer chains and the matrix. Typically, we studied the phase behaviors of polymethyl methacrylate grafted silica nanoparticles (PMMA-SiO_2) mixed with both chemically dissimilar polymer matrix (polystyrene grafted silica nanoparticles PS-SiO_2 in Chapter III and polystyrene-acrylonitrile homopolymer PSAN in Chapter V) and chemically identical but smaller sized PMMA-SiO_2 (Chapter IV). The objectives of this dissertation can be summarized as: 1) elucidate the thermodynamics and kinetics for the phase behaviors of binary high molecular mass PGNPs and compare it with its parent binary homopolymer blends and PGNPs/homopolymer nanocomposite films; 2) develop new approaches to change both the entropic and enthalpic interactions between the grafted polymer chains and the matrix to control the phase behaviors of PGNPs blends; 3) determine the optimal conditions to use topographic confinement to control the distribution of PGNPs in a nanopatterned films.

Recent research from our group and collaborators has found that melt phase separation for high molecular mass PGNPs (degree of polymerization for each chain: $N > 350$) blends through thermal annealing is a challenging task due to the lack of melt mobility of large particle brushes. In Chapter III, we proposed and demonstrated the use of an innovative solvent assisted method, direct immersion annealing (DIA), to help induce the phase separation of high molecular mass PMMA-SiO_2 (N=650) and PS-SiO_2 (N=360) blends. In this method, the polymer films are directly immersed into a miscible mixture of good and poor solvent, where the good solvent swells the film, decreases the glass transition temperature (T_g), and increases the mobility of the polymer. The poor solvent helps reduce the degree of good solvents interaction to prevent the dissolution or dewetting of the films while maintaining high mobility.

We examine both kinetics and thermodynamics of large binary PGNP blend films annealed by DIA. Several new results are presented in our paper on these unique systems: 1) We show that the phase morphologies could be readily switched between phase-separated and homogenous state by changing the thermodynamic conditions of DIA solution quality, between selective solvent (to PMMA-SiO_2) and neutral solvent (good solvent for both of the PGNPs), respectively. In comparison, thermal annealed PGNP blend films using thermal annealing at 180℃ produces no evolution from the as-cast structure. 2) The in-plane correlation length (ξ) to out-of-plane surface roughness (R_{rms}) stabilizes to a thermodynamic limit of surface to interfacial tension. 3) The kinetics of in-plane DIA phase separation shows unique ultrafast (~ few minutes) phase separation kinetics, $\xi \sim K t^n$, driven by a large pre-factor K due to a large DIA solvent mobility parameter, despite a smaller growth exponent, n ≈ 0.2, than

the classic 0.33 diffusive melt regime. 4) A pinning regime that prevents further evolution of phase separated PGNPs, apparently due to finite size effect of film confinement. 5) Progressively tunability of the phase-separated morphology from 2-phase all the way up and into the 1-phase state (analog of moving within thermal phase separation boundary), via tuning the interaction parameter χ, by carefully dialing in the fraction of good solvent in the DIA mixture.

We have thoroughly verified the consistency of the reversible phase through the entire film using Neutron Reflectivity (NR), AFM, etching the film by Time-of-Flight Secondary Ion Mass Spectroscopy (ToF-SIMS) for depth composition profile, and even doing AFM on etched areas, coupled with Ultra Small-Angle Neutron Scattering (USANS). We have proven that the reversible phase separation happens due to the change in the Flory-Huggings interaction parameter of the two grafted polymers ($\chi_{\mathrm{PMMA-SiO_2/PS-SiO_2}}$) with different DIA solvents. The selective solvent for PMMA-SiO_2 increases the $\chi_{\mathrm{PMMA-SiO_2/PS-SiO_2}}$, inducing the phase separation. While the neutral solvent decreases the $\chi_{\mathrm{PMMA-SiO_2/PS-SiO_2}}$, making PMMA-$SiO_2$ and PS-SiO_2 compatible with each other, resulting in a homogenous state.

We also investigated approaches to exert the precise control over the distribution of the high molecular mass PGNPs in a nanopatterned films. Recent research from our group indicates that the topographic nanoimprint patterning can be used to induce the selective segregation of low molecular mass PGNPs in both chemically dissimilar and identical homopolymer matrix. However, our results indicate that the traditional thermal annealing soft lithography (TA-SL) cannot induce

the preferential partitioning due to the lack of mobility from these high molecular mass systems. We develop a solvent vapor annealing soft lithography (SVA-SL) method, where the PGNPs blends with the topographic polydimethylsiloxane (PDMS) pattern are directly put into the solvent vapor (acetic acid for our PMMA-SiO_2) that only swell the PGNPs. During the SVA-SL process, the PMMA-SiO_2 is plasticized by the acetic acid, and the T_g decreases below the room temperature, which makes the PMMA-SiO_2 gain mobility to move in the film. The swelling process also relaxes the high molecular mass PMMA-SiO_2 from the entangled state, which increases its mobility in the film compared to the TA-SL process. As the topographic PDMS pattern is applied on the PGNPs film, the minimization of the entropic free energy from the topographic pattern along with the increased mobilities from SVA-SL process drives the high molecular mass PGNPs to selectively segregated in the less confined "mesa" region of the nanopatterned films. We quantified the extension of partitioning using a partition parameter K_p. We elucidated that the degree of partition can be easily tunned with the variation of molecular mass for the grafted polymer chains and the initial film thickness before patterning. We also determined the optimal condition for the selective segregation of PGNPs in the nanopatterned films through the degree of confinement (h_{brush} / $h_{confine}$). Only when the h_{brush} / $h_{confine}$ is larger than the critical value (1.5 for the system we studied), the entropic driving force can be larger enough to drive the selective segregation. Interestingly, it is not always good to have strong confinement. For the 44K PGNP system in Chapter IV, the pinning effect from the finite "trench" thickness is not negligible and impede the selective partitioning when h_{brush} / $h_{confine}$ > 5. In general, we overcome the technique processing

difficulties of nanopatterned high molecular mass PGNPs and develop a new SVA-SL process to induce the selective partitioning of these PGNPs. We elucidate the thermodynamic driving force for the preferential segregation *via* K_p and determined the optimal condition with h_{brush} / $h_{confine.}$

Furthermore, we also investigated the influence of enthalpic interactions on the distribution of PGNPs in nanopattern polymer matrix. We incorporated the high molecular mass PMMA-SiO_2 (N = 440) into the polystyrene-acrylonitrile (PSAN) homopolymer matrix. This is a polymer blends with lower critical solution temperature (LCST) transition, where the enthalpic interactions can be tunned by changing the annealing temperature above or below LCST. When the annealing temperature of the thermal annealing soft lithography (TA-SL) is above the LCST, the positive enthalpic interaction between the grafted PMMA layer and the PSAN matrix, which drives the blend to phase separate in a smooth film, drives the PMMA-SiO_2 to selectively partitioned in the "mesa" region as a synergistic effect from the entropic driving force from the topographic confinement. At the same time, when the nanopatterned films, along with the topographic PDMS pattern, are annealed below the LCST while still above the T_g, the negative enthalpic driving force, which leads to homogenization in smooth films, compensates the entropy penalty from the topographic confinement and redistributes the PGNPs evenly in the nanopatterned films. Kinetic study indicates that the reversible partitioning can be achieved as soon as 24 hours. We also determined the optimal condition for the reversible process through the partition parameter K_p. Interestingly, as the entanglement between the PGNPs increases as the loading of it increases, the reversible process disappears when

the mass ratio of PGNPs is above 10 %. This reversible organization of nanopatterned PGNPs film is novel. It expands the usage of a single film and makes it possible to be adapted to different advanced applications as needed.

REFERENCES

(1) Narayanan, S.; Choi, J.; Porter, L.; Bockstaller, M. R. Flexible Transparent Metal/Polymer Composite Materials Based on Optical Resonant Laminate Structures. *ACS Appl. Mater. Interfaces* **2013**, *5*, 4093–4099.

(2) Balazs, A. C.; Emrick, T.; Russell, T. P. Nanoparticle Polymer Composites: Where Two Small Worlds Meet. *Science (80-.).* **2006**, *314*, 1107–1110.

(3) Kumar, S. K.; Benicewicz, B. C.; Vaia, R. A.; Winey, K. I. 50th Anniversary Perspective : Are Polymer Nanocomposites Practical for Applications? *Macromolecules* **2017**, *50*, 714–731.

(4) Choi, J.; Dong, H.; Matyjaszewski, K.; Bockstaller, M. R. Flexible Particle Array Structures by Controlling Polymer Graft Architecture. *J. Am. Chem. Soc.* **2010**, *132*, 12537–12539.

(5) Ethier, J. G.; Hall, L. M. Structure and Entanglement Network of Model Polymer-Grafted Nanoparticle Monolayers. *Macromolecules* **2018**, *51*, 9878–9889.

(6) Ethier, J. G.; Drummy, L. F.; Vaia, R. A.; Hall, L. M. Uniaxial Deformation and Crazing in Glassy Polymer-Grafted Nanoparticle Ultrathin Films. *ACS Nano* **2019**, *13*, 12816–12829.

(7) Schmitt, M.; Choi, J.; Min Hui, C.; Chen, B.; Korkmaz, E.; Yan, J.; Margel, S.; Burak Ozdoganlar, O.; Matyjaszewski, K.; Bockstaller, M. R. Processing Fragile Matter: Effect of Polymer Graft Modification on the Mechanical Properties and Processibility of (Nano-) Particulate Solids. *Soft Matter* **2016**, *12*, 3527–3537.

(8) Bhadauriya, S.; Wang, X.; Pitliya, P.; Zhang, J.; Raghavan, D.; Bockstaller, M. R.; Stafford, C. M.; Douglas, J. F.; Karim, A. Tuning the Relaxation of Nanopatterned Polymer Films with Polymer-Grafted Nanoparticles: Observation of Entropy–Enthalpy Compensation. *Nano Lett.* **2018**, *18*, 7441–7447.

(9) Bhadauriya, S.; Wang, X.; Nallapaneni, A.; Masud, A.; Wang, Z.; Lee, J.; Bockstaller, M. R.; Al-Enizi, A. M.; Camp Jr, C. H.; Stafford, C. M.; Douglas, J. F.; Karim, A. Observation of General Entropy–Enthalpy Compensation Effect in the Relaxation of Wrinkled Polymer Nanocomposite Films. *Nano Lett.* **2021**, *21*, 1274–1281.

(10) Prateek; Thakur, V. K.; Gupta, R. K. Recent Progress on Ferroelectric Polymer-Based Nanocomposites for High Energy Density Capacitors: Synthesis, Dielectric Properties, and Future Aspects. *Chem. Rev.* **2016**, *116*, 4260–4317.

(11) C., M. T.; D., F. B.; J., S. R.; Z., H.; I., P.; P., M.; J., H. A. Ultrapermeable, Reverse-Selective Nanocomposite Membranes. *Science (80-.).* **2002**, *296*, 519–522.

(12) Choi, J.; Hui, C. M.; Pietrasik, J.; Dong, H.; Matyjaszewski, K.; Bockstaller, M. R. Toughening Fragile Matter: Mechanical Properties of Particle Solids Assembled from Polymer-Grafted Hybrid Particles Synthesized by ATRP. *Soft Matter* **2012**, *8*, 4072.

(13) Hore, M. J. A.; Korley, L. T. J.; Kumar, S. K. Polymer-Grafted Nanoparticles. *J. Appl. Phys.* **2020**, *128*, 030401.

(14) Bhat, R. R.; Tomlinson, M. R.; Wu, T.; Genzer, J. Surface-Grafted Polymer

Gradients: Formation, Characterization, and Applications. In *Surface-Initiated Polymerization II*; Springer-Verlag: Berlin/Heidelberg, 2006; Vol. 198, pp 51–124.

(15) Han, J.; Zhai, Y.; Wang, Z.; Bleuel, M.; Liu, T.; Yin, R.; Wu, W.; Hakem, I. F.; Karim, A.; Matyjaszewski, K.; Bockstaller, M. R. Nanosized Organo-Silica Particles with "Built-In" Surface-Initiated Atom Transfer Radical Polymerization Capability as a Platform for Brush Particle Synthesis. *ACS Macro Lett.* **2020**, *9*, 1218–1223.

(16) Matyjaszewski, K.; Gaynor, S.; Greszta, D.; Mardare, D.; Shigemoto, T. 'Living' and Controlled Radical Polymerization. *J. Phys. Org. Chem.* **1995**, *8*, 306–315.

(17) Edmondson, S.; Osborne, V. L.; Huck, W. T. S. Polymer Brushes via Surface-Initiated Polymerizations. *Chem. Soc. Rev.* **2004**, *33*, 14.

(18) Bockstaller, M. R.; Thomas, E. L. Proximity Effects in Self-Organized Binary Particle–Block Copolymer Blends. *Phys. Rev. Lett.* **2004**, *93*, 166106.

(19) Darling, S. B.; Yufa, N. A.; Cisse, A. L.; Bader, S. D.; Sibener, S. J. Self-Organization of FePt Nanoparticles on Photochemically Modified Diblock Copolymer Templates. *Adv. Mater.* **2005**, *17*, 2446–2450.

(20) Wang, X.; Bhadauriya, S.; Zhang, R.; Pitliya, P.; Raghavan, D.; Zhang, J.; Bockstaller, M. R.; Douglas, J. F.; Karim, A. Nanoimprint Directed Assembly of Associating Polymer-Grafted Nanoparticles for Polymer Thin Films with Enhanced Stability. *ACS Appl. Polym. Mater.* **2019**, *1*, 3242–3252.

(21) Zhang, R.; Lee, B.; Bockstaller, M. R.; Kumar, S. K.; Stafford, C. M.; Douglas,

J. F.; Raghavan, D.; Karim, A. Pattern-Directed Phase Separation of Polymer-Grafted Nanoparticles in a Homopolymer Matrix. *Macromolecules* **2016**, *49*, 3965–3974.

(22) Zhang, R.; Lee, B.; Bockstaller, M. R.; Al-Enizi, A. M.; Elzatahry, A.; Berry, B. C.; Karim, A. Soft-Shear Induced Phase-Separated Nanoparticle String-Structures in Polymer Thin Films. *Faraday Discuss.* **2016**, *186*, 31–43.

(23) Zhang, R.; Lee, B.; Stafford, C. M.; Douglas, J. F.; Dobrynin, A. V.; Bockstaller, M. R.; Karim, A. Entropy-Driven Segregation of Polymer-Grafted Nanoparticles under Confinement. *Proc. Natl. Acad. Sci.* **2017**, *114*, 2462–2467.

(24) Wu, W.; Singh, M.; Masud, A.; Wang, X.; Nallapaneni, A.; Xiao, Z.; Zhai, Y.; Wang, Z.; Terlier, T.; Bleuel, M.; Yuan, G.; Satija, S. K.; Douglas, J. F.; Matyjaszewski, K.; Bockstaller, M. R.; Karim, A. Control of Phase Morphology of Binary Polymer Grafted Nanoparticle Blend Films via Direct Immersion Annealing. *ACS Nano* **2021**, *15*, 12042–12056.

(25) Schmitt, M.; Zhang, J.; Lee, J.; Lee, B.; Ning, X.; Zhang, R.; Karim, A.; Davis, R. F.; Matyjaszewski, K.; Bockstaller, M. R. Polymer Ligand–Induced Autonomous Sorting and Reversible Phase Separation in Binary Particle Blends. *Sci. Adv.* **2016**, *2*, e1601484.

(26) Midya, J.; Cang, Y.; Egorov, S. A.; Matyjaszewski, K.; Bockstaller, M. R.; Nikoubashman, A.; Fytas, G. Disentangling the Role of Chain Conformation on the Mechanics of Polymer Tethered Particle Materials. *Nano Lett.* **2019**, *19*, 2715–2722.

(27) Bilchak, C. R.; Jhalaria, M.; Huang, Y.; Abbas, Z.; Midya, J.; Benedetti, F. M.; Parisi, D.; Egger, W.; Dickmann, M.; Minelli, M.; Doghieri, F.; Nikoubashman, A.; Durning, C. J.; Vlassopoulos, D.; Jestin, J.; Smith, Z. P.; Benicewicz, B. C.; Rubinstein, M.; Leibler, L.; Kumar, S. K. Tuning Selectivities in Gas Separation Membranes Based on Polymer-Grafted Nanoparticles. *ACS Nano* **2020**, *14*, 17174–17183.

(28) Talapin, D. V; Lee, J.-S.; Kovalenko, M. V; Shevchenko, E. V. Prospects of Colloidal Nanocrystals for Electronic and Optoelectronic Applications. *Chem. Rev.* **2010**, *110*, 389–458.

(29) Anikeeva, P. O.; Halpert, J. E.; Bawendi, M. G.; Bulović, V. Electroluminescence from a Mixed Red−Green−Blue Colloidal Quantum Dot Monolayer. *Nano Lett.* **2007**, *7*, 2196–2200.

(30) Li, Z.; Du, A. J.; Sun, Q.; Aljada, M.; Zhu, Z. H.; Lu, G. Q. (Max). Field-Effect Transistors Fabricated from Diluted Magnetic Semiconductor Colloidal Nanowires. *Nanoscale* **2012**, *4*, 1263.

(31) Winey, K. I.; Vaia, R. A. Polymer Nanocomposites. *MRS Bull.* **2007**, *32*, 314–322.

(32) Baekeland, L. H. The Synthesis, Constitution, and Uses of Bakelite. *J. Ind. Eng. Chem.* **1909**, *1*, 149–161.

(33) Rawal, S.; Brantley, J.; Karabudak, N. Development of Carbon Nanotube-Based Composite for Spacecraft Components. In *2013 6th International Conference on Recent Advances in Space Technologies (RAST)*; IEEE, 2013; pp 13–19.

(34) Paul, D. R.; Robeson, L. M. Polymer Nanotechnology : Nanocomposites. **2008**, *49*, 3187–3204.

(35) Yan, J.; Bockstaller, M. R.; Matyjaszewski, K. Brush-Modified Materials: Control of Molecular Architecture, Assembly Behavior, Properties and Applications. *Prog. Polym. Sci.* **2020**, *100*, 101180.

(36) Matyjaszewski, K. Atom Transfer Radical Polymerization (ATRP): Current Status and Future Perspectives. *Macromolecules* **2012**, *45*, 4015–4039.

(37) Hui, C. M.; Pietrasik, J.; Schmitt, M.; Mahoney, C.; Choi, J.; Bockstaller, M. R.; Matyjaszewski, K. Surface-Initiated Polymerization as an Enabling Tool for Multifunctional (Nano-)Engineered Hybrid Materials. *Chem. Mater.* **2014**, *26*, 745–762.

(38) Xie, G.; Ding, H.; Daniel, W. F. M.; Wang, Z.; Pietrasik, J.; Sheiko, S. S.; Matyjaszewski, K. Preparation of Titania Nanoparticles with Tunable Anisotropy and Branched Structures from Core–Shell Molecular Bottlebrushes. *Polymer (Guildf).* **2016**, *98*, 481–486.

(39) Zhang, J.; Song, Y.; Zhao, Y.; Zhao, S.; Yan, J.; Lee, J.; Wang, Z.; Liu, S.; Yuan, R.; Luo, D.; Kopeć, M.; Gottlieb, E.; Kowalewski, T.; Matyjaszewski, K.; Bockstaller, M. R. Organosilica with Grafted Polyacrylonitrile Brushes for High Surface Area Nitrogen-Enriched Nanoporous Carbons. *Chem. Mater.* **2018**, *30*, 2208–2212.

(40) Pino-Ramos, V. H.; Ramos-Ballesteros, A.; López-Saucedo, F.; López-Barriguete, J. E.; Varca, G. H. C.; Bucio, E. Radiation Grafting for the Functionalization and Development of Smart Polymeric Materials. *Top. Curr.*

Chem. **2016**, *374*, 63.

(41) Matyjaszewski, K. Advanced Materials by Atom Transfer Radical Polymerization. *Adv. Mater.* **2018**, *30*, 1706441.

(42) Liu, S.; Tang, Z. Nanoparticle Assemblies for Biological and Chemical Sensing. *J. Mater. Chem.* **2010**, *20*, 24–35.

(43) Yuan, H.; Zvonkina, I. J.; Al-Enizi, A. M.; Elzatahry, A. A.; Pyun, J.; Karim, A. Facile Assembly of Aligned Magnetic Nanoparticle Chains in Polymer Nanocomposite Films by Magnetic Flow Coating. *ACS Appl. Mater. Interfaces* **2017**, *9*, 11290–11298.

(44) Stuart, M. A. C.; Huck, W. T. S.; Genzer, J.; Müller, M.; Ober, C.; Stamm, M.; Sukhorukov, G. B.; Szleifer, I.; Tsukruk, V. V.; Urban, M.; Winnik, F.; Zauscher, S.; Luzinov, I.; Minko, S. Emerging Applications of Stimuli-Responsive Polymer Materials. *Nat. Mater.* **2010**, *9*, 101–113.

(45) Grabowski, C. A.; Koerner, H.; Meth, J. S.; Dang, A.; Hui, C. M.; Matyjaszewski, K.; Bockstaller, M. R.; Durstock, M. F.; Vaia, R. A. Performance of Dielectric Nanocomposites: Matrix-Free, Hairy Nanoparticle Assemblies and Amorphous Polymer–Nanoparticle Blends. *ACS Appl. Mater. Interfaces* **2014**, *6*, 21500–21509.

(46) Grabowski, C. A.; Fillery, S. P.; Koerner, H.; Tchoul, M.; Drummy, L.; Beier, C. W.; Brutchey, R. L.; Durstock, M. F.; Vaia, R. A. Dielectric Performance of High Permitivity Nanocomposites: Impact of Polystyrene Grafting on BaTiO3 and TiO2. *Nanocomposites* **2016**, *2*, 117–124.

(47) Che, J.; Jawaid, A.; Grabowski, C. A.; Yi, Y. J.; Louis, G. C.; Ramakrishnan,

S.; Vaia, R. A. Stability of Polymer Grafted Nanoparticle Monolayers: Impact of Architecture and Polymer-Substrate Interactions on Dewetting. *ACS Macro Lett.* **2016**, *5*, 1369–1374.

(48) Milner, S. T. Polymer Brushes. *Science (80-.).* **1991**, *251*, 905–914.

(49) Parkatzidis, K.; Wang, H. S.; Truong, N. P.; Anastasaki, A. Recent Developments and Future Challenges in Controlled Radical Polymerization: A 2020 Update. *Chem* **2020**, *6*, 1575–1588.

(50) Ślusarczyk, K.; Flejszar, M.; Chmielarz, P. Less Is More: A Review of ML-Scale of SI-ATRP in Polymer Brushes Synthesis. *Polymer (Guildf).* **2021**, *233*, 124212.

(51) Watanabe, H.; Kilbey, S. M.; Tirrell, M. A Scaling Model for Osmotic Energy of Polymer Brushes. *Macromolecules* **2000**, *33*, 9146–9151.

(52) Gennes, P. G. de (Pierre-G. de). *Scaling Concepts in Polymer Physics / Pierre-Gilles de Gennes*; Cornell University Press: Ithaca, N.Y, 1979.

(53) Alexander, S. Polymer Adsorption on Small Spheres. A Scaling Approach. *J. Phys.* **1977**, *38*, 977–981.

(54) Karim, A.; Satija, S. K.; Douglas, J. F.; Ankner, J. F.; Fetters, L. J. Neutron Reflectivity Study of the Density Profile of a Model End-Grafted Polymer Brush: Influence of Solvent Quality. *Phys. Rev. Lett.* **1994**, *73*, 3407–3410.

(55) Wijmans, C. M.; Zhulina, E. B. Polymer Brushes at Curved Surfaces. *Macromolecules* **1993**, *26*, 7214–7224.

(56) Ohno, K.; Morinaga, T.; Takeno, S.; Tsujii, Y.; Fukuda, T. Suspensions of Silica Particles Grafted with Concentrated Polymer Brush : Effects of Graft

Chain Length on Brush Layer Thickness and Colloidal Crystallization. **2007**, 9143–9150.

(57) Daoud, M.; Cotton, J. P. Star Shaped Polymers : A Model for the Conformation and Its Concentration Dependence. **1982**, *43*, 531–538.

(58) Dukes, D.; Li, Y.; Lewis, S.; Benicewicz, B.; Schadler, L.; Kumar, S. K. Conformational Transitions of Spherical Polymer Brushes: Synthesis, Characterization, and Theory. *Macromolecules* **2010**, *43*, 1564–1570.

(59) Robeson, L. M. *Polymer Blends: A Comprehensive Review*; 2007.

(60) Chung, H.; Wang, H.; Composto, R. J. A Morphology Map Based on Phase Evolution in Polymer Blend Films. *Macromolecules* **2006**, *39*, 153–161.

(61) Oh, H.; Green, P. F. Polymer Chain Dynamics and Glass Transition in Athermal Polymer/Nanoparticle Mixtures. *Nat. Mater.* **2009**, *8*, 139–143.

(62) Borukhov, I.; Leibler, L. Enthalpic Stabilization of Brush-Coated Particles in a Polymer Melt. *Macromolecules* **2002**, *35*, 5171–5182.

(63) Ferreira, P. G.; Ajdari, A.; Leibler, L. Scaling Law for Entropic Effects at Interfaces between Grafted Layers and Polymer Melts. *Macromolecules* **1998**, *31*, 3994–4003.

(64) Trombly, D. M.; Ganesan, V. Curvature Effects upon Interactions of Polymer-Grafted Nanoparticles in Chemically Identical Polymer Matrices. *J. Chem. Phys.* **2010**, *133*.

(65) Bansal, A.; Yang, H.; Li, C.; Benicewicz, B. C.; Kumar, S. K.; Schadler, L. S. Controlling the Thermomechanical Properties of Polymer Nanocomposites by Tailoring the Polymer-Particle Interface. *J. Polym. Sci. Part B Polym. Phys.*

2006, *44*, 2944–2950.

(66) Meli, L.; Arceo, A.; Green, P. F. Control of the Entropic Interactions and Phase Behavior of Athermal Nanoparticle/Homopolymer Thin Film Mixtures. *Soft Matter* **2009**, *5*, 533–537.

(67) Jayaraman, A.; Schweizer, K. S. Effective Interactions, Structure, and Phase Behavior of Lightly Tethered Nanoparticles in Polymer Melts. *Macromolecules* **2008**, *41*, 9430–9438.

(68) Akcora, P.; Liu, H.; Kumar, S. K.; Moll, J.; Li, Y.; Benicewicz, B. C.; Schadler, L. S.; Acehan, D.; Panagiotopoulos, A. Z.; Pryamitsyn, V.; Ganesan, V.; Ilavsky, J.; Thiyagarajan, P.; Colby, R. H.; Douglas, J. F. Anisotropic Self-Assembly of Spherical Polymer-Grafted Nanoparticles. *Nat. Mater.* **2009**, *8*, 354–359.

(69) Kumar, S. K.; Jouault, N.; Benicewicz, B.; Neely, T. Nanocomposites with Polymer Grafted Nanoparticles. *Macromolecules* **2013**, *46*, 3199–3214.

(70) Borukhov, I.; Leibler, L. Stabilizing Grafted Colloids in a Polymer Melt: Favorable Enthalpic Interactions. *Phys. Rev. E* **2000**, *62*, R41–R44.

(71) Martin, T. B.; Mongcopa, K. I. S.; Ashkar, R.; Butler, P.; Krishnamoorti, R.; Jayaraman, A. Wetting–Dewetting and Dispersion–Aggregation Transitions Are Distinct for Polymer Grafted Nanoparticles in Chemically Dissimilar Polymer Matrix. *J. Am. Chem. Soc.* **2015**, *137*, 10624–10631.

(72) Lifshitz, I. M.; Slyozov, V. V. The Kinetics of Precipitation from Supersaturated Solid Solutions. *J. Phys. Chem. Solids* **1961**, *19*, 35–50.

(73) Watkins, J. J.; Brown, G. D.; RamachandraRao, V. S.; Pollard, M. A.; Russell,

T. P. Phase Separation in Polymer Blends and Diblock Copolymers Induced by Compressible Solvents. *Macromolecules* **1999**, *32*, 7737–7740.

(74) Strobl, G. R.; Bendler, J. T.; Kambour, R. P.; Shultz, A. R. Thermally Reversible Phase Separation in Polystyrene/Poly(Styrene-Co-4-Bromostyrene) Blends. *Macromolecules* **1986**, *19*, 2683–2689.

(75) Karim, A.; Slawecki, T. M.; Kumar, S. K.; Douglas, J. F.; Satija, S. K.; Han, C. C.; Russell, T. P.; Liu, Y.; Overney, R.; Sokolov, J.; Rafailovich, M. H. Phase-Separation-Induced Surface Patterns in Thin Polymer Blend Films. *Macromolecules* **1998**, *31*, 857–862.

(76) Chen, K.; Yu, J.; Guzman, G.; Es-haghi, S. S.; Becker, M. L.; Cakmak, M. Role of Hydrogen Bonding on Nonlinear Mechano-Optical Behavior of l-Phenylalanine-Based Poly(Ester Urea)S. *Macromolecules* **2017**, *50*, 1075–1084.

(77) Chen, K.; Dreger, N. Z.; Peng, F.; Vogt, B. D.; Becker, M. L.; Cakmak, M. Nonlinear Mechano-Optical Behavior and Strain-Induced Structural Changes of l-Valine-Based Poly(Ester Urea)S. *Macromolecules* **2018**, *51*, 8114–8126.

(78) Thunga, M.; Chen, K.; Grewell, D.; Kessler, M. R. Bio-Renewable Precursor Fibers from Lignin/Polylactide Blends for Conversion to Carbon Fibers. *Carbon N. Y.* **2014**, *68*, 159–166.

(79) Peng, F.; Chen, K.; Yildirim, A.; Xia, X.; Vogt, B. D.; Cakmak, M. M. Tunable Piezoresistivity from Magnetically Aligned Ni(Core)@Ag(Shell) Particles in an Elastomer Matrix. *ACS Appl. Mater. Interfaces* **2019**, *11*, 20360–20369.

(80) Vaia, R. A.; Maguire, J. F. Polymer Nanocomposites with Prescribed

Morphology: Going beyond Nanoparticle-Filled Polymers. *Chem. Mater.* **2007**, *19*, 2736–2751.

(81) Mathur, A.; Brown, A.-D.; Erlebacher, J. Self-Ordering of Colloidal Particles in Shallow Nanoscale Surface Corrugations. *Langmuir* **2006**, *22*, 582–589.

(82) Zhang, R.; Singh, G.; Dang, A.; Dai, L.; Bockstaller, M. R.; Akgun, B.; Satija, S.; Karim, A. Nanoparticle-Driven Orientation Transition and Soft-Shear Alignment in Diblock Copolymer Films via Dynamic Thermal Gradient Field. *Macromol. Rapid Commun.* **2013**, *34*, 1642–1647.

(83) Gangwal, S.; Cayre, O. J.; Velev, O. D. Dielectrophoretic Assembly of Metallodielectric Janus Particles in AC Electric Fields. *Langmuir* **2008**, *24*, 13312–13320.

(84) Singh, J. P.; Lele, P. P.; Nettesheim, F.; Wagner, N. J.; Furst, E. M. One- and Two-Dimensional Assembly of Colloidal Ellipsoids in Ac Electric Fields. *Phys. Rev. E - Stat. Nonlinear, Soft Matter Phys.* **2009**, *79*.

(85) Grzelczak, M.; Vermant, J.; Furst, E. M.; Liz-marza, L. M. Directed Self-Assembly of Nanoparticles. **2010**, *4*, 3591–3605.

(86) Lumsdon, S. O.; Kaler, E. W.; Velev, O. D. Two-Dimensional Crystallization of Microspheres by a Coplanar AC Electric Field. *Langmuir* **2004**, *20*, 2108–2116.

(87) Thompson, R. B.; Ginzburg, V. V.; Matsen, M. W.; Balazs, A. C. Predicting the Mesophases of Copolymer-Nanoparticle Composites. *Science (80-.).* **2001**, *292*, 2469–2472.

(88) Huh, J.; Ginzburg, V. V.; Balazs, A. C. Thermodynamic Behavior of

Particle/Diblock Copolymer Mixtures: Simulation and Theory. *Macromolecules* **2000**, *33*, 8085–8096.

(89) Bockstaller, M. R.; Mickiewicz, R. A.; Thomas, E. L. Block Copolymer Nanocomposites: Perspectives for Tailored Functional Materials. *Adv. Mater.* **2005**, *17*, 1331–1349.

(90) Bockstaller, M. R.; Lapetnikov, Y.; Margel, S.; Thomas, E. L. Size-Selective Organization of Enthalpic Compatibilized Nanocrystals in Ternary Block Copolymer/Particle Mixtures. *J. Am. Chem. Soc.* **2003**, *125*, 5276–5277.

(91) Jang, S. G.; Kramer, E. J.; Hawker, C. J. Controlled Supramolecular Assembly of Micelle-Like Gold Nanoparticles in PS- b -P2VP Diblock Copolymers via Hydrogen Bonding. *J. Am. Chem. Soc.* **2011**, *133*, 16986–16996.

(92) Nepal, D.; Onses, M. S.; Park, K.; Jespersen, M.; Thode, C. J.; Nealey, P. F.; Vaia, R. A. Control over Position, Orientation, and Spacing of Arrays of Gold Nanorods Using Chemically Nanopatterned Surfaces and Tailored Particle–Particle–Surface Interactions. *ACS Nano* **2012**, *6*, 5693–5701.

(93) Chen, Y.; Yoon, Y. J.; Pang, X.; He, Y.; Jung, J.; Feng, C.; Zhang, G.; Lin, Z. Precisely Size-Tunable Monodisperse Hairy Plasmonic Nanoparticles via Amphiphilic Star-Like Block Copolymers. *Small* **2016**, *12*, 6714–6723.

(94) Chen, Y.; Wang, Z.; Harn, Y. W.; Pan, S.; Li, Z.; Lin, S.; Peng, J.; Zhang, G.; Lin, Z. Resolving Optical and Catalytic Activities in Thermoresponsive Nanoparticles by Permanent Ligation with Temperature-Sensitive Polymers. *Angew. Chemie Int. Ed.* **2019**, *58*, 11910–11917.

(95) Chevigny, C.; Dalmas, F.; Di Cola, E.; Gigmes, D.; Bertin, D.; Boué, F.; Jestin,

J. Polymer-Grafted-Nanoparticles Nanocomposites: Dispersion, Grafted Chain Conformation, and Rheological Behavior. *Macromolecules* **2011**, *44*, 122–133.

(96) Hore, M. J. A. Polymers on Nanoparticles: Structure & Dynamics. *Soft Matter* **2019**, *15*, 1120–1134.

(97) Luzinov, I.; Minko, S.; Tsukruk, V. V. Responsive Brush Layers: From Tailored Gradients to Reversibly Assembled Nanoparticles. *Soft Matter* **2008**, *4*, 714.

(98) Quan, B.; Lee, C.; Yoo, J. S.; Piao, Y. Facile Scalable Synthesis of Highly Monodisperse Small Silica Nanoparticles Using Alkaline Buffer Solution and Their Application for Efficient Sentinel Lymph Node Mapping. *J. Mater. Chem. B* **2017**, *5*, 586–594.

(99) Prucker, O.; Rühe, J. Synthesis of Poly(Styrene) Monolayers Attached to High Surface Area Silica Gels through Self-Assembled Monolayers of Azo Initiators. *Macromolecules* **1998**, *31*, 592–601.

(100) Vargas–Lara, F.; Starr, F. W.; Douglas, J. F. Hydrodynamic Radius Fluctuations in Model DNA–Grafted Nanoparticles. *AIP Conf. Proc.* **2016**, *1736*, 020080.

(101) Midya, J.; Rubinstein, M.; Kumar, S. K.; Nikoubashman, A. Structure of Polymer-Grafted Nanoparticle Melts. *ACS Nano* **2020**, *14*, 15505–15516.

(102) Harton, S. E.; Kumar, S. K. Mean-Field Theoretical Analysis of Brush-Coated Nanoparticle Dispersion in Polymer Matrices. *J. Polym. Sci. Part B Polym. Phys.* **2008**, *46*, 351–358.

(103) Rostom, S.; Dadmun, M. D. The Impact of Nanoparticle Softness on Its Tracer

Diffusion Coefficient in All Polymer Nanocomposites. *J. Appl. Phys.* **2020**, *127*, 074303.

(104) Sung, L.; Karim, A.; Douglas, J. F.; Han, C. C. Dimensional Crossover in the Phase Separation Kinetics of Thin Polymer Blend Films. *Phys. Rev. Lett.* **1996**, *76*, 4368–4371.

(105) Chung, H.; Composto, R. J. Breakdown of Dynamic Scaling in Thin Film Binary Liquids Undergoing Phase Separation. *Phys. Rev. Lett.* **2004**, *92*, 185704.

(106) Dudowicz, J.; Freed, K. F.; Douglas, J. F. New Patterns of Polymer Blend Miscibility Associated with Monomer Shape and Size Asymmetry. *J. Chem. Phys.* **2002**, *116*, 9983–9996.

(107) Dudowicz, J.; Freed, K. F.; Douglas, J. F. Concentration Fluctuations in Miscible Polymer Blends: Influence of Temperature and Chain Rigidity. *J. Chem. Phys.* **2014**, *140*, 194901.

(108) Yatsyshin, P.; Fytas, N. G.; Theodorakis, P. E. Mixing–Demixing Transition in Polymer-Grafted Spherical Nanoparticles. *Soft Matter* **2020**, *16*, 703–708.

(109) Longanecker, M.; Modi, A.; Dobrynin, A.; Kim, S.; Yuan, G.; Jones, R.; Satija, S.; Bang, J.; Karim, A. Reduced Domain Size and Interfacial Width in Fast Ordering Nanofilled Block Copolymer Films by Direct Immersion Annealing. *Macromolecules* **2016**, *49*, 8563–8571.

(110) Modi, A.; Bhaway, S. M.; Vogt, B. D.; Douglas, J. F.; Al-Enizi, A.; Elzatahry, A.; Sharma, A.; Karim, A. Direct Immersion Annealing of Thin Block Copolymer Films. *ACS Appl. Mater. Interfaces* **2015**, *7*, 21639–21645.

(111) Park, W. I.; Kim, J. M.; Jeong, J. W.; Jung, Y. S. Deep-Nanoscale Pattern Engineering by Immersion-Induced Self-Assembly. *ACS Nano* **2014**, *8*, 10009–10018.

(112) Singh, M.; Wu, W.; Basutkar, M. N.; Strzalka, J.; Al-Enizi, A. M.; Douglas, J. F.; Karim, A. Ultra-Fast Vertical Ordering of Lamellar Block Copolymer Films on Unmodified Substrates. *Macromolecules* **2021**, *54*, 1564–1573.

(113) Hore, M. J. A.; Ford, J.; Ohno, K.; Composto, R. J.; Hammouda, B. Direct Measurements of Polymer Brush Conformation Using Small-Angle Neutron Scattering (SANS) from Highly Grafted Iron Oxide Nanoparticles in Homopolymer Melts. *Macromolecules* **2013**, *46*, 9341–9348.

(114) Samant, S.; Basutkar, M.; Singh, M.; Masud, A.; Grabowski, C. A.; Kisslinger, K.; Strzalka, J.; Yuan, G.; Satija, S.; Apata, I.; Raghavan, D.; Durstock, M.; Karim, A. Effect of Molecular Weight and Layer Thickness on the Dielectric Breakdown Strength of Neat and Homopolymer Swollen Lamellar Block Copolymer Films. *ACS Appl. Polym. Mater.* **2020**, *2*, 3072–3083.

(115) Luo, Y.; Wang, X.; Zhang, R.; Singh, M.; Ammar, A.; Cousins, D.; Hassan, M. K.; Ponnamma, D.; Adham, S.; Al-Maadeed, M. A. A.; Karim, A. Vertically Oriented Nanoporous Block Copolymer Membranes for Oil/Water Separation and Filtration. *Soft Matter* **2020**, *16*, 9648–9654.

(116) Singh, M.; Wu, W.; Nuka, V.; Strzalka, J.; Douglas, J. F.; Karim, A. Late Stage Domain Coarsening Dynamics of Lamellar Block Copolymers. *ACS Macro Lett.* **2021**, *10*, 727–731.

(117) Singh, M.; Apata, I. E.; Samant, S.; Wu, W.; Tawade, B. V.; Pradhan, N.;

Raghavan, D.; Karim, A. Nanoscale Strategies to Enhance the Energy Storage Capacity of Polymeric Dielectric Capacitors: Review of Recent Advances. *Polym. Rev.* **2021**, *0*, 1–50.

(118) Samant, S.; Hailu, S.; Singh, M.; Pradhan, N.; Yager, K.; Al-Enizi, A. M.; Raghavan, D.; Karim, A. Alignment Frustration in Block Copolymer Films with Block Copolymer Grafted <scp> TiO_2 </Scp> Nanoparticles under <scp>soft-shear</Scp> Cold Zone Annealing. *Polym. Adv. Technol.* **2021**, *32*, 2052–2060.

(119) Tawade, B. V.; Apata, I. E.; Singh, M.; Das, P.; Pradhan, N.; Al-Enizi, A. M.; Karim, A.; Raghavan, D. Recent Developments in the Synthesis of Chemically Modified Nanomaterials for Use in Dielectric and Electronics Applications. *Nanotechnology* **2021**, *32*, 142004.

(120) Masud, A.; Longanecker, M.; Bhadauriya, S.; Singh, M.; Wu, W.; Sharma, K.; Terlier, T.; Al-Enizi, A. M.; Satija, S.; Douglas, J. F.; Karim, A. Ionic Liquid Enhanced Parallel Lamellar Ordering in Block Copolymer Films. *Macromolecules* **2021**, *54*, 4531–4545.

(121) Kent, M. S.; Factor, B. J.; Satija, S.; Smith, G. S. Structure of Bimodal Polymer Brushes in a Good Solvent by Neutron Reflectivity. *Macromolecules* **1996**, *29*, 2843–2849.

(122) Espinosa-Marzal, R. M.; Nalam, P. C.; Bolisetty, S.; Spencer, N. D. Impact of Solvation on Equilibrium Conformation of Polymer Brushes in Solvent Mixtures. *Soft Matter* **2013**, *9*, 4045.

(123) Liu, S.; Walton, M.; Tarakina, N. V.; Akcora, P. Solvation in Ionic Liquids with

Polymer-Grafted Nanoparticles. *J. Phys. Chem. B* **2020**, *124*, 4843–4850.

(124) Auroy, P.; Auvray, L. Collapse-Stretching Transition for Polymer Brushes: Preferential Solvation. *Macromolecules* **1992**, *25*, 4134–4141.

(125) Birshtein, T. M.; Lyatskaya, Y. V. Theory of the Collapse-Stretching Transition of a Polymer Brush in a Mixed Solvent. *Macromolecules* **1994**, *27*, 1256–1266.

(126) Dudowicz, J.; Freed, K. F.; Douglas, J. F. Modification of the Phase Stability of Polymer Blends by Diblock Copolymer Additives. *Macromolecules* **1995**, *28*, 2276–2287.

(127) Maranville, B.; Ratcliff II, W.; Kienzle, P. Reductus : A Stateless Python Data Reduction Service with a Browser Front End. *J. Appl. Crystallogr.* **2018**, *51*, 1500–1506.

(128) Gaikwad, A. M.; Khan, Y.; Ostfeld, A. E.; Pandya, S.; Abraham, S.; Arias, A. C. Identifying Orthogonal Solvents for Solution Processed Organic Transistors. *Org. Electron.* **2016**, *30*, 18–29.

(129) Hansen, C. M. *Hansen Solubility Parameters : A User's Handbook, Second Edition*; CRC Press: Boca Raton, 2007.

(130) Terlier, T.; Zappalà, G.; Marie, C.; Leonard, D.; Barnes, J. P.; Licciardello, A. ToF-SIMS Depth Profiling of PS-b-PMMA Block Copolymers Using Arn+, C60++, and Cs+ Sputtering Ions. *Anal. Chem.* **2017**, *89*, 6984–6991.

(131) Flory, P. J. Thermodynamics of High Polymer Solutions. *J. Chem. Phys.* **1942**, *10*, 51–61.

(132) Huggins, M. L. Theory of Solutions of High Polymers 1. *J. Am. Chem. Soc.* **1942**, *64*, 1712–1719.

(133) Bates, F. S. Polymer-Polymer Phase Behavior. *Science (80-.).* **1991**, *251*, 898–905.

(134) Robeson, L. M. Fundamentals of Polymer Blends. In *Polymer Blends*; Carl Hanser Verlag GmbH & Co. KG: München, 2007; pp 11–64.

(135) Zeman, L.; Patterson, D. Effect of the Solvent on Polymer Incompatibility in Solution. *Macromolecules* **1972**, *5*, 513–516.

(136) Bank, M.; Leffingwell, J.; Thies, C. The Influence of Solvent upon the Compatibility of Polystyrene and Poly(Vinyl Methyl Ether). *Macromolecules* **1971**, *4*, 43–46.

(137) Douglas, J. F.; Johnson, H. E.; Granick, S. A Simple Kinetic Model of Polymer Adsorption and Desorption. *Science (80-.).* **1993**, *262*, 2010–2012.

(138) Chung, H.-J.; Taubert, A.; Deshmukh, R. D.; Composto, R. J. Mobile Nanoparticles and Their Effect on Phase Separation Dynamics in Thin-Film Polymer Blends. *Europhys. Lett.* **2004**, *68*, 219–225.

(139) Wilcoxon, J. P.; Martin, J. E.; Odinek, J. Anomalous Phase Separation Kinetics Observed in a Micelle Solution. *Phys. Rev. Lett.* **1995**, *75*, 1558–1561.

(140) Tateno, M.; Tanaka, H. Numerical Prediction of Colloidal Phase Separation by Direct Computation of Navier–Stokes Equation. *npj Comput. Mater.* **2019**, *5*, 40.

(141) Kawasaki, K.; Ohta, T. Kinetics of Fluctuations for Systems Undergoing Phase Transitions - Interfacial Approach. *Phys. A Stat. Mech. its Appl.* **1983**, *118*, 175–190.

(142) Midya, J.; Rubinstein, M.; Kumar, S. K.; Nikoubashman, A. Structure of

Polymer-Grafted Nanoparticle Melts. *ACS Nano* **2020**, *14*, 15505–15516.

(143) Chremos, A.; Douglas, J. F. Particle Localization and Hyperuniformity of Polymer-grafted Nanoparticle Materials. *Ann. Phys.* **2017**, *529*, 1600342.

(144) Chremos, A.; Douglas, J. F. Hidden Hyperuniformity in Soft Polymeric Materials. *Phys. Rev. Lett.* **2018**, *121*, 258002.

(145) Song, K.-X.; Jia, Y.-X.; Sun, Z.-Y.; An, L.-J. Lattice Boltzmann Study of Hydrodynamic Effects in Lamellar Ordering Process of Two-Dimensional Quenched Block Copolymers. *J. Chem. Phys.* **2008**, *129*, 144901.

(146) Bilchak, C. R.; Buenning, E.; Asai, M.; Zhang, K.; Durning, C. J.; Kumar, S. K.; Huang, Y.; Benicewicz, B. C.; Gidley, D. W.; Cheng, S.; Sokolov, A. P.; Minelli, M.; Doghieri, F. Polymer-Grafted Nanoparticle Membranes with Controllable Free Volume. *Macromolecules* **2017**, *50*, 7111–7120.

(147) Yu, J.-W.; Douglas, J. F.; Hobbie, E. K.; Kim, S.; Han, C. C. Shear-Induced "Homogenization" of a Diluted Polymer Blend. *Phys. Rev. Lett.* **1997**, *78*, 2664–2667.

(148) Beysens, D.; Gbadamassi, M.; Boyer, L. Light-Scattering Study of a Critical Mixture with Shear Flow. *Phys. Rev. Lett.* **1979**, *43*, 1253–1256.

(149) Takebe, T.; Sawaoka, R.; Hashimoto, T. Shear-Induced Homogenization of Semidilute Solution of Polymer Mixture and Unmixing after Cessation of the Shear. *J. Chem. Phys.* **1989**, *91*, 4369–4379.

(150) Douglas, J. F. "Shift" in Polymer Blend Phase-Separation Temperature in Shear Flow. *Macromolecules* **1992**, *25*, 1468–1474.

(151) Nakatani, A. I.; Sung, L.; Hobbie, E. K.; Han, C. C. Shear-Induced Order in a

Homopolymer Blend with Block Copolymer Surfactant. *Phys. Rev. Lett.* **1997**, *79*, 4693–4696.

(152) Goel, V.; Pietrasik, J.; Dong, H.; Sharma, J.; Matyjaszewski, K.; Krishnamoorti, R. Structure of Polymer Tethered Highly Grafted Nanoparticles. *Macromolecules* **2011**, *44*, 8129–8135.

(153) Hore, M. J. A.; Ford, J.; Ohno, K.; Composto, R. J.; Hammouda, B. Direct Measurements of Polymer Brush Conformation Using Small-Angle Neutron Scattering (SANS) from Highly Grafted Iron Oxide Nanoparticles in Homopolymer Melts. *Macromolecules* **2013**, *46*, 9341–9348.

(154) Vargas-Lara, F.; Pazmiño Betancourt, B. A.; Douglas, J. F. Communication: A Comparison between the Solution Properties of Knotted Ring and Star Polymers. *J. Chem. Phys.* **2018**, *149*, 161101.

(155) Chremos, A.; Douglas, J. F. Self-Assembly of Polymer-Grafted Nanoparticles in Solvent-Free Conditions. *Soft Matter* **2016**, *12*, 9527–9537.

(156) Barnett, J. W.; Kumar, S. K. Modeling Gas Transport in Polymer-Grafted Nanoparticle Membranes. *Soft Matter* **2019**, *15*, 424–432.

(157) Chremos, A. Design of Nearly Perfect Hyperuniform Polymeric Materials. *J. Chem. Phys.* **2020**, *153*, 054902.

(158) Chremos, A. Design of Nearly Perfect Hyperuniform Polymeric Materials. *J. Chem. Phys.* **2020**, *153*, 054902.

(159) Bilchak, C. R.; Huang, Y.; Benicewicz, B. C.; Durning, C. J.; Kumar, S. K. High-Frequency Mechanical Behavior of Pure Polymer-Grafted Nanoparticle Constructs. *ACS Macro Lett.* **2019**, *8*, 294–298.

(160) Liu, S.; Tyagi, M.; Akcora, P. Polymer-Coupled Local Dynamics Enhances Conductivity of Ionic Liquids. *Macromolecules* **2020**, *53*, 6538–6546.

(161) Liu, S.; Wu, D.; Akcora, P. Ion-Containing Polymer-Grafted Nanoparticles in Ionic Liquids: Implications for Polymer Electrolyte Membranes. *ACS Appl. Nano Mater.* **2021**, *4*, 8108–8115.

(162) Singh, M.; Wu, W.; Basutkar, M. N.; Strzalka, J.; Al-Enizi, A. M.; Douglas, J. F.; Karim, A. Ultra-Fast Vertical Ordering of Lamellar Block Copolymer Films on Unmodified Substrates. *Macromolecules* **2021**, *54*, 1564–1573.

(163) Koh, C.; Grest, G. S.; Kumar, S. K. Assembly of Polymer-Grafted Nanoparticles in Polymer Matrices. *ACS Nano* **2020**, *14*, 13491–13499.

(164) Alkhodairi, H.; Russell, S. T.; Pribyl, J.; Benicewicz, B. C.; Kumar, S. K. Compatibilizing Immiscible Polymer Blends with Sparsely Grafted Nanoparticles. *Macromolecules* **2020**, *53*, 10330–10338.

(165) Maguire, S. M.; Boyle, M. J.; Bilchak, C. R.; Demaree, J. D.; Keller, A. W.; Krook, N. M.; Ohno, K.; Kagan, C. R.; Murray, C. B.; Rannou, P.; Composto, R. J. Grafted Nanoparticle Surface Wetting during Phase Separation in Polymer Nanocomposite Films. *ACS Appl. Mater. Interfaces* **2021**, *13*, 37628–37637.

(166) Maguire, S. M.; Krook, N. M.; Kulshreshtha, A.; Bilchak, C. R.; Brosnan, R.; Pana, A.-M.; Rannou, P.; Maréchal, M.; Ohno, K.; Jayaraman, A.; Composto, R. J. Interfacial Compatibilization in Ternary Polymer Nanocomposites: Comparing Theory and Experiments. *Macromolecules* **2021**, *54*, 797–811.

(167) Koski, J. P.; Krook, N. M.; Ford, J.; Yahata, Y.; Ohno, K.; Murray, C. B.; Frischknecht, A. L.; Composto, R. J.; Riggleman, R. A. Phase Behavior of

Grafted Polymer Nanocomposites from Field-Based Simulations. *Macromolecules* **2019**, *52*, 5110–5121.

(168) Masud, A.; Wu, W.; Singh, M.; Tonny, W.; Ammar, A.; Sharma, K.; Strzalka, J. W.; Terlier, T.; Douglas, J. F.; Karim, A. Solvent Processing and Ionic Liquid-Enabled Long-Range Vertical Ordering in Block Copolymer Films with Enhanced Film Stability. *Macromolecules* **2021**, *54*, 8512–8525.

(169) Bilchak, C. R.; Huang, Y.; Benicewicz, B. C.; Durning, C. J.; Kumar, S. K. High-Frequency Mechanical Behavior of Pure Polymer-Grafted Nanoparticle Constructs. *ACS Macro Lett.* **2019**, *8*, 294–298.

(170) Lin, C.-C.; Griffin, P. J.; Chao, H.; Hore, M. J. A.; Ohno, K.; Clarke, N.; Riggleman, R. A.; Winey, K. I.; Composto, R. J. Grafted Polymer Chains Suppress Nanoparticle Diffusion in Athermal Polymer Melts. *J. Chem. Phys.* **2017**, *146*, 203332.

(171) Hore, M. J. A.; Ford, J.; Ohno, K.; Composto, R. J.; Hammouda, B. Direct Measurements of Polymer Brush Conformation Using Small-Angle Neutron Scattering (SANS) from Highly Grafted Iron Oxide Nanoparticles in Homopolymer Melts. *Macromolecules* **2013**, *46*, 9341–9348.

(172) Goel, V.; Pietrasik, J.; Dong, H.; Sharma, J.; Matyjaszewski, K.; Krishnamoorti, R. Structure of Polymer Tethered Highly Grafted Nanoparticles. *Macromolecules* **2011**, *44*, 8129–8135.

(173) Lee, J. N.; Park, C.; Whitesides, G. M. Solvent Compatibility of Poly(Dimethylsiloxane)-Based Microfluidic Devices. *Anal. Chem.* **2003**, *75*, 6544–6554.

(174) You, J.; Zhang, S.; Huang, G.; Shi, T.; Li, Y. Solvent Annealing Induced Phase Separation and Dewetting in PMMA/SAN Blend Film: Film Thickness and Solvent Dependence. *J. Chem. Phys.* **2013**, *138*, 244907.

(175) Bilchak, C. R.; Buenning, E.; Asai, M.; Zhang, K.; Durning, C. J.; Kumar, S. K.; Huang, Y.; Benicewicz, B. C.; Gidley, D. W.; Cheng, S.; Sokolov, A. P.; Minelli, M.; Doghieri, F. Polymer-Grafted Nanoparticle Membranes with Controllable Free Volume. *Macromolecules* **2017**, *50*, 7111–7120.